ENERGETIC VERSATILITY OF MUSCLE

A Dissertation
Presented to
The Academic Faculty

By

Travis Carver Tune

In Partial Fulfillment
of the Requirements for the Degree
Doctor of Philosophy in the
School of Physics

Georgia Institute of Technology

December 2020

ENERGETIC VERSATILITY OF MUSCLE

Approved by:

Dr. Simon Sponberg, Advisor
School of Biology and Physics
Georgia Institute of Technology

Dr. Thomas Irving
School of Biology and Physics
Illinois Institute of Technology

Dr. Peter Yunker
School of Physics
Georgia Institute of Technology

Dr. Flavio Fenton
School of Physics
Georgia Institute of Technology

Dr. Zeb Rocklin
School of Physics
Georgia Institute of Technology

Date Approved: August 21, 2020

Still theory

Grandmaster Ben Finegold

Dedicated to eV

ACKNOWLEDGEMENTS

I would first like to thank my advisor Simon Sponberg, for all his help and mentoring throughout my graduate research.

I would also like to thank Tom Irving, Weikang Ma, Rick Heurich, and Mark Vukonich for all their help at Argonne National Lab and data interpretation and analysis.

Thanks also to Tom Daniel, Dave Williams, Sage Malingen, Anthony Cass, and Jose Alvarado for their helpful discussions.

I would also like to thank all the members of the lab, as well as all my friends from the Physics Department.

I would also like to thank my parents Martha Carver and Richard Tune, as well as my brother Will Tune for their support and encouragement.

TABLE OF CONTENTS

LIST OF TABLES

LIST OF FIGURES

SUMMARY

Muscle in an incredibly versatile, active, soft, crystalline material which makes it very unique. It is ubiquitous in animals across many scales, enabling a diverse range of locomotion types and mechanical functions, capable of operating as a motor, brake, or spring. The fact that muscle is a highly ordered, crystalline material means that x-ray diffraction can be used to observe structural changes at the nanometer scale in muscle, linking its crystal structure to function. While muscle x-ray diffraction is a very well established field, it has only been in the last 15 or so years that very high frequency x-ray detectors have allowed x-ray diffraction experiments to be performed on muscles operating under conditions mimicking their *in vivo* behavior. In this thesis we use x-ray diffraction combined with stress-strain measurements of muscle operating under *in vivo*-like conditions in order to link its nanometer scale structure to macroscopic mechanical function. This is difficult because muscle is also a hierarchical material, and interactions between structures on different length scales can have unexpected, emergent effects.

We first examine a pair of muscles in the cockroach *Blaberus discoidalis* previously established as having very similar quasi-static properties yet very different dynamic stress-strain curves, and therefore mechanical function. Since force in muscle is generated by the interaction between two types of filaments in a crystal lattice, we hypothesized that we could find differences in their lattice structure which may explain these similarities and differences. We show that the radial spacing between these filaments is different between the two muscles, and is of an order of magnitude sufficient to affect force production.

We next used a spatially explicit model in order to further establish that changes at the nanometer scale can affect macroscopic mechanical function. Using a spatially explicit model allows us to examine how small changes at the nanometer scale can affect function at a much larger scale. Using this model, we show that lattice structure changes like those we found in *B. discoidalis* are able to affect mechanical function of muscle.

Finally we return to the simultaneous x-ray diffraction and physiological force experiments and examine the large flight muscles of the hawkmoth *Manduca sexta*. This muscle is very well ordered and provides many structural features at high time resolution. While there have been previous high-frequency stress-strain x-ray diffraction experiments, these did not examine the behavior of the muscle under physiological conditions mimicking its *in vivo* conditions. Using *M. sexta* invertebrate flight muscle operating under dynamic conditions, we examine four hypotheses that have been established using x-ray diffraction in quasi-static and vertebrate skeletal muscles. This is important because these assumptions are sometimes extended to invertebrate muscles under dynamic conditions. We show that we can obtain features from highly time-resolved x-ray diffraction data which can be used to predict macroscopic force through a machine learning model. We also found several structural changes during dynamic oscillations which were inconsistent with expectations established from quasi-static and vertebrate skeletal muscles and offer several hypotheses, including that the relatively slow *M. sexta* flight muscle may share properties which have been previously thought to be found in high frequency flight muscle.

CHAPTER 1
MUSCLE VERSATILITY AND STRUCTURE

1.1 Motivation

Muscle has the remarkable ability to fill many roles in organisms, being able to operate as different elements such as motors, brakes, or springs [1]. It is even possible for different parts of a single muscle to behave as more than one such element [2, 3]. This is what is meant by "Energetic Versatility of Muscle" - the ability of muscle to perform many different mechanical functions. Muscle is an active material, and is able to generate internal tension. A muscle's mechanical function is characterized by its work loop, a stress-strain curve in which a muscle is phasically activated. The net work (or mass-specific work) produced, and therefore mechanical function, is taken as the area of the force-length (or stress-strain) curve [4]. For example, the pectoral muscles of birds must act as a motor, producing net positive work in order to generate lift [5]. Other muscles act like brakes, dissipating energy, such as the quadriceps during the landing portion of a jump, or a control muscle in the leg of a cockroach [6]. Muscles may also be spring-like or strut-like, generating zero net work [7].

Often work loops are performed under conditions which mimic the *in vivo* conditions as closely as possible in order to characterize the *in vivo* behavior of the muscle [8, 9, 10]. Strain amplitude and frequency, as well as timing (or phase) of activation of a particular muscle can be measured in an intact animal [11, 12, 13]. In vertebrates the length and force of the tendon must also be measured since its stiffness is comparable to that of the muscle, typically through tendon buckles [14], force transducers which measure the force in the tendon. The length of the muscle in those cases is measured via piezoelectric sonomicrometry crystals [15]. In invertebrates, because of their exoskeleton, high speed videography

makes length measurements easier because they can be directly inferred from the strain of the exoskeleton or the join kinematics. After these measurements have been made, the muscle can then be excised and the same strain trajectory and activation patterns can be play into the muscle with a precise motor. We can then collect simultaneous measurement of the force generated by the muscle [4]. While much is known about how force is generated in muscle, it can still be difficult to explain or predict muscle mechanical function, that is the amount of mechanical work a muscle does under different conditions [16, 17, 9, 18]. This central goal of this thesis is understanding how the nanometer scale structure of muscle relates to whole muscle mechanical function and contributes to it versatile function.

As with many biological systems, the structure of muscle is hierarchical at multiple length scales [19]. What makes muscle so exceptional is that it is also active matter, able to generate internal stress and strain, to enable animal locomotion. A whole muscle is made up of individual muscle cells whose orientation can influence muscle force and function [20]. Muscle cells (10s of mm) are made of bundles called myofibrils, which are divided longitudinally into sarcomeres (1-10 m). In sarcomeres, force is generated at the nanometer scale by the collective action of myosin motors, arranged on thick filaments, which bind to binding sites on actin, located on the thin filaments [18]. A bound myosin head is termed a "crossbridge" because it spans the radial distance between think and thin filaments. There are also myriad regulatory and structural filaments such as titin and its analogs [21, 22], nebulin [23], and dystrophin [24], all of which contribute to muscle function. The force that can be generated by each sarcomere depends strongly on its strain and velocity [25]. Strain changes can be imposed by macroscopic forces on the muscle during locomotion as well as internal forces generated by crossbridge binding. This means that coupling between factors at the nanometer, micrometer and centimeter (whole muscle) scale makes a multiscale understanding of muscle behavior difficult [26].

However, despite muscle's structure being so complicated, the fact that it is also highly ordered means that x-ray crystallographic techniques can be used to study its structure,

even when the tissue is *in vivo*. This is what makes muscle such an interesting material to study - it is soft, crystalline, active matter. The thin and thick filaments that comprise sarcomeres are arranged in a well ordered hexagonal lattice [27]. The myosin motors on the thick filaments and actin binding sites on the thin filaments are spaced at regular intervals. Because of how well ordered these structures are, the radial spacing between the thin and thick filaments, as well as the axial strain in the filaments and position of the myosin heads can all be measured with x-ray diffraction [28, 29]. With a high intensity synchrotron source, such as the BioCAT Beamline 18ID at the Advanced Photon Source, Argonne National Laboratory, in concert with modern high sensitivity, high speed, X-ray detectors, the nanometer scale structure of this soft active crystal can be studied with millisecond time resolution under conditions which mimic its *in vivo* behavior. We can now acquire X-ray diffraction images simultaneously with the whole isolated muscle work loops, or even from muscle inside a tethered, intact animal activating its muscles [10, 30, 2, 31, 32].

The combination of high speed x-ray diffraction recordings with simultaneous work loop experiments is a powerful tool that lets us ask how the structure of muscle can influence mechanical function. While much is known about how muscle's functional versatility arises, it is still not possible to definitively predict muscle function based on the its quasistatic physiological properties or it structural features alone. Recently the nanometer scale structure has been implicated in partially determining the isometric force a muscle can produce [33, 34, 35]. Several structural features have also be linked to the specialized function of specific muscles [10, 2, 30]. In my thesis, I take the opportunity afforded by multiscale experiments and new advances in complementary spatially explicit modeling of muscle to show how the nanometer scale structure of muscle can influence whole muscle mechanical function. In this chapter I first provide some background on the standard physiological measurements of muscle function, their limitations, and the analysis of x-ray images. I then provide an overview of the three core results of my dissertation work.

1.2 Background

1.2.1 Sliding Filament Theory and Crossbridge Dynamics

The sliding filament theory states that muscle contraction is accomplished by the sliding of two protein filaments past each other. Using electron and interference microscopy, these groups observed light and dark bands in muscle, and were able to identify that these bands came from two kinds of filaments, one which polarized light and one which did not [36]. It was noticed that during contraction one band remained at constant length while the other band makes up the change in length. This evidence implied that the two protein filaments, the myosin-containing thick filaments and the actin-containing thin filaments, contract by sliding past each other [36, 37]. In parallel, another group reasoned that characteristic four phase force-length curve of active muscle could arise from a population of active molecules that were arrayed on overlapping filaments and produced different amounts of overlap as the filaments slide past one another (Figure 1.1).

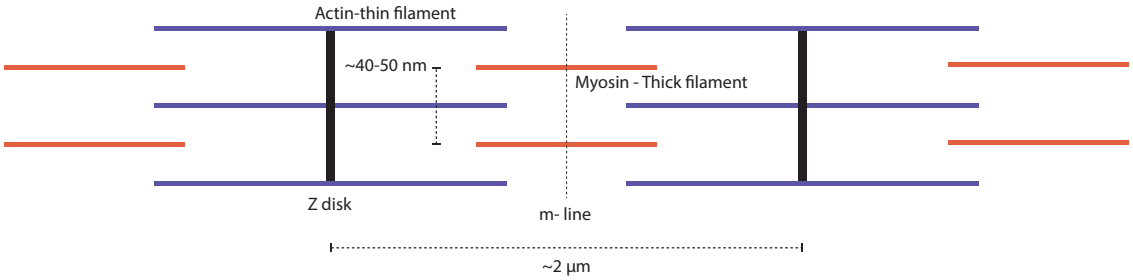

Figure 1.1: Representation of a sarcomere, indicating the actin-containing thin filaments (blue) and myosin-containing thick filaments (red). The z-disks define the longitudinal boundaries of a sarcomere.

The axial force generated in muscle comes from interaction between the two filaments, when myosin heads on the thick filament form crossbridges by binding to the thin filament. The initial basis for our understanding of the nature of crossbridge dynamics comes from work done in 1971 [38]. In order to study the kinetics of the myosin-actin power stroke, experiments were performed in which the maximally activated muscle undergoes a step

change in length while force recovery is measured. The recovery of force over time can be modeled as several exponential processes with time constants related to the elementary rate kinetic steps of the crossbridge cycle [38, 39].

In passive muscle, binding of myosin heads to actin is prevented by tropomyosin, a protein which covers the myosin binding site on actin. When muscle is activated by electrical stimulation by neurons, calcium is released from the sarcoplasmic reticulum inside the cell [40]. When calcium binds to troponin, it causes a conformational change which removes the tropomyosin from the binding site, which allows for myosin-actin binding [41].

The power cycle of a crossbridge involves transitions between multiple states (Fig. 1.2) [38]. The crossbridge cycle begins with ADP and an inorganic phosphate attached to the myosin head, which leads to attachment with the binding site on actin and the release of the phosphate. When ADP is released, a conformational change occurs in the myosin head which leads to the power stroke of muscle. When ATP binds to the myosin head, the bond between actin and myosin breaks, and ATP is converted into ADP and P so that the cycle can repeat [42]. We will use this understanding of the cycling of a crossbridge when we develop models (Chapter 3) to understand of muscle force generation and energetic versatility.

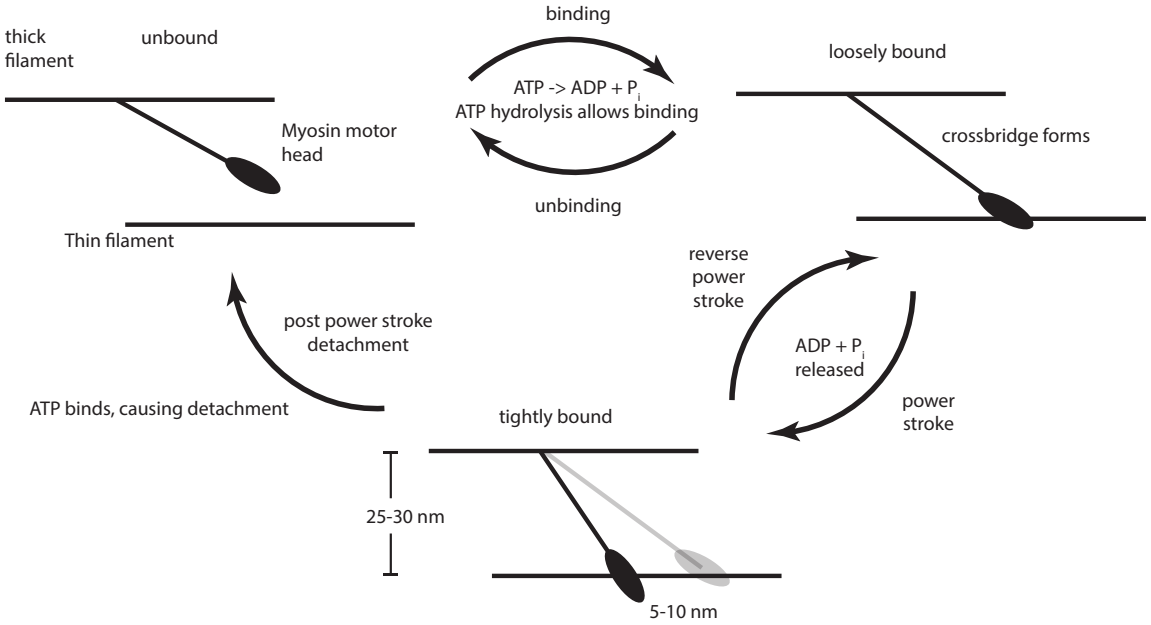

Figure 1.2: The force in muscle is generated by state changes in the myosin motors on the thick filament, which bind to the thin filament then undergo a power stroke. After undergoing a power stroke, the myosin motor detaches, ready to bind again.

1.2.2 The Work Loop Technique

Many of the early studies of muscle were done under isometric maximally activated conditions. These experiments were aimed at establishing the sliding filament model and uncovering the rate equations for the force generation mechanism of muscle [38]. However, the information they provide does not directly tell us about muscle's energetic versatility or its function at the macroscopic scale under physiological conditions [16, 10].

More recently muscle function has been defined in the context of "work loops," which are phasically activated force length curves that capture periodic contractions of muscle [4, 10, 43]. In a work loop experiment, a muscle is typically mounted between a length controller and force transducer or on an ergometer that does both. The allows the strain amplitude, frequency, and duty cycle (time shortening vs lengthening) to be prescribed. Stimulating wires are inserted into the muscle, and voltage can be applied across the muscle, which activates the muscle. The time course of force is simultaneously measured.

When length and force are plotted against each other, the net work is then the area of the curve, or mass specific work if stress and strain are plotted.

Initially, the focus of these experiments was to find the peak power output of muscle [4], rather than *in vivo* function. However, it later became apparent that muscles operate under a wide variety of conditions, and that peak power may only be expressed in certain muscles or certain behaviors (Fig. 1.3) [10]. This recognition has led to an increasing effort to understand how muscles behave under conditions mimicking their *in vivo* patterns of strain and activation, which has led to uncovering control principles of locomotion [44, 45].

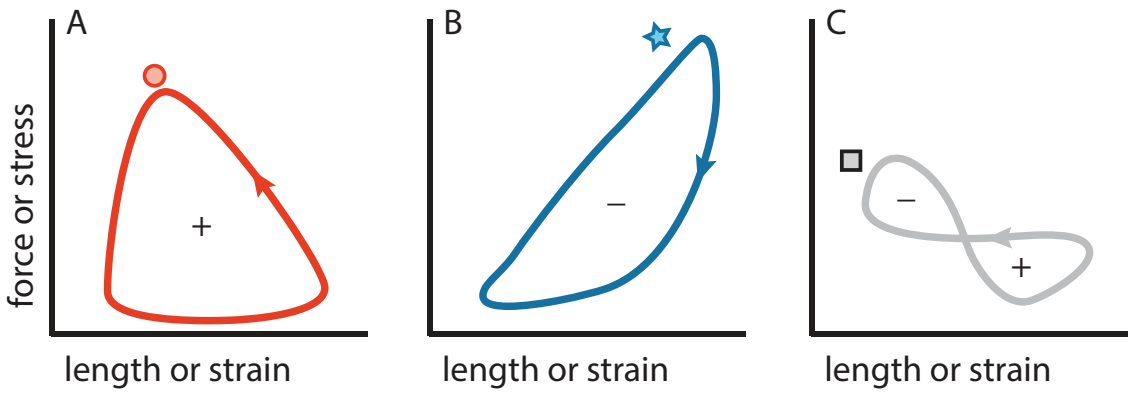

Figure 1.3: Example work loops showing net positive work (A – motor), and net negative work (B – brake), approximately zero (C – nonlinear spring).

1.2.3 Determinants of Work Loops and Muscle Functions

There are many ways that the dynamics of active muscle might be tuned by an organism in order to produce a particular work loop. These include temperature regulation, phase of activation, force-length or force-velocity relationships, coupling to series elastic elements (e.g. tendons), differences in moment arms, and changes in strain patterns [1, 3, 43]. However, even in systems where these parameters are similar, certain pairs of muscles with similar inputs known to affect work loops can still yield different work loops and hence different functions [16].

First, we describe some of the primary quasistatic determinants of muscle function.

The material properties of muscle discussed below are all known factors that can shape a muscle's work loop.

Force-Length Relationship of Muscle

The force-length (or length-tension) curve of a sarcomere increases as sarcomere length increases up to a maximal force plateau, then decreases with further length increase (Fig. 1.4). The force-length curve is taken under isometric, maximally activated conditions over lengths outside the physiological operating range. A muscle under physiological conditions will only operate over a portion of the force length curve. Force, and therefore work, will depend on what section of the curve the muscle operates on. Both the location of the sarcomere rest length and strain amplitude will affect work output [1].

The force-length relationship in muscle has traditionally been explained by the amount of overlap between the two filaments. As a sarcomere contracts, force increases as overlap increases up to a plateau where a maximum overlap of actin and myosin occurs. Active force will decrease for shortening past the optimal length, and is thought to occur because of interference between actin filaments and eventually with compression of the filaments as they interfere with the z-disks [4, 25]. However, it is now known that the force relationship is in part explainable by changes in the thick-thin filament spacing, which changes as sarcomere length changes [33, 34]. This is because the cross bridge binding rate and force depends in part on the radial spacing between the filaments. In addition to the active force generated, muscle produces a nonlinear passive stiffness at large tension.

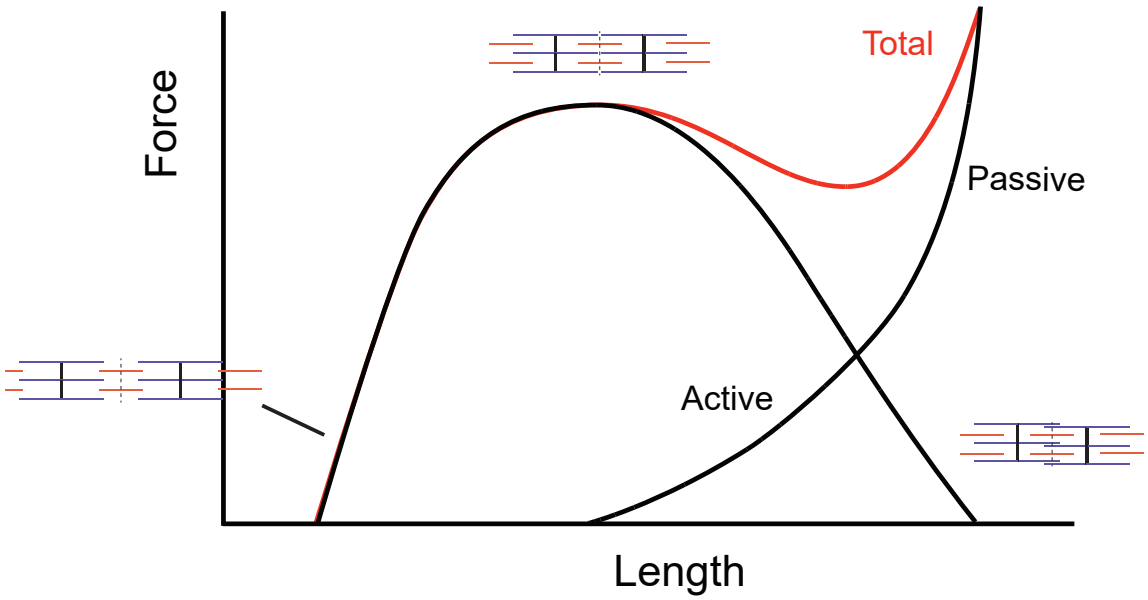

Figure 1.4: Typical force length relationship for an intact muscle. The active contribution comes from the variable overlap of crossbridges and the radial expansion of the filament lattice. The passive component arise from the nonlinear material stiffness a muscle demonstrates under tension (but not compression). By convention positive force is the direction of shortening.

Force-Velocity Relationship of Muscle

For concentric contractions, or active shortening defined as positive velocity, force decreases as velocity increases (Fig. 1.5). This is explained by the crossbridge model and sliding filament theory: since a crossbridge requires a characteristic time to form, for higher shortening velocities fewer crossbridges undergo a full, force producing power stroke [46]. For eccentric contractions, or where muscle force resists lengthening, force is larger than isometric force, and plateaus after low velocities. This is the basis of negative mechanical work, giving muscle a brake-like function [13, 16].

Force-velocity experiments are performed under quasi-static conditions, at constant activation and constant load (isotonic). Like the force-length curve, this relationship is composed of multiple separate measurements taken at a fixed load, then the muscle is allowed to totally relax, and the next data point, at a different load, is taken. Neither measure therefore

capture the dynamic time-varying influences that shape muscle function under periodic and unsteady conditions.

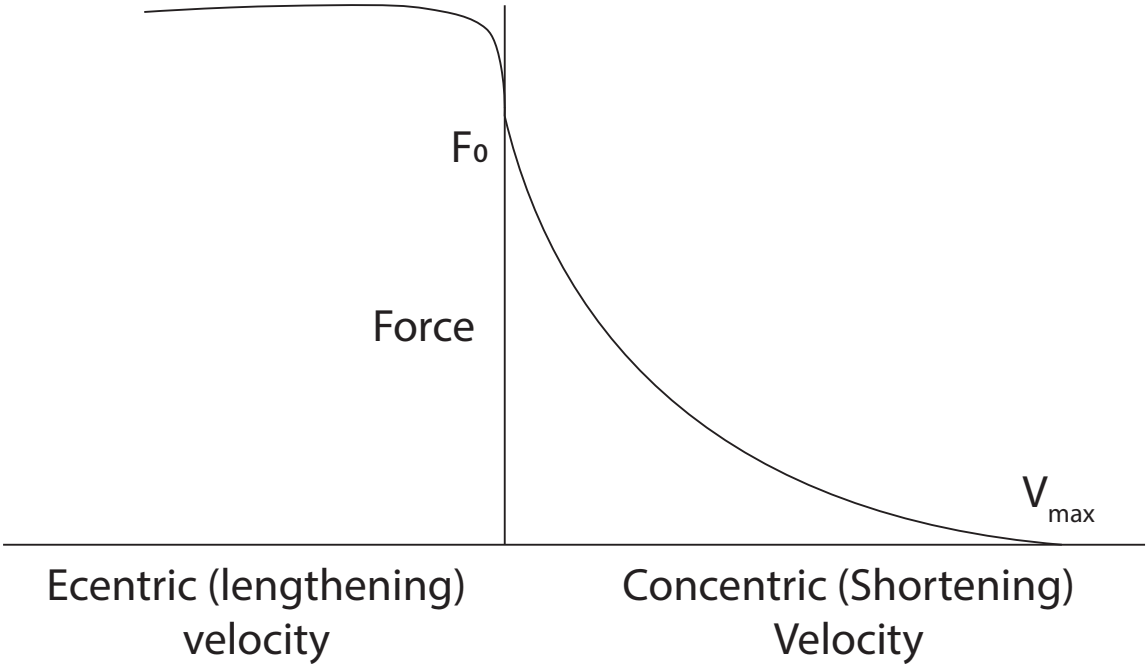

Figure 1.5: Force vs. velocity curve for muscle. F_0 is the peak isometric force, and V_{max} is the maximum unloaded velocity of contraction. Eccentric contractions, or contractions during lengthening are the basis of negative work in muscle. Concentric contractions, or contractions during shortening, decrease with increasing velocity, since transitions between states in the crossbridge cycle take a characteristic time, increasing shortening velocity will not allow significant crossbridge formation [47].

Force Response Depends on Pattern of Activation

When a muscle fiber (a single cell) is activated by a single motor neuron action potential, force rises and falls in a twitch response (Fig. 1.6). By increasing the frequency of action potentials so that the force response of two twitches overlap, force output can be modulated. At sufficiently high frequencies of activation muscle force will begin to fuse and will plateau into a steady force production state called tetanus [41]. This characterization is done under isometric conditions. The frequency of activation will therefore affect work loops by affecting peak force. Phase of activation is also important since the work output

will depend strongly on whether the muscle is active during the shortening or lengthening phase of the length cycle: active shortening will lead to net positive work (motor), while active lengthening will lead to net negative work (brake) [4]. In vertebrates, muscles are made up of multiple motor units, and each motor unit can be individually activated, allowing a gradation of force via more or fewer motor units, or a different times. In invertebrates, by contrast, muscles contain only one or very few motor units, which can make them easier to examine [48].

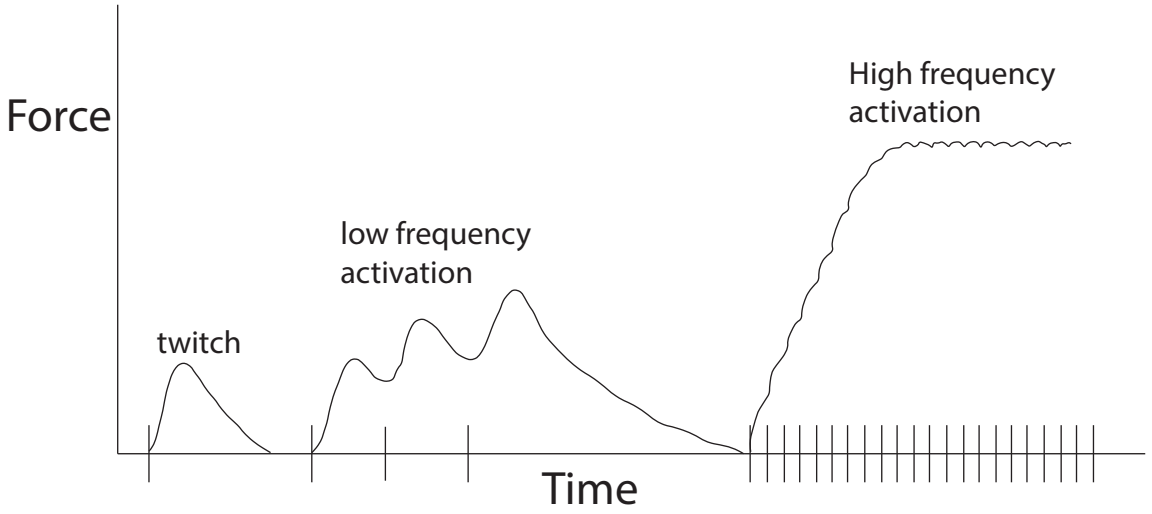

Figure 1.6: A twitch is when a muscle is activated with a single action potential. The force of a muscle can be increased by increasing the frequency of activation. Tetanus occurs when a muscle is maximally activated with high frequency stimulation.

Moving beyond quasi-static determinants of Work Loops

While the force-length curve, force-velocity response, twitch and tetanus are often used as the constituent physiological properties that are significant factor in determining muscle work loop output, they are not the only variables which can affect muscle function. Importantly, these measurements are all quasi-static, and do not capture the full behavior of muscle under dynamic conditions. For example, the patterns of strain and activation in these types of experiments are far from the *in vivo* patterns, since they are constant activation, length, and velocity. In *in vivo* muscle on the other hand, the level of activation is

changing, sometimes over each stride as an animal moves. A muscle's work also can depend on how the animal interacts with its environment, though mechanical feedback [49]. Variable loads, contacts, and other imposed forces can apply external strains on muscles. Also, muscle has complicated history dependent properties that are not easy to capture with quasi-static measurements, and may be emergent from multiscale interactions [26, 50].

Structural differences in muscle can alter its behavior at macroscopic scales. It has recently become known how the lattice spacing in a muscle contributes to the static force-length curve [34]. However, it is still unclear how it affects and is affected by dynamic muscle behavior. Since myosin and actin form a hexagonally repeating array, it can be considered as an active crystal, which means techniques such as x-ray diffraction can be used to measure the lattice spacing of muscle during dynamic behavior, such as a work loop [51].

Micro- and nanoscale features of muscle's structure and how they couple to macroscopic strain could contribute to force production under dynamic conditions and thus to mechanical work and function. Because of the recent improvements in sensitivity and time resolution in the BioCAT Beamline 18ID at the Advanced Photon Source, we have the opportunity to connect mechanical characterization of muscle performance via work loops with simultaneous structural information at the nanometer and millisecond scales. The broad goal of this dissertation is to connect the structural features of muscle's myofilament lattice, especially lattice spacing, to the energetic versatility of muscle for locomotion.

Small angle X-Ray (SAX) fiber diffraction

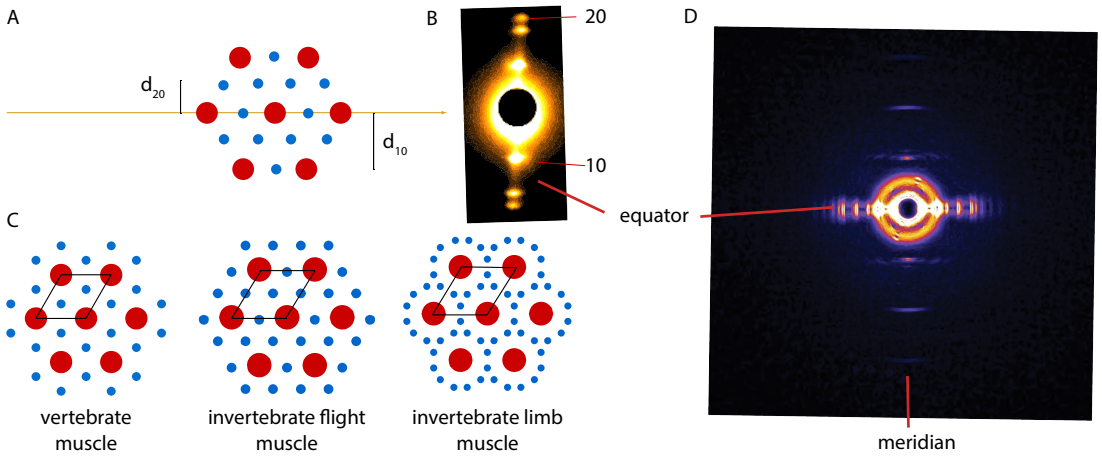

Figure 1.7: A: Cross section of a sarcomere. Red represents the myosin containing thick filaments, blue represents the actin containing thin filaments. The d_{10} spacing is proportional to the distance between the thin and thick filaments. B: example x-ray diffraction image from *Blaberus discoidalis* [31]. C: While vertebrates and invertebrates have the same hexagonal arrangement of thick filaments, the number and geometry of the thin filaments are different. D: A zoomed out image of an example x-ray diffraction image, showing the equatorial peaks, which indicate radial repeats, and the meridian, indicating axial repeats.

Because of the highly ordered crystal lattice of muscle, we can use x-ray diffraction to measure the spacing between thick and thin filaments (Fig 1.7). Equatorial reflections in a muscle's x-ray diffraction image are related by Bragg's Law to the spacing of actin-containing thin and myosin-containing thick filaments. Since muscle will contract under a constant volume constraint (at least approximately), absent other forces the filament spacing will change according to the equation $\frac{2*d_{10}^2}{\sqrt{3}} * L = volume = constant$ where L is the sarcomere length and d_{10} is related to the myosin lattice spacing [51]. However, cross-bridge binding also generates a radial force which can influence the lattice spacing [35] and the probability of myosin heads attaching to actin binding sites is dependent on the distance between filaments and the stiffness of the crossbridges themselves [33]. The relationship between axial strain and binding is complex. The equatorial (1,0), (1,1), and (2,0) peaks are labeled by their crystallographic Miller indices, and define planes of diffraction. The

(1,0) spacing therefore gives the spacing between (1,0) planes, and the (1,0) intensity is related to amount of mass oriented along the (1,0) planes [28].

The equatorial intensity distribution can also be used to obtain information about the structure and dynamics of the myosin heads and the thick and thin filaments, although such information is aggregated over a large number individual filaments. For example: the brightest peak is the 1,0, with the next brightest peaks (1,1 and 2,0) indicating the packing pattern of actin relative to myosin [51]. In the dyad arrangement, in which one actin filament is between each pair of myosin, the 2,0 peak will be brighter than the 1,0 peak along the equatorial axis. This pattern is typically associated with insect flight muscle. The triad arrangement, with one actin filament located between three myosin filaments will have the 1,1 peak brighter than the 2,0 peak. This pattern is typically associated with vertebrate muscle [27].

The ratio of intensity between the 1,0 peak and either the 1,1 or 2,0 peak, depending on the packing pattern, can be used to obtain the relative degree of association of myosin heads with the thin filaments. This is because if myosin heads move toward mysoin binding sites on actin, more mass will be associated with the actin filaments. Since the diffraction intensity is related to the electron density distribution, either the 1,1 or 2,0 peak will increase in intensity as crossbridge binding increases [51].

The meridional peaks are orthogonal to the equatorial peaks and contain information about the axial repeats in the filaments. Repeating structures in the helical thick and thin filaments diffract along this axis. Also the actin binding sites and myosin heads themselves are spaced at regular intervals, which deform when crossbridges are bound.

The most important advance for us is the recently improved time resolution of the Bio-Cat x-ray beamline 18ID at the Advanced Photon Source, Argonne National Laboratory with new detector technology (Fig. 1.8). Since we not only wish to measure the lattice spacing of muscle, but connect it to energetic versatility, we need to be able to measure the changing lattice structure under physiological conditions.

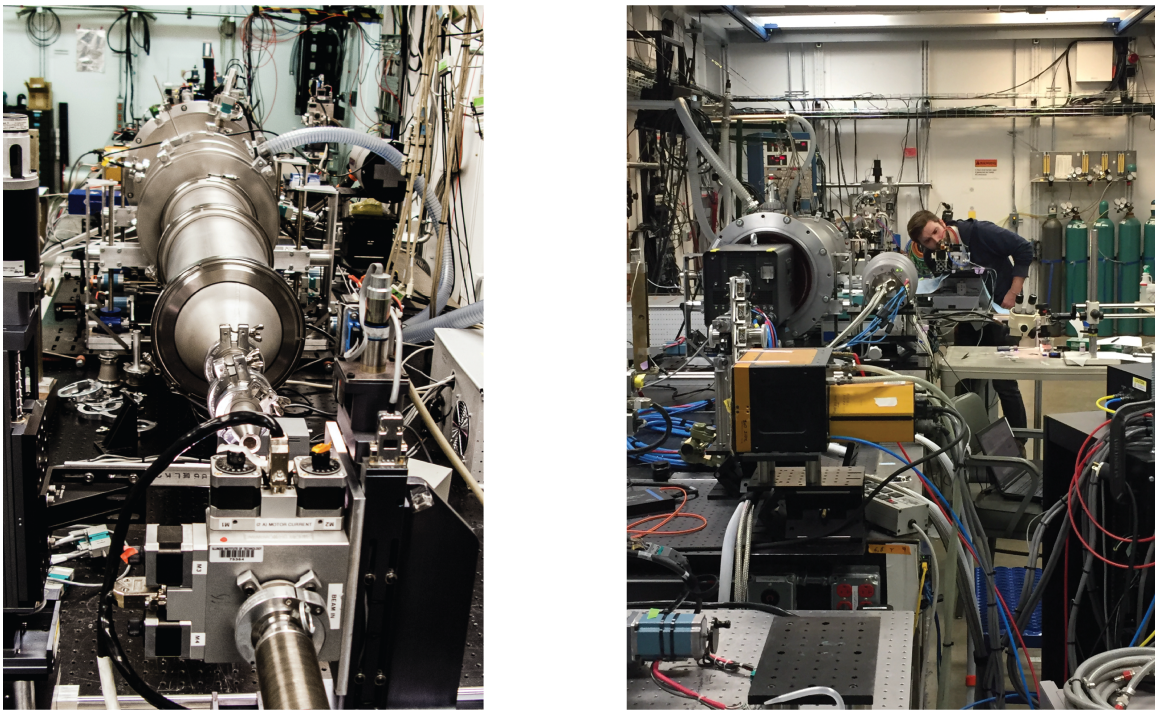

Figure 1.8: Images taken from the BioCAT eamline 18ID at the Advanced Photon Source, Argonne National Laboratory small angle x-ray scattering beam line at the Advanced Photon Source (APS), Argonne National Lab.

1.3 Overview

Using time resolved small angle fiber diffraction and a spatially explicit model, the next three chapters will address how myofilament structural differences, especially lattice spacing, can contribute to functional diversity that muscle shows at the whole tissue level.

In chapter 2, we introduce a system of two muscles in the cockroach *Blaberus discoidalis* in which both muscles' quasi-static and history dependent properties are very similar, yet their work output is different, as first described in [16]. We hypothesize that we could explain the difference in work between these two muscles in *B. discoidalis* by a difference in their radial spacing between thin and thick filaments. The radial spacing could be very important for force production since not only is the binding rate of myosin and actin dependent on the radial spacing, the radial force of a crossbridge is enough to change the radial spacing [35, 52]. This is because not only does the structure of the filament lattice

of muscle affect the force development, but the force generated by muscle will change the filament lattice of muscle, forming a coupled system [33, 34]. We find that the two muscles' actin-myosin spacing differed in passive conditions by one nm, and that on activation one of the muscle's spacing increased, reaching the same spacing as the other muscle. We connect this result to their similar quasi-static whole muscle properties, then show that the lattice spacing during work loops correlates to force output in both muscles.

While the results of chapter 2 implicate lattice spacing structural changes at level of a single nanometer could be a determinant of muscle function, because of muscle's complicated hierarchical structure, involving multiple length scales and numerous structures besides the lattice spacing, we were not able to show definitively there was a causal relationship. Therefore, in chapter 3, we adapt the model described in [33, 34] to show that net work production can depend on lattice spacing. We chose this model as a basis in which to explore this question because it is a spatially explicit model in which individual filaments and crossbridges are described as spring elements in a lattice. This lets us independently change lattice structure in order to see how net work changes. We find that net work increases as the radial (thick-thin) spacing increases up to a certain value, at which it plateaus and slowly decreases. We then incorporate *in vivo*–like lattice spacing changes in the work loop by forcing the lattice to change in an isovolumetric fashion with sarcomere length, and show work can depend on the trajectory of lattice spacing changes, not just the mean spacing.

Finally, in the chapter 4 we try to bridge quasi-static measurements of muscle structure with dynamic work loop experiments. Quasi-static experiments combined with x-ray diffraction are useful for investigating the origins of specific mechanisms in muscles. However, it is not always clear how results from these experiments relate to dynamic work loops. For example, hypotheses about how muscle nanometer scale structure relates to macroscopic force are proposed and verified based on isometric experiments in model vertebrates [53, 54, 55]. However, interpretations are then made in sometimes very different

systems under very different conditions, such as intact flying invertebrates [30, 32], or invertebrates during dynamic work loops [56, 2]. We wanted to see if we could bridge the gap between these types of experiments by investigating four hypotheses in dynamic work loops. To do this we chose to look at *Manduca sexta*, the tobacco hawk moth. We chose this animal because its net work has been characterized under many conditions [11, 12, 44], has exceptionally well ordered muscle filaments affording excellent fiber diffraction images and has served as a model organism to investigate how lattice structure relates to force [2, 32]. We show that the 7.2 meridional myosin reflection in diffraction experiments, which in vertebrates is assumed to be indicative of force, has a hysteretic relationship with force in *Manduca sexta*. We also show how a neural network machine learning model can predict phase of activation and force based on equatorial x-ray data establishing that the time course of structural changes can predict macroscopic force.

CHAPTER 2

NANOMETER-SCALE STRUCTURE DIFFERENCES IN THE MYOFILAMENT LATTICE SPACING OF TWO COCKROACH LEG MUSCLES CORRESPOND TO THEIR DIFFERENT FUNCTIONS

2.1 Introduction

Many biological structures, especially tissues have hierarchical, multiscale organization [19]. Of these, muscle is exceptional because it is also active: capable of producing internal stress based on the collective action of billions of myosin motors [57]. At the macroscopic scale, muscle can perform many roles in organisms, acting like a motor, brake, or spring depending on the task required [4, 10]. It is even possible for different parts of a single muscle to behave with different mechanical functions, defined by their mechanical work and force production [7, 2]. This functional versatility enables muscle's diverse roles in animal locomotion and behavior. Muscle's mechanical functional can be difficult to predict, especially under perturbed conditions, because of muscle's hierarchical structure across multiple length scales [58, 16, 59].

Muscle's mechanical function during locomotion is typically characterized through a work loop: a stress-strain (or force-length) curve in which the length (or strain) of the muscle is prescribed through a trajectory and electrically activated at specific phases during the cycle of shortening and lengthening [4, 43]. The area inside the loop gives the net work done by the muscle and can be positive, negative, or zero. Work loops that produce zero net work can still have different behavior being spring-like, isometric and strut-like [60],

This chapter is published in a co-authored manuscript with Dr. Weikang Ma (IIT/Argonne NL) and Prof. Thomas Irving (IIT/Argonne NL). Travis Tune is the lead author and researcher.

or biphasic with a period of negative and positive work. Work loop parameters typically mimic either *in vivo* or power maximizing conditions.

Many other physiological characterizations of muscle are steady state in some respect. Twitch responses are isometric. The length-tension curve is obtained under constant, usually tetanic activation. Even the force-velocity curve is taken as the force at constant activation during constant velocity shortening for a given load. These macroscopic properties arise from and, in fact, helped establish the crossbridge basis for muscle contraction and sliding filament theory [25, 38]. Although these steady state macroscopic measurements are important determinants of muscle work loops, they are not sufficient to account for the variability of muscle work output and hence mechanical function under dynamic conditions [1]. The multiscale nature of muscle suggests that subtle differences in structure of the contractile apparatus at the micro to nanometer scale could also be playing an underappreciated role in determining differences in work output and hence macroscopic mechanical function [33, 34, 28]. Here we determine if there are structural differences in muscles with functional differences that cannot be explained by classical steady state measurements

The structural arrangement of actin-containing thin filaments and myosin-containing thick filaments in a sarcomere forms a regular lattice with spacings on the scale of 10's of nanometers [27]. This myofilament lattice inside each sarcomere is a crystal in cross section even under physiological conditions. As a result, its structure can be studied by x-ray diffraction even during force production and length changes [51, 30]. Here we use "lattice spacing" to refer to the distances between the repeating planes of actin and myosin filaments in this lattice. Lattice spacing depends in part on the axial length of the muscle, stemming from the strain placed on the muscle fibers during contraction. However, the filament lattice spacing in muscle also depends on the presence of radial forces, stemming from structural proteins such as titin, as well as crossbridge attachment which can generate radial forces [61, 35] that are of the same order as crossbridge axial forces [34].

Differences in lattice structure even at the nanometer scale can have profound effects

of force development in muscle. Lattice spacing influences myosin binding probability and hence axial and radial force production [62, 33, 63, 64]. Changing only lattice spacing can enhance Ca^{2+} sensitivity (the shape of force-pCa curves) [65] and change crossbridge kinetics [66]. A change in lattice spacing of just several nanometers even accounts for up to 50% of the force change in a typical muscle's force-length curve [34]. Temperature differences in insect flight muscle have been shown to change crossbridge binding, lattice spacing, and work output [2]. What is still unknown is whether or not myofilament lattice structure (its packing arrangement and spacing) might correspond to macroscopic work in the absence of other differences in physiology, and hence if differences in lattice structure might be important in the functional role of muscle during locomotion.

To explore the potential significance of structural differences, we looked for two very similar muscles that have unexplained differences in their work production. Two of the femoral extensors of the cockroach, *Blaberus discoidalis*, are ideal in this respect (Figure 2.1a). These two muscles have the same tetanic force-length curves, twitch response, force-velocity curve, phase of activation, force enhancement due to passive pre-stretch, and force depression due to active shortening [6, 16]. They are even innervated by the same single, fast-type motor neuron [67, 68] and share the same synaptic transmission properties [69] meaning that both muscles are activated as a single motor unit in all conditions. These muscles share the same anatomical and steady state physiological properties typically used to characterize muscle performance. However, when the two muscles undergo dynamic patterns of strain and activation which match those that they experience during *in vivo* running, one muscle acts like a brake with a dissipative work loop, while the other is more like a motor with a net positive, biphasic work loop (Figure 2.1b). It is difficult to reconcile the similarities between these muscle under steady state, and their difference in actual muscle function. [16] did observe differences in these muscles' submaximal force-length curves bur only at short lengths and conclude that these differences alone could not account for the differences in function. Moreover the origin of these submaximal differences was un-

known, although they did suggest that structural differences in the myofilament lattice may account for the differences under dynamic conditions.

Critically, any structural feature that would be consistent with the differences in work output would not only have to correspond to the dynamic differences between the two muscles, but also their stead-state similarities. We tested two possible, and not mutually exclusive, hypotheses. First, we hypothesized that the myofilament lattice in the two muscles might have a different packing structure. Actin and myosin vary in their ratio and packing pattern across muscles [27, 70], which can be inferred from how the muscle diffracts x-rays [51]. Different packing structures could produce different dynamics of force development, since changing the packing pattern will change the spacing between myosin and actin filaments [27], which changes their binding probability [33]. Second, we hypothesized that the myofilament lattice spacing might change, but only under dynamic (i.e. work work loop conditions that mimic *in vivo* running) while remaining the same during steady-state activation. Because of constraints involving simultaneous work loop and x-ray imaging, we cannot exactly replicate the conditions of previous *in situ* work loop studies and must rely on isolated muscle preparations. Nonetheless we can examine myofilament lattice spacing both during twitches and then during work loop conditions matching those in [16] as closely as possible. The overall goal of these hypotheses is to test whether these muscles have structural differences in their actin-myosin lattice which might be large enough to effect force macroscopic force production and mechanical function. If so, we predict that structural differences must manifest under dyanmic conditions, but not under steady-state conditions.

2.2 Methods and Materials

2.2.1 Animals

Blaberus discoidalis were maintained in a colony at Georgia Tech under a 12:12 light dark cycle and provided food *ad libitum*. Muscles 178 and 179 are located on the mediodorsal

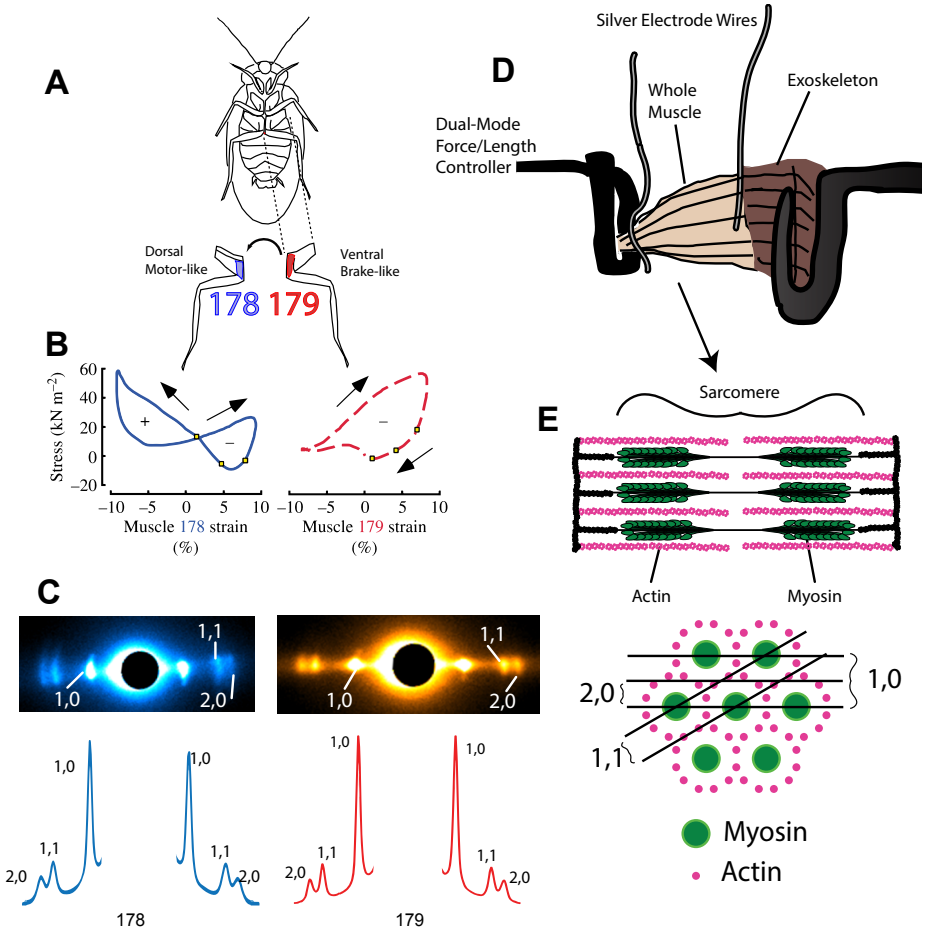

Figure 2.1: A) Ventral View of *Blaberus discoidalis* showing the hind-limb femoral extensors 178 and 179 (notation from [71]). B) *In situ* work loops performed on muscles 178 and 179 show a difference in function despite near identical steady state behavior (work loop figures reproduced from [16]). C) X-ray diffraction patterns from muscles 178 and 179 with the most prominent peaks labeled. Also shown, is the intensity profile along the equatorial axis. D) A diagram shows the experimental set-up. The X-ray beam path is perpendicular to the contraction axis. E) Multiscale hierarchy of muscle structure, showing a single sarcomere (1-10 μm) of a muscle (1-10 mm) and the sarcomere cross-section, with diffraction planes (10's of nm) corresponding to the peaks indicated in C. Spacing between diffraction planes in E is related by Bragg's Law to the spacing between peaks in C, while the intensity of peaks shown in C are related to the mass lying along depicted planes in E.

and medioventral sides of the coxa respectively [16]. After removing the whole hind-limb, the leg was pinned such that the femur formed a 90° angle with the axis of contraction for 178 and 179 with either dorsal or ventral side facing up, which defined the muscles rest length (RL). After removing enough exoskeleton to view the muscle of interest, its rest length was measured from a characteristic colored spot on the apodeme to the anterior side of the coxa where the muscle originates [6]. We also measured the width of the muscle at mid-length. Once dissected from the coxa, the muscle was mounted between a dual-mode muscle lever (model 305C, Aurora Scientific, Aurora, Canada) and a rigid hook, and length was set to 104.4% RL for muscle 178 and 105% for muscle 179. This is because during *in vivo* running the mean length of the muscle is not the rest length. We define this as the operating length (OL) of the muscle, or the mean length during *in vivo* running [16, 13]. All strain measurements later in the text are relative to this operating length. Silver wire electrode leads were placed at opposite ends of the muscle for extra-cellular activation as in [49].

2.2.2 Time Resolved x-ray Diffraction

Small angle X-ray fiber diffraction was done using the Biophysics Collaborative Access team (BioCat) Beamline 18ID at the Advanced Photon Source (APS), Argonne National Laboratory. The beam dimensions at the focus were 60 x 150 μm, vertically and horizontally respectively with a wavelength of .103 nm (12 keV). Initial beam intensity is 10^{13} photons/s, which we attenuated with 12 sheets of 20 μm thick aluminum, about a 65% reduction. For all cases, diffraction images were recorded on a Pilatus 3 1M pixel array detector (Dectris Inc) with an exposure time of 4 ms with a 4 ms period between images during which a fast shutter was closed to reduce radiation damage.

2.2.3 Experimental Protocol

After being extracted and mounted, muscles were placed in the beam-line and set to the *in vivo* operating length we measured pre-dissection. We then stimulated with a twitch stimulation pattern consisting of 3 spikes separated by 10 ms. The three spike pattern we chose was based on previous work [16, 13] which showed this was the *in vivo* activation pattern during running. Time resolved x-ray images were taken starting from $t = -25$ ms, from which we obtained passive isometric measurements, and ending at $t = 175$ ms, with $t = 0$ defining the moment of stimulation. We performed these isometric twitch experiments at mean strain offsets of -10, -5, 0, +5, +10% OL each for both muscles. We estimated cross-sectional area from the diameter of the muscle assuming a cylindrical shape, and used this to calculate stress. The x-ray frame closest to peak stress was used for the active quasistatic measurements. Since these muscles rarely experience tetanic activation *in vivo*, and because repeated tetanic stimulation combined with heat and radiation damage from repeated x-ray imaging would have reduced the viability of each sample, we chose not to examine lattice spacing changes under tetanic stimulation.

Next, we tested the muscles' responses under several different work loop conditions. First, strain amplitude (peak to peak) was 18.5% of OL for muscle 178 and 16.4% of OL for muscle 179. Strain amplitude was different for the two muscles because the muscles are slightly different lengths but must have identical absolute length change during *in vivo* running. The driving frequency was 8 Hz, with activation consisting of 3 spikes at 6 volts at 100 Hz, at a phase of activation of 8%, with 0 defined as the start of shortening. These are the *in vivo* conditions of these muscles during running [6, 16], except with the muscle isolated and extracellularly stimulated. We then changed the oscillation frequency to 11 Hz while keeping the same phase of activation, which matched the conditions from [49] including the same method of stimulation. We then performed work loops under the same phase of activation, 8 Hz oscillation frequency and amplitude as before but with mean changes in length (offset strain) of -10, -5, 0, +5, +10 percent OL. We also performed passive work

loop measurements for every active work loop condition. Each work loop trial consisted of 8 cycles, and we discarded the first cycle. Muscle stress was calculated using the average mass values from [16] and the measured resting lengths because these measurements produced less variation than attempts to measure mass following x-ray experiments. During our limited beam time we gathered data from 8 samples of muscle 178 and 10 of muscle 179 which were not consistently from the same individual animal. Because prep viability decreases rapidly during prolonged x-ray exposure, not every condition reported has the same number of individuals. Therefore each figure reports the number of samples which are included in that analysis.

2.2.4 Analysis

The most prominent peaks in the muscle diffraction patterns are the (1,0), (1,1), (2,0) equatorial peaks, all of which correspond to crystallographic diffraction planes in the muscle crystal lattice (see Figure 2.1 C and E). Since the intensity is related to the mass which lies along the associated plane, we can use the (1,1) and (2,0) peaks to determine the arrangement of actin in the lattice. If more mass is located along the (1,1) plane, as in vertebrate muscle, the (1,1) peak will be much brighter than the (2,0) peak, and $\frac{I_{11}}{I_{20}} >> 1$ [51]. In invertebrate flight muscle, more mass is aligned with the (2,0), which will mean the (2,0) peak is brighter than the (1,1): $\frac{I_{11}}{I_{20}} << 1$ [51]. Also, the spacing between two peaks gives the spacing between the corresponding planes in the lattice via Bragg's Law, $\lambda = 2d\frac{s}{L}$, where L is the sample to detector distance and λ is the wavelength of the x-ray [51]. We can use the (1,0) peaks to determine the lattice spacing d_{10}, which is proportional to the inter-myosin distance, and therefore proportional to the distance between thick and thin filaments.

Lattice spacing changes are usually on the order of 1-3 nm (2-5%) necessitating image analysis to resolve [51]. X-ray diffraction patterns were analyzed by automated software [72], a subset of which was verified by hand fitting with *fityk*, a curve fitting program [73].

Individual frames for which the automated software failed to resolve peaks were discarded. Trials with frames that consistently failed during multiple cycles to resolve peaks were discarded totally.

2.3 Results

2.3.1 Similarity in packing structure cannot explain functional differences

We first tested whether the two muscles had the same lattice packing structure (Figure 2.1E). In invertebrates, there can be a wide variety of actin packing patterns. Two muscles with different myosin-actin ratios and geometry might have similar steady state behavior since they have the same number of myosin heads available for crossbridge binding, but could have different dynamic behavior due to having more or fewer actin filaments. We can use the ratio ($\frac{I_{11}}{I_{20}} = I_{11/20}$) of intensity in the (1,1) and (2,0) peaks (Figure 2.1, peaks labeled) to determine if muscles 178 and 179 have similar packing patterns (see methods).

We measured the intensity of the (1,1) and (2,0) peaks of muscles 178 and 179 and found $I_{11/20} = 2.47 \pm 0.4$ and $I_{11/20} = 2.68 \pm 0.4$ for muscle 179 (mean and 95% confidence of mean) for muscles 178 and 179 respectively. Although we have not modeled what packing pattern would produced such an intensity ratio, we know from previous electron microscopy work that muscle 137, the midlimb analog of 179, has a 6:1 packing pattern common among insect limb muscle [74]. The similar ratios ($p = .44$, Wilcoxon rank sum test) mean it is likely muscle 179 also has this packing pattern. Regardless, based on the intensity ratio of 178 compared to 179, we determined 178 to have the same structure as 179. Since the two muscles have the same packing structure, this alone cannot account for their different work loops.

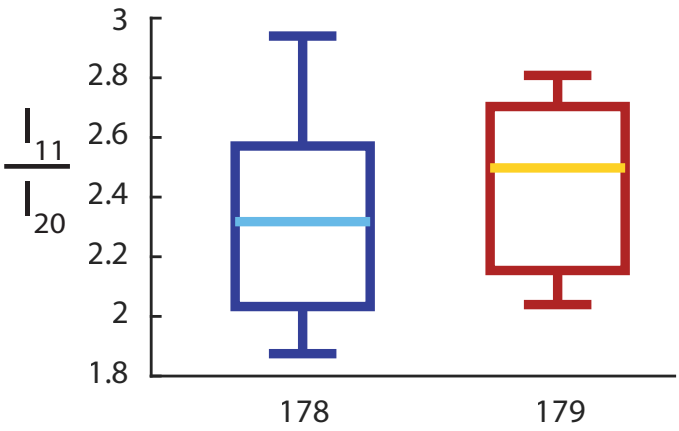

Figure 2.2: Boxplots of the intensity ratio $I_{11/20}$ for muscles 178 (n=8, left) and 179 (n=9, right), with median and 25th and 75th percentiles. There is no significant difference between the two muscles' intensity ratios, indicating that they have same packing pattern (p =.44, Wilcoxon rank sum test).

2.3.2 A 1 nm difference in lattice spacing under passive conditions disappears when muscles are activated to steady state

Since we did not observe a difference in packing structure between the two muscles, we next asked if the lattice spacing under isometric conditions differed between the two muscles. We used the value of d_{10} at peak stress as the steady state active lattice spacing (Figure 2.3). The peak stress values at each strain for both muscles are recorded in Table 2.1, and passive and active d_{10} are shown.

We found a significant structural difference between the two muscle at rest, but not when activated. Under passive conditions muscle 178's lattice spacing was 1.01 $\pm$ 0.41 nm (mean $\pm$ 95% CI of the mean) smaller than 179 across all 5 strain conditions (p = .005). When activated, the myofilament lattice of muscle 178 expanded radially by about 1 nm (see inset in Figure 2.3) under all strain conditions, but activating muscle 179 caused no statistically significant change in lattice spacing at any strain condition (Figure 2.3, $p = 0.008$ and $p = 0.52$, two-factor ANOVA accounting for activation and strain, for 178 and 179 respectively). As a result, the two muscle has statistically indistinguishable lattice spacings when both were activated under steady conditions (0.05 nm $\pm$ 0.4 apart, $p = 0.86$). Taken together, these measurements show that under passive conditions, the lattice spacing of these two muscles are different, but that under quasi-static submaximal conditions, their lattice spacing is the same. This is because the lattice spacing of muscle

178 increased to match muscle 179's lattice spacing, which did not change.

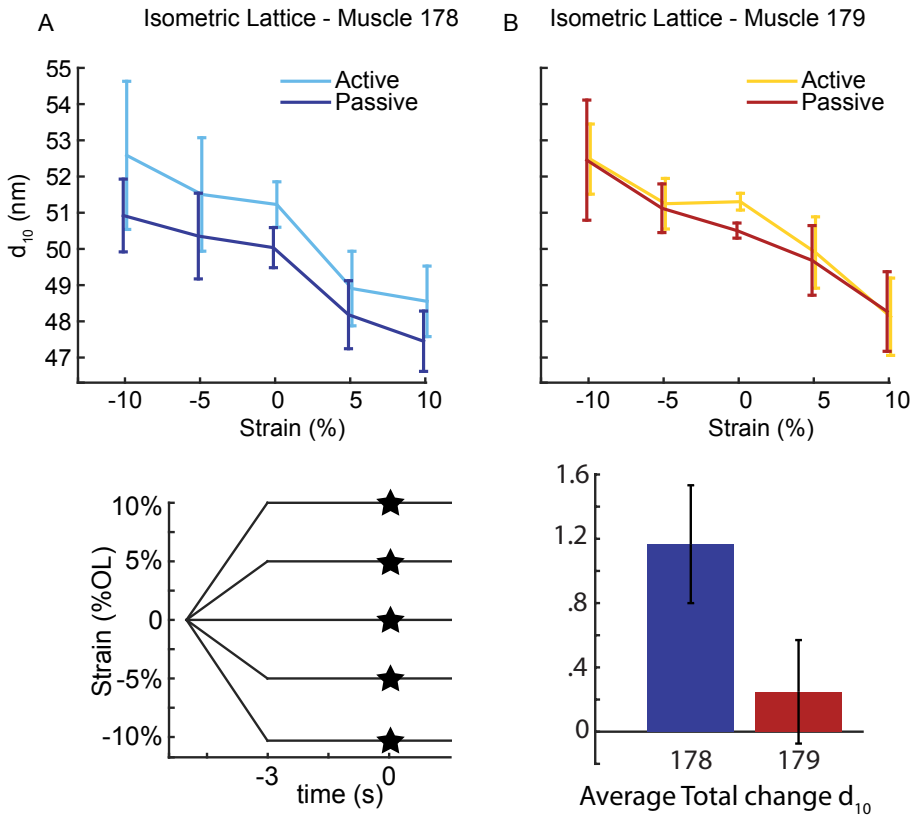

Figure 2.3: Muscle 178 (A) and 179 (B) passive and active d_{10} at strains of -10% to +10% of operating length, with 95% confidence of the mean. Inset shows the total average change under activation in d_{10} across all strains with 95% confidence of the mean, showing a difference in the mean of 0.92 nm ($p < 10^{-3}$). Sample size, n, at strains (-10,-5,0,5,10) was: (7,6,8,7,7) for muscle 178; (8,9,8,9,9) for muscle 179. The inset also indicates the strain conditions we used, with the timing of activation indicated by the star at $t = 0$.

2.3.3 The two muscles have different lattice spacing dynamics

The isometric comparison shows that there is a structural difference between the two muscles under passive conditions which is not manifest under steady-state activation. This is consistent with the two muscles having similar twitch, force-length, and force-velocity properties which are all taken at steady activation. We wanted to see what structural differences might exist under conditions mimicking *in vivo* behavior, so we next examined how lattice spacing behaves during dynamic contractions. We measured d_{10} during passive

work loops and work loops at 8 Hz with the *in vivo* activation pattern and phase (see methods). When activated, the time course of d_{10} in muscle 178 differed significantly in the active vs. the passive case, while 179 lattice spacing did not ($p = .008$ and $p = .11$, two factor ANOVA between strain and activation. Figure 2.4 shows the mean subtracted 8 Hz results in order to compare the peak-to-peak differences in lattice spacing during active and passive work loops. In both muscles, passive (unstimulated) muscle underwent comparable peak-to-peak lattice spacing change. Activation produced additional lattice spacing expansion of 1.1 $\pm$ .5 nm at the peak stress plateau. Peak lattice spacing change in muscle 179 was .4 $\pm$ .4 nm (see Figure 2.5 for a representative lattice spacing, stress, and incremental work time series). Therefore under dynamic conditions we found that peak-to-peak d_{10} increased more in 178 than in 179 (Figure 2.4), continuing the structural motif we found in the steady state case.

2.3.4 8 Hz and 11 Hz work loops differed in net work

For technical reasons, we could not exactly prepare the muscles in the same ways as in the experiments from [16] where the muscle was left *in situ* in the limb and the motor neuron directly stimulated. Our preparation required isolating the muscles from the cockroach leg and directly stimulating them with silver wire electrodes [49]. This was necessary to restrict x-ray imaging to a single muscle and because of size constraints for fitting the experimental apparatus in the beam line. When extracellularly stimulating, muscle force rise times are faster (approximately 8 ms) because of the lack of transmission and synaptic delays, and decrease faster likely because all sarcomeres are simultaneously activated [49]. Consequently, under identical 8 Hz running conditions, force develops sooner in our muscle preparations than in the neural stimulation, *in situ* work loops of [16]. As a result, under extracellular stimulation both muscles 178 and 179 produce small but significant positive work and more negative work (Table 2.1). In prior experiments, faster 11 Hz running conditions were also implemented in work loops [49]. In muscle 137, the midleg equivalent

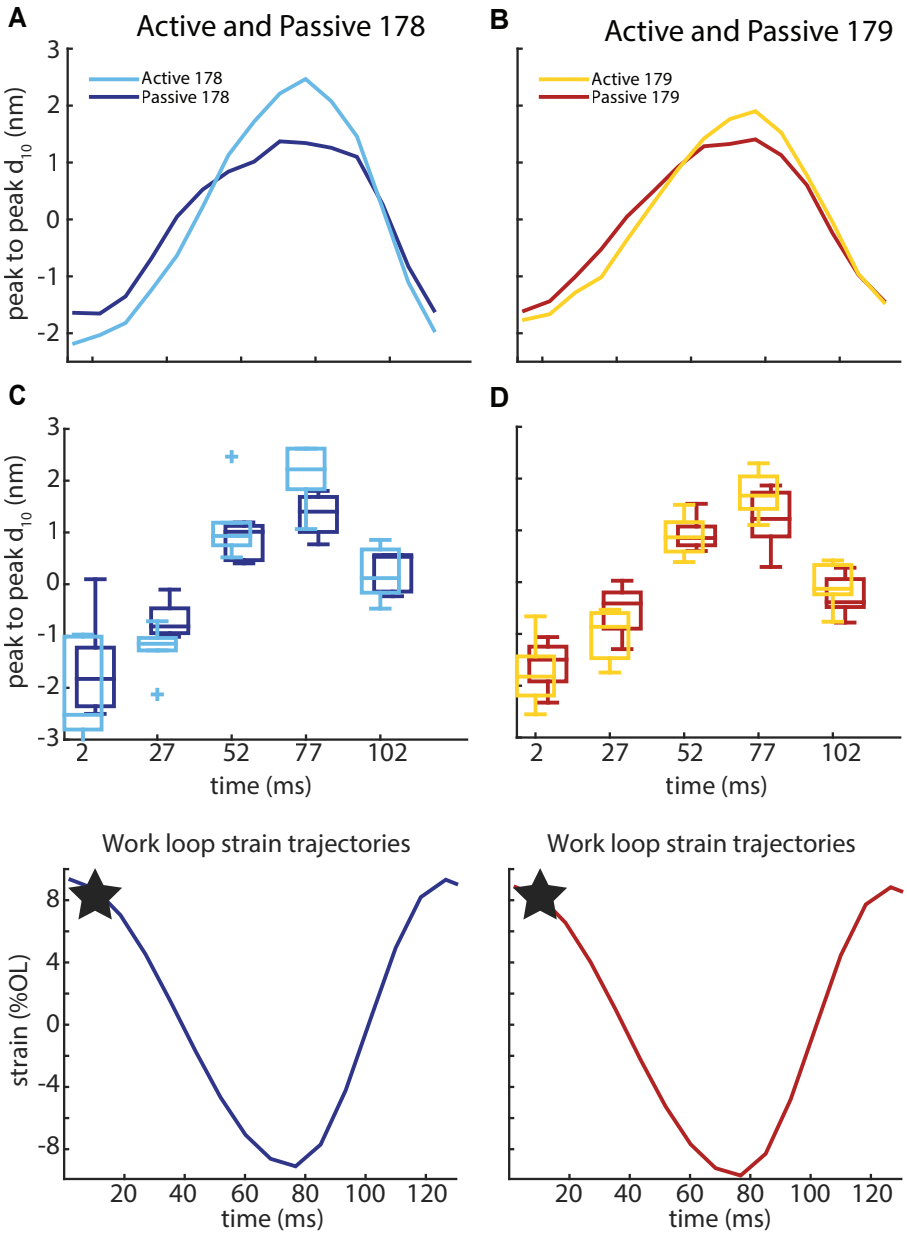

Figure 2.4: A) and B) show the mean subtracted active and passive d_{10} lattice spacing, respectively. These were obtained similarly to Figure 2.3, but under dynamic work loop conditions. C) and D) show the variation in the mean at times corresponding to $.02T$, $0.23T$, $0.43T$, $0.64T$, $0.84T$, which corresponded to the time points nearest maximum strain amplitude $\frac{\Delta L}{L_0}$, 0.5*$\frac{\Delta L}{L_0}$, -0.5*$\frac{\Delta L}{L_0}$, minimum strain amplitude $\frac{\Delta L}{L_0}$, and 0% strain, respectively, where T = 120 ms is the cycle period. Boxplots show the median spacing as well as 25$^{\text{th}}$ and 75$^{\text{th}}$ percentiles, with + indicating data points considered outliers defined as being 1.5 times greater than the interquartile range. Sample size, n, was: 5 for passive muscle 178 , 6 for active muscle 178, 8 for active and passive muscle 179. E) indicates strain trajectories of our work loop protocol, with the timing of activation indicated by the star.

of 179, these 11 Hz conditions with extracellular stimulation gave more similar work to the [16] and [6] conditions. The faster frequency reduced stride period correspondingly. To compare with these conditions, we repeated all of our trials with 11 Hz work loops. In this case, we found results more consistent with previous work loops, although the difference between the two muscles was still not as dramatic as those from the [16] *in situ* work loops. Muscle 178 produced positive work statistically indistinguishable from the 8 Hz condition ($p = .56$, *t*-test), but muscle 179 produced significantly less ($p = .017$, *t*-test) and both muscles produced even more negative work than in the 8 Hz conditions ($p = .07$ and $p = .002$, *t*-test, for muscles 178 and 179, respectively). The differences in preparation between previous *in situ* work and our isolated muscle protocols are likely the main source of discrepancy. However, negative work also has large variation (50-75$\%$) from experiment to experiment both here (see Table 2.1) and in previous studies at these conditions [16, 49], suggesting that there might be a large range of typical responses across individuals.

		Muscle 178		Muscle 179	
8 Hz	Work per cycle (active) (J\Kg)	Total positive	Total negative	Total positive	Total negative
		0.35 ± 0.11	-1.23 ± 0.30	0.67 ± 0.31	-1.27 ± 0.35
11 Hz	Work per cycle (active) (J/Kg)	Total positive	Total negative	Total positive	Total negative
		0.46 ± 0.25	-2.95 ± 1.54	0.25 ± 0.12	-3.74 ± 1.08
	Length (mm)	3.59 ± 0.20		3.78 ± 0.15	
	Width (mm)	2.17 ± 0.28		1.69 ± 0.27	
	Stress (mN/mm^2) at -10%, -5%, 0, 5%, 10%	50.9 ± 20.5 78.8 ± 29.2 101.6 ± 18.8 124.0 ± 24.0 129.2 ± 27.8		60.1 ± 35.4 89.7 ± 35.9 158.5 ± 22.2 166.3 ± 34.8 190.4 ± 40.7	

Table 2.1: All values are means $\pm 95\%$ confidence intervals of the mean. For the 8 Hz conditions, $n = 6$ for muscle 178, and $n = 7$ for muscle 179. For the 11 Hz conditions, $n = 4$ for muscle 178, and $n = 9$ for muscle 179. Stress values are peak stress during isometric conditions under submaximal three spike stimulation pattern. We report total positive and total negative work, rather than net work, to better emphasize the differences between 11 Hz and 8 Hz work loops, and the differences between muscles.

2.3.5 Lattice spacing dynamics correlate to changes in stress

Given the lattice spacing difference between muscle 178 and 179, we next tested whether these changes correlated to the timing of stress differences in the two muscle's dynamic behavior. The two muscles have nearly identical strain patterns so differences in mechanical work arise from different stress profiles. Given individual variation, we considered the correlations between lattice spacing and stress in every individual from both the 8 Hz and 11 Hz work loops. We paired active and passive work loop conditions for each individual and subtracted the passive spacing changes which gave us the spacing changes due to activation - $\Delta d_{10} = d_{10,\ active} - d_{10,\ passive}$. We cross correlated Δd_{10} with the instantaneous muscles stress (force per cross sectional area).

In all 8 Hz and 11 Hz trials, changes in lattice spacing from passive to active work loop conditions correlated with stress. Figure 2.5 shows a representative time series of Δd_{10}, stress (active - passive), and incremental work for muscle 178 and 179 at 8 Hz and 11 Hz. Stimulation occurs just after the start of shortening. Following stimulation, in 8 Hz trials, stress begins to develop in both muscles, but falls off earlier in muscle 179 and plateaus in muscle 178. During this stress plateau, peak Δd_{10} occurs in muscle 178 (Figure 2.5 A) while Δd_{10} in muscle 179 returns to baseline (Figure 2.5 B). In 11 Hz trials, stress peaks at the start of shortening in both muscles, which in general is when the peak of Δd_{10} also occurs. However in 11 Hz trials, Δd_{10} was sometimes negative during the end of shortening, indicating the lattice spacing deceases from the passive value, although the magnitude of change is still greater in muscle 178 than 179 (Figure 2.5 C, D).

2.3.6 Lattice spacing dynamics depend on strain

Under perturbed conditions during locomotion these muscles can undergo many different strain patterns [49, 50]. We next changed the mean strain of the work loop conditions by shifting the mean length by $\pm$5 and +10% of OL. In this way, we tested if changes in lattice spacing dynamics during the work loops were sensitive to specific length (or strain)

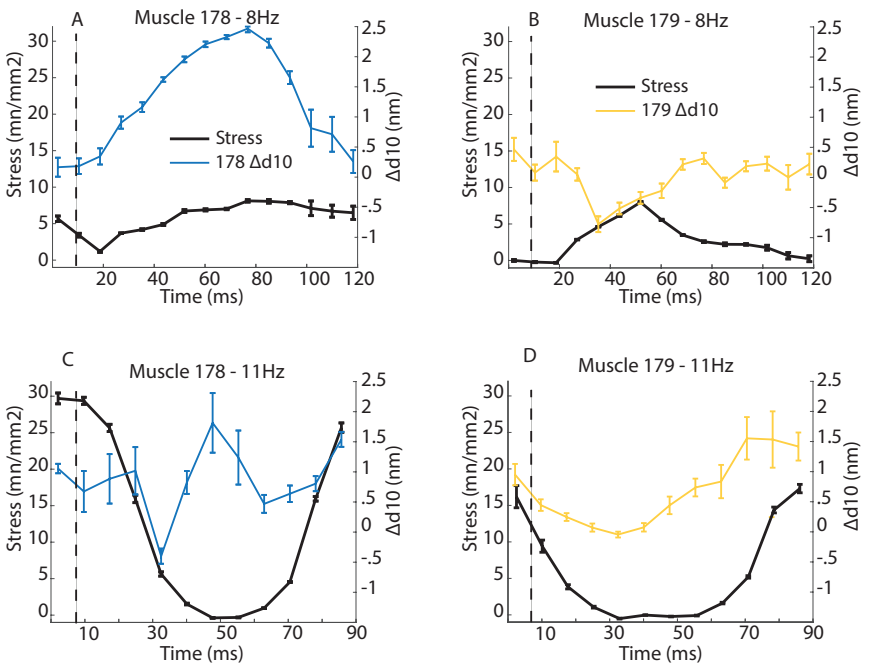

178 - 8 Hz

Correlation Coefficient	*p*-Value	Time shift (ms)
0.34	$<10^{-2}$	24
0.47	$<10^{-2}$	16
0.45	$<10^{-2}$	0
0.21	0.01	32
0.77	$<10^{-2}$	-8

179 - 8 Hz

Correlation Coefficient	*p*-Value	Time shift (ms)
0.29	$<10^{-2}$	0
0.41	$<10^{-2}$	16
0.46	$<10^{-2}$	16
0.09	.2	-40
0.57	$<10^{-2}$	24
0.34	$<10^{-2}$	-40
0.50	$<10^{-2}$	0

178 - 11 Hz

Correlation Coefficient	*p*-Value	Time shift (ms)
0.45	$<10^{-2}$	-22.8
0.35	$<10^{-2}$	-22.8
0.35	$<10^{-2}$	22.8
0.16	0.01	53.2

179 - 11 Hz

Correlation Coefficient	*p*-Value	Time shift (ms)
0.46	$<10^{-2}$	-15.2
0.48	$<10^{-2}$	15.2
0.55	$<10^{-2}$	-7.6
0.41	$<10^{-2}$	30.4
0.61	$<10^{-2}$	7.6
0.44	$<10^{-2}$	-22.8

Figure 2.5: A) Muscle 178 under 8 Hz work loop conditions. B) Muscle 179 under 8 Hz work loop conditions. C) Muscle 179 under 11 Hz work loop conditions. D) Muscle 179 under 11 Hz work loop conditions. Black solid lines show stress in mN/mm^2, colored bars show Δd_{10}, black dashed lines show the timing of stimulation. Lattice spacing changes in 178 were larger for muscle 178 than 179 under both conditions. Stress under the 11 Hz conditions more closely matched previous results [16], with higher stress during shortening in muscle 178 leading to more positive work than in muscle 179, and both muscles having substantial stress during lengthening, leading to negative work. Under the 11 Hz and 8 Hz conditions, Δd_{10} correlated with stress.The bottom table shows the Pearson linear correlation coefficient between stress and Δd_{10} of each individual. Timing differences are the peak cross correlations for each work loop condition in each individual. Our convention is that negative timing difference indicate stress changes follow Δd_{10}, although conditions are periodic.

trajectories. The midleg homolog to muscle 179 has a large functional range, shifting from a brake to a motor under different activation and strain conditions [49]. If lattice spacing covaries with work, we might expect corresponding large variations in lattice spacing dynamics under different strain trajectories.

The difference in lattice spacing dynamics between the two muscles was present at every mean offset condition we measured. The peak-to-peak amplitude of d_{10} in muscle 178 always increased during activated work loops compared to passive conditions (Figures 2.6 and 2.7). This change was larger than the Δd_{10} for muscle 179 in every case except at -5%, where d_{10} decreased in muscle 179. In many cases the lattice spacing was actually reduced when the muscle was activated, indicating that activation constrained the radial expansion of the lattice. Overall the lattice spacing change in muscle 179 is more dependent on the specific length trajectory of the muscle, which is consistent with is variable role as a motor or a brake under perturbed conditions.

2.4 Discussion

A single nanometer difference in the myofilament lattice is the first structural difference detected in these otherwise identical muscles that match their function difference in mechanical function and their similar steady-state properties. Before activation, d_{10} in muscle 178 has a smaller lattice spacing than muscle 179 by approximately 1 nm at 10% strain, which is where activation occurs *in vivo* (figure 2.8). Simply showing that there is a passive lattice spacing difference is insufficient to explain the two muscles' different work production because under steady state (isometric and isotonic) conditions, these two muscles produce the same force. However, stimulation causes muscle 178's lattice spacing to increase, eventually matching 179, whereas muscle 179 is already at its steady state lattice spacing. So muscle 178 has dynamic lattice spacing changes due to activation whereas muscle 179 does not. The 1 nm lattice spacing difference disappears at the plateau of isometric twitches, which is consistent with the identical steady state macroscopic properties

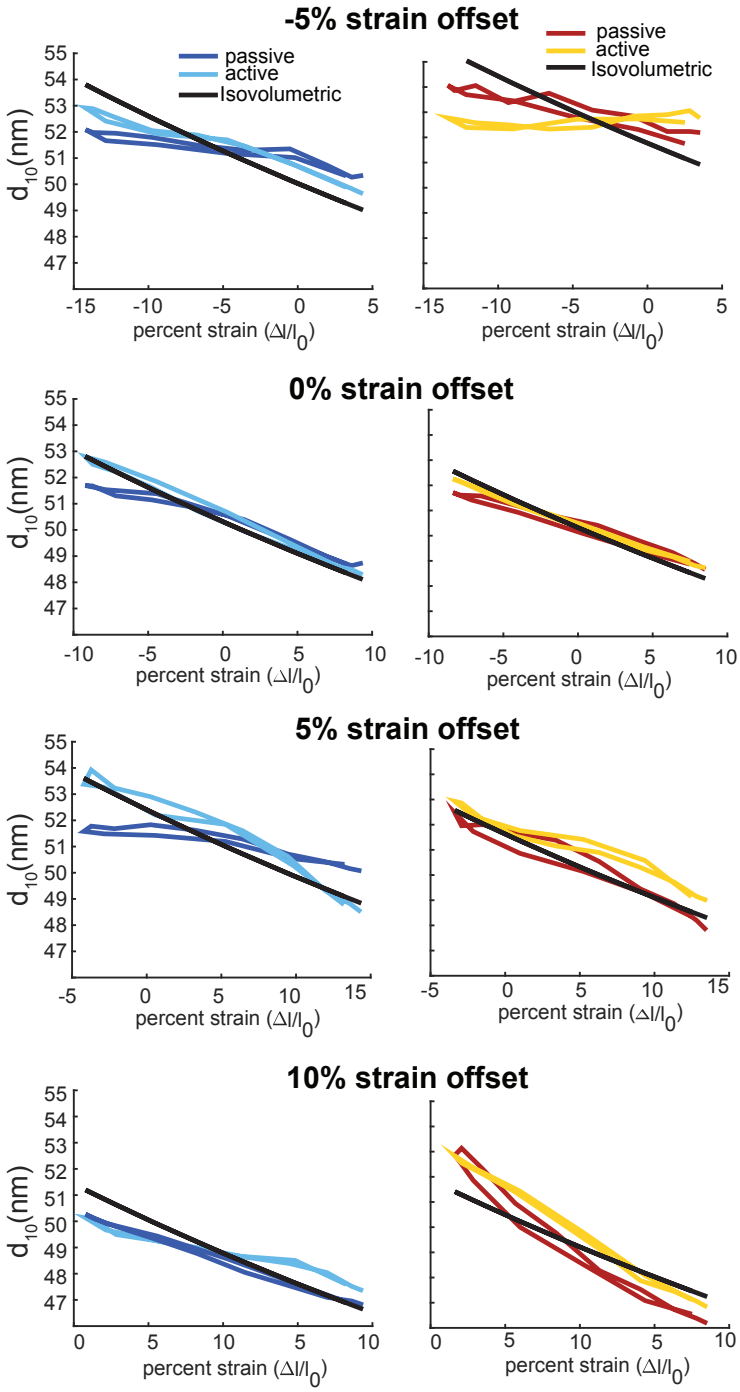

Figure 2.6: Lattice loops (d_{10} vs. strain) during work loops with mean offsets of -5%, +0%, +5%, +10% OL (top to bottom) for muscles 178 and 179 (left and right). The lattice spacing change in passive conditions is due to the axial strain of the myofilament lattice during compression and tension. Under activated conditions the spacing patterns change in part due to the action of active myosin binding and activation of other proteins, such as titin. Sample size, n, for strain conditions (-5,0,5,10) was: passive muscle 178, n=5 for all strains; active muscle 178, n=(5,6,5,5); passive and active muscle 179, n=(5,8,8,5). See Figure 2.7 for variation in d_{10}.

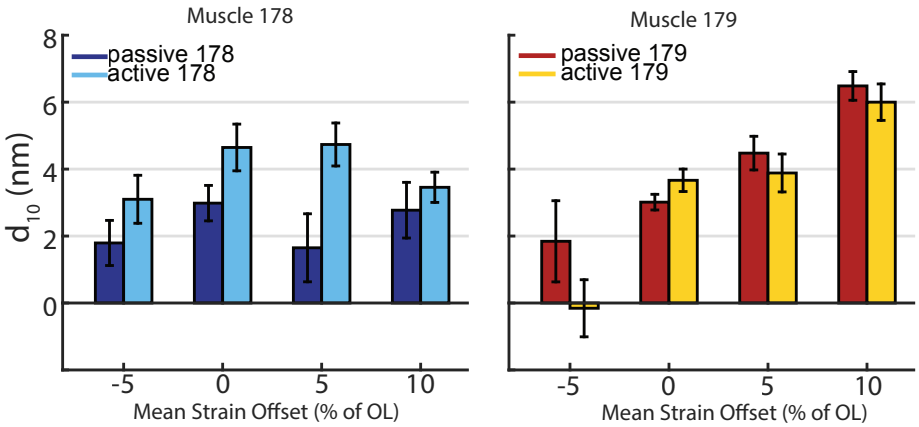

Figure 2.7: Mean change in lattice spacing from start of shortening to end of shortening with 95% confidence of the mean for muscles 178 (left) and 179 (right) during passive and active work loops. We found that strain greatly affected lattice spacing for muscle 179 (p <.001), but not for muscle 178 ($p = .43$). In contrast, we found activation greatly affected muscle 178 ($p = .007$) but did not significantly affect muscle 179 ($p = .24$). Statistics were calculated by 2-factor ANOVA (strain and activation). See Figure 2.6 for sample sizes.

(force-length and force-velocity curves).

During cyclic contractions where the muscles activate and relax, the muscles' lattice spacing will change both with muscle length (comparable in both msucles) and as they go from passive to activated states. As a result, muscle 178 undergoes a 0.82 nm larger change in lattice spacing during periodic contractions compared to muscle 179. Figure 2.8 shows the range of Δd_{10} in order to demonstrate the effect of activation. Since the amount of force that is generated axially is dependent on the lattice spacing, as is the crossbridge binding probability [62, 33], it is reasonable this increased change in lattice spacing could have functional consequences.

Figure 2.8 shows a representation of the lattice spacing changes during activation. At rest, the muscles are offset in lattice spacing (*). Under isometric conditions, the lattice spacing in muscle 178 increases while muscle 179's does not, leaving them at the same lattice spacing at peak activation (green lines). During passive, unactivated work loops, lattice spacing changes due to axial strain (Figure 2.4). We subtracted that passive cycling off to show the difference in lattice spacing due solely to activation of muscle during work

loops, Δd_{10} (solid blue and yellow lines). During early shortening (*i* to *ii* in 2.8) muscle 178 produces more positive work (Table 2.1), presumably because it is in a more favorable position for myosin heads to bind, and undergoes a larger transient in lattice spacing change (dashed blue to dash red line). By the end of shortening (*iii*) and into lengthening, the myosin heads have bound and the thin filaments (pink) have expanded out to the steady state value (red dashed line). This expansion is greater in muscle 178 and likely due to myosin heads producing greater outward radial force in the more constrained configuration. Even though constraints on doing work loops within the x-ray beamline required different methods of stimulation and muscle preparation compared to previous work, changes in lattice spacing correlate with stress production in both muscles 178 and 179 (Figure 2.5). The increased transient change in 178's d_{10} after activation corresponds to the plateau in stress development during this portion of the contraction cycle (Figure 2.5 A). We cannot currently manipulate lattice spacing within intact muscle independent of cross bridge activity to causally connect to muscle function. However, our results suggest structural differences in these two muscles might explain both the dynamic differences and the steady state similarities of these two cockroach muscles.

2.4.1 Packing structure cannot account for the differences in these two muscles

Although the packing pattern of these two cockroach muscles does not explain their work loop differences, it is still an open question how different packing structures might affect muscle function and energetic versatility. Structure indeed does seem to be related to function. In vertebrate muscle (human gastrocnemius [76], rabbit psoas [77], frog sartorius [78], all seen by electron microscopy, and others [27, 70]) actin is arranged such that one thin filament is located equidistant from 3 thick filaments, which makes a 1:2 myosin:actin ratio per unit cell. Invertebrate muscle actin packing can vary greatly, with even adjacent muscles in the same animal having different actin arrangement. Flight muscle (*drosophila* [51], *Lethocerus cordofanus* [79]), for example has one think filament located equidistant

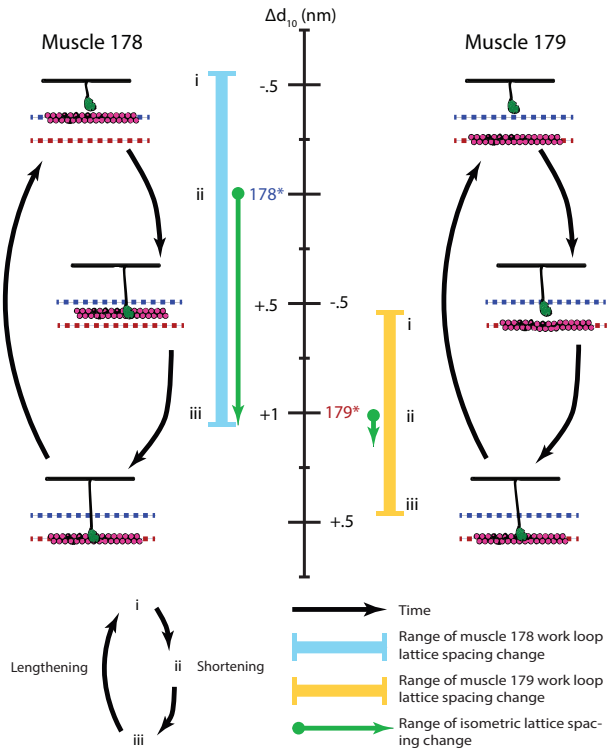

Figure 2.8: Lattice spacing has larger dynamic transients in Muscle 178 than 179. Crossbridge schematics on the left and right indicate lattice spacing at different times during a cyclic contraction (i.e. work loop conditions). Times represented by i, ii, and iii, correspond to the start of shortening (stimulation occurs right after onset), mid-way through shortening, and the transition from shortening to lengthening. Right before stimulation (i), muscle 178's lattice spacing is tighter (blue dashed line) than 179's (red dashed line). During activation (ii), muscle 178's lattice spacing increases until it reaches the red dashed line (iii), while muscle 179's does not significantly change (see Fig. 3). The muscles then relax during lengthening and the cycle repeats. The central scale bar shows the change in lattice spacing compared to the mean passive lattice spacing at rest for each muscle (indicated by blue178* and red179*). These are offset because of the passive differences in the muscle. The green arrows indicate the range of lattice spacing under isometric activation and show that the initial lattice spacing difference disappears at state state. Both muscles undergo lattice spacing change during periodic contractions because of axial length change. However, muscle 178 has a 0.82 nm larger range in lattice spacing (cyan line) during periodic contractions compared to muscle 179 (yellow line) because of the addition of activation dependent lattice spacing. Lattice spacing arises from a balance of radial forces from many potential sources including crossbridges and other sarcomeric proteins (e.g. titin and titin-like molecules [75]). Both the amount of force that is generated axially and radially by crossbridges and crossbridge binding rates are dependent on the lattice spacing [62, 33]. These influences could enable even a 1 nm difference to have the potential to drive differences in muscle's mechanical work output, but we must further explore causal mechanisms.

between every 2 thick filament, which makes a 1:3 myosin:actin ratio per unit cell, whereas invertebrate limb muscle (crab leg muscle [80], crayfish leg [81]) has 12 thin filaments surrounding each thick filaments, which makes which makes a 1:6 myosin:actin ratio per unit cell. Different packing structures will have different actin-myosin spacing even if d_{10} is the same between muscles since the geometry of actin relative to myosin has changed but myosin geometry has not [27]. Different ratios will also affect the availability of actin binding sites for myosin heads. The broad interspecific correlation with muscle locomotor type suggests that packing structure may still be an important determinant of work.

However, in this case no statistically significant difference was found in the measurements we took of $\frac{I_{20}}{I_{11}}$ for the two muscles and we determined them to have the same ratio and arrangement of myosin to actin filaments. Since the muscles are both femoral extensors acting at the same joint, it might seem natural to assume from the beginning that they have the same packing structure. However, even though *B. discoidalis* is flightless, electron micrographs have shown that the largest of the femoral extensors in the middle leg which is in between the homologs of these two muscles actually has flight muscle packing arrangement [74], in which thin filaments are located equidistant between two thick filaments, for a 1:3 myosin to actin filament ratio. Despite being a limb muscle, that femoral extensor is bifunctional and also actuates the wings [71]. Conversely a wing actuation muscle in the beetle *Mecynorrhina torquata*, which act as a steering muscle, has a packing pattern usually associated with limb muscle [82]. So it is not always possible to assume a given packing geometry based only on muscle function. However in the two muscles considered here, packing structure cannot explain their differences.

2.4.2 Structural differences at the micro-scale could explain functional differences at the macro-scale

It is perhaps surprising that a 1 nm spacing difference could link to such a dramatic functional consequence. Even when we consider the change relative to the absolute lattice

spacing of $\approx$ 50 nm, it is only a 2% difference (figure 2.3). However small differences in myofilament configuration can have dramatic effects because of the sensitivity of myosin's spatial orientation relative to its binding site on the thin filament. Crossbridge kinetics depend on lattice spacing and vice versa [62, 66, 63, 34]. By undergoing a larger range of lattice spacing during a typical contraction, muscle 178's crossbridge kinetics will likely change more than 179's crossbridge kinetics.

It is not unprecedented for relatively small lattice spacing changes to have multiscale physiological consequences. Temperature has been shown to affect crossbridge activity enough to change d_{10} by as much as 1 nm in hawk moth flight muscle [2]. In that case the temperature difference also corresponds to a functional difference where the cooler superficial part of the muscle acts like a spring while the warmer interior does net positive work [3]. In the cockroach muscles there is unlikely to be any temperature difference because both muscles are small and superficial. While the origin of the lattice spacing differences in these muscles is unknown (discussed below), it is reasonable that a 1 nm difference in lattice spacing could influence crossbridge activity enough to make a sizable change in work output. While we do not yet know the full multiscale mechanisms of work differences in these two muscles we have now shown that there are significant structural differences that correlate with different mechanical functions and are of a magnitude that can impact stress production.

The importance of small nanometer differences in lattice spacing reflects the more general feature of muscle's multiscale nature. Multiscale effects manifest when there is coupling between different length scales and when physiological properties arise which are not predicted by the behavior of other length scales. As myosin crossbridges form, lattice spacing can change due to the radial forces generated, aiding or impeding further crossbridge attachment [33]. Also, crossbridge formation strains myosin thick filaments axially, which can influence myosin cooperativity [63]. This means crossbridges (10's of nanometer scale) influence and are influenced by the length change of the whole sarcomere (micron

scale). The deformation of the sarcomere is also a product of strain imposed on the whole muscle fiber (100s of microns), which introduces coupling between whole muscle dynamics and crossbridge kinetics. Spatially explicit models have shown that lattice spacing can affect force, but these models cannot yet predict work under dynamic conditions for a full 3-D lattice [33, 63]. Other detailed half-sarcomere models can capture work differences but cannot yet explicitly incorporate myofilament lattice differences (e.g. [17, 83]. We generally cannot yet predict mechanical work from steady-state physiological properties, especially during perturbed conditions [58, 16, 59, 50] but our results link nanometer scale structural differences with functional differences relevant for locomotion.

2.4.3 How might different time courses of lattice spacing arise?

Lattice spacing changes are variable across different muscles, and although the whole muscle is isovolumetric, the myofilament lattice may or may not be [35]. In frog muscles, the lattice is isovolumetric as rest [84] while in active indirect flight muscle lattice change is minimal [29]. However, our results show that under some strain conditions (see Figure 2.6, 0 and +5% strain offset in muscle 178) even passive muscle is not strictly isovolumetric, and that the lattice spacing increase after activation can make muscles more isovolumetric. This indicates that individual muscles might have different dependencies on length change as well as activation, as we see in Figure 2.7.

Many experiments have shown that the relationship between sarcomere length and lattice spacing may be regulated by titin [85]. For example, by enzymatically lowering the passive tension of titin in mice, it was seen that lattice spacing increased and pCa sensitivity decreased, implying there exists a strong radial component of titin force which influences actin-myosin interaction possibly by regulating the lattice structure [86]. Bovine left ventricles and left aortas express higher and lower titin stiffness, respectively. Ca^{2+} sensitivity with sarcomere length is much stronger in the ventricle with stiffer titin, and this is coupled with smaller lattice spacing, as seen with x-ray diffraction [87].

In the muscles in our study, lattice spacing differences might be explained by differences in projectin or sallimus, the titin-like proteins found in insects [22, 88, 89, 90]. It is possible that the passive radial force component of elastic proteins decreases as muscle strain increases in muscle 179, but remains constant with respect to strain in muscle 178 because lattice spacing change is independent of changes in mean length (mean strain offset) in muscle 178 but not in muscle 179 (Figure 2.6 and 2.7). However, titin is thought to become stiffer when activated [75], suggesting a more complicate force balance. Nonetheless, if the stiffness in the projectin or sallimus proteins (the titin analogs in invertebrate muscle [22]) increased by different amounts upon activation, crossbridge forces would have different affects on the lattice spacing. If elastic protein stiffness increases under activation in such a way as to balance radial forces generated by bound crossbridges in muscle 179 but not in muscle 178, it could help explain our results.

The offset in filament spacing between the two muscles could also arise from differences in Z disk proteins, like α-actinin, which cross-link actin [91]. While this could account for the passive offset it is less clear how such structural differences in the anchoring of thin filaments alone could explain why the d_{10} difference between the two muscle disappears under steady state activation. Overall expansion and contraction of the myofilament lattice arises from a balance of radial forces from many elements.

2.4.4 Structural elements of the actin-myosin lattice have implications for understanding control

In addition to similar muscles producing different amounts of mechanical work under comparable conditions, the same muscle can also have a great deal of functional variation. How lattice spacing interplays with macroscopic force production might contribute to how a muscle changes function under perturbed conditions. The way a muscle's lattice spacing changes during periodic contractions at different mean offsets might give clues to how muscles can achieve such versatile mechanical functions. Muscle 179's lattice spacing has

a more sensitive dependence on strain (Figure 2.6), and a smaller dependence on activation compared to muscle 178 (Figure 2.7). On flat terrain while running, this muscle's *in vivo* function is to act as a brake. However when perturbed, it could perform large amounts of positive work which can affect center of mass behavior of the whole insect. In muscle 137, the mid-limb analogue of muscle 179, a large change in function can arise from small changes in strain and phase of activation which arise from either neural or mechanical feedback [92, 49]. By having lattice spacings with different dependencies on muscle length and activation, different muscles may be able achieve large functional variation such as muscle 137, or be robust in their function even as activation changes.

2.4.5 Conclusion

A 1 nm difference in the spacing of the myofilament lattice is the first feature that matches the steady-state and dyanmic similarities and differences in two nearly identical leg muscles in the cockroach. Nanometer size differences in lattice spacing not only influence myosin binding, but may explain categorical shifts in muscle function that have effects at the scale of locomotion. A single nanometer change in spacing could have this profound effect because of the multiscale coupling from the molecular lattice to the tissue. Simultaneous time resolved x-ray diffraction and physiological mechanism are starting to link biophysical differences in muscle structure to macroscopic function even under dynamic conditions.

2.5 Acknowledgement

The authors thank George Steven Chandler and Chidinma Chukwueke for help in data collection and Sage Malingen, Tom Libby, and Tom Daniel for helpful discussions.

This work was supported by grant W911NF-14-1-0396 from the Army Research Office. This research used resources of the Advanced Photon Source, a U.S. Department of Energy (DOE) Office of Science User Facility operated for the DOE Office of Science by Argonne National Laboratory under Contract No. DE-AC02-06CH11357. The work was

supported by GUP beamtime awards 47291 and 52213. Use of the Pilatus 3 1M detector was provided by grant 1S10OD018090-01 from the National Institute of General Medical Sciences of the National Institutes of Health. This project was also supported by grant 9 P41 GM103622 from NIGMS. The content is solely the responsibility of the authors and does not necessarily reflect the official views of the National Institute of General Medical Sciences or the National Institutes of Health.

CHAPTER 3
NANOMETER SCALE DIFFERENCE IN MYOFILAMENT LATTICE STRUCTURE OF MUSCLE ALTER MUSCLE FUNCTION IN A SPATIALLY EXPLICIT MODEL

3.1 Introduction

In muscle, force is generated by the collective action of billions of myosin motors all undergoing nanometer scale conformational changes. The mechanical work output of a whole muscle, which is often the physiologically relevant parameter for animal locomotion, however, happens at the centimeter scale [4]. Because of muscle's highly ordered, hierarchical structure across multiple length scales, the way in which force is modulated through hierarchical structure can make bulk muscle's behavior on the centimeter scale difficult to predict [26]. For example, the interactions between chains of sarcomeres can produce emergent history dependent behavior that single sarcomeres might not [17, 83]. While this multiscale interplay has led to perhaps a greater understanding of molecular to macroscopic function in muscle than in any other tissue, it has proved challenging to extend this mechanistic understanding from quasi-static regimes to the dynamic behavior that makes muscle so versatile during movement. Here, we show in a spatially explicit, half sarcomere model how the nanometer scale lattice structure of muscle may affect whole muscle mechanical function.

Many of the physiological properties of whole muscle have been linked to the underlying structure and geometry of muscle sarcomeres. For example, whole muscle's force-length relationship was originally attributed to the amount of overlap between myosin containing thick filaments and the actin containing thin filaments at the micron scale [1, 25]. This led to the sliding filament theory and allowed many of muscle's small scale structure-

function relationships to be inferred from whole muscle properties. However, it was later observed that the radial spacing between the thick and thin filaments was not constant, but rather could change with sarcomere axial strain changes [18]. Not only that, but cross-bridges (myosin motors bound to actin) in fact generate radial forces of comparable strength to axial forces, which can deform the lattice [35, 27, 52]. The probability of crossbridge attachment depends on the spacing between the filaments. Therefore, the radial spacing and crossbridges form a coupled system where strain changes imposed on the whole muscle can affect the thick-thin filaments spacing, which affects crossbridge binding. These ideas led researchers to re-investigate the origin of the force-length curve, and they concluded that the radial separation of thick and thin filaments - which is dependent on the length of the sarcomere - could contribute between 20% - 50% of the change in force in the force-length curve as the filament axial overlap [72, 33]. Radial separation of the thick and thin filaments is an important determinant of muscle force.

Because these previous modeling and experimental efforts indicated the force-length curve of muscle is significantly affected by this radial spacing, we wanted to investigate if this radial separation could significantly affect a whole muscle's mechanical function, defined by it net mechanical work during periodic contractions. This can, in part, be investigated experimentally. Because thick and thin filaments are arranged in a highly ordered hexagonal crystal lattice, the thick-thin spacing can be measured while simultaneously measuring force and length with high time resolved x-ray diffraction [28, 10]. Previously, it was found (Chapter 2) that two muscles in the cockroach *Blaberus discoidalis*, which had very similar quasistatic properties yet very dissimilar work outputs, had very similar lattice spacing under quasistatic conditions, but differed in the magnitude and timing of lattice spacing changes. It was also shown that force during a work loop correlated to lattice spacing changes. This suggested that the nanometer-scale lattice spacing of a muscle can have an affect on the macroscopic whole muscle function [31].

However, it is experimentally hard to show that a lattice spacing change can by itself

change the work output of a whole muscle. While chemicals like Dextran can be used to increase lattice spacing osmotically, this usually requires removing the cellular membrane ("skinning"). Skinning the muscle which makes isolating the effect of lattice spacing on mechanical work of the intact muscle difficult because the sarcolemma provides a stabilizing radial force to the lattice [93, 94]. So to test the effect of lattice spacing on muscle mechanical work output independent of other changes, we turned to a spatially explicit three-dimensional model of a muscle half sarcomere. The fact that the model is spatially explicit means that the model can allow us to investigate how the spatial arrangement of crossbridges and the biophysics of crossbridge formation at the nanometer scale can affect force and work at the sarcomere scale. These models were initially developed to investigate how cooperativity between myosin heads could enhance force production in muscle, which is why it was necessary to make them spatially explicit, as opposed to a mass action model like MyoSim [95]. This spatially explicit model was later used to explore work production under periodic contractions, however, they had no dependence on radial spacing, which meant they could not investigate the effect of lattice spacing [96]. Our model is based on the model that was used to show that force-length properties are dependent on the lattice spacing [33, 34]. While that model was able to produce good quasi-static results, it was unable to produce physiological amounts of net work at *in vivo* frequencies.

Since the lattice spacing of muscle has been implicated in whole muscle mechanical function, here we use this spatially explicit modeling approach to test if nanometer differences in lattice spacing alone could have potentially significant impacts on whole muscle mechanical work. We first have to adapt previous models to produce reasonable work loops, periodically activated stress strain curve, in a physiologically accurate range. We ground the model by comparing to twitch, tetanus, and mechanical work at different phases of activation. As with previous modeling efforts we use the physiological data from the dorsal longitudinal flight muscle (DLM) of *Manduca sexta* [12, 11, 96]. We chose this muscle not only because the twitch, tetanus, and work vs. phase of activation have been

well established, but also because very detailed, high time resolution measurements of the actin-myosin spacing changes simultaneous with work measurements have been obtained through x-ray diffraction [32, 2, 97].

In some muscles, such as invertebrate asynchronous flight muscle, the lattice spacing is approximately constant with length change [29]. However, in many muscles, the lattice spacing depends strongly on length, in some cases expanding under an isovolumetric constraint [61, 10, 32, 31, 97]. So not only can a static lattice spacing affect work, but muscles with different dependencies on length could have different relationships between net work and lattice offset and trajectory. In the spatially explicit model we can prescribe different patterns of lattice spacing and axial strain to guide our examination of how lattice spacing changes affect net work. We first investigate the net work for lattice spacing offsets which remain constant over the course of the work loop, then we show the relationship between work and lattice spacing where the lattice spacing is isovolumetric – the myofilament lattice expands or contract proportionally to the axial strain as defined by a fixed Poisson ratio of 0.5.

3.2 Materials and methods

3.2.1 Model overview

Our basis for the model is taken from [33] and [34]. Each time step in the model follows a sequence of steps that ultimately give a scalable estimate of axial force produced by the myofilament lattice. Starting at the current spatial configuration of the model, each myosin head first undergoes thermal forcing by drawing energies from a Boltzmann distribution for each spring that comprises the myosin head, which is then used to update the position of the heads. Then binding probabilities for each myosin head are calculated for the new spatial configuration of the half sarcomere and a set of prescribed rate equations. After transitions between the states have been performed, the nodes which make up the thick and thin filaments undergo a minimization procedure to find the equilibrium configuration of

the half sarcomere. This loop of diffusion, stochastic transition, and then force balancing is repeated at each time step.

3.2.2 Model geometry

A half sarcomere is represented as a 3 dimensional spring lattice. Myosin-containing thick and actin-containing thin filaments are composed of a series of linear springs (Fig. 3.1A) where nodes between springs represent either the origin of a myosin motor (in the case of the thick filament) or a potential binding site (in the case of the thin filament). The model consists of 4 thick filaments and 8 thin filaments arranged such that one thin filament is located equidistant between three thick filaments, as in vertebrate muscle [27]. This spatially explicit unit (Fig. 3.1B) is the repeating motif that composes the regular myofilament lattice in a sarcomere. Periodic boundary conditions are enforced so that each thick filament interacts with 6 thin filaments and allow us to scale to arbitrary size. Interactions with the boundary of sarcomere and fluid interaction within the sarcomere are currently ignored.

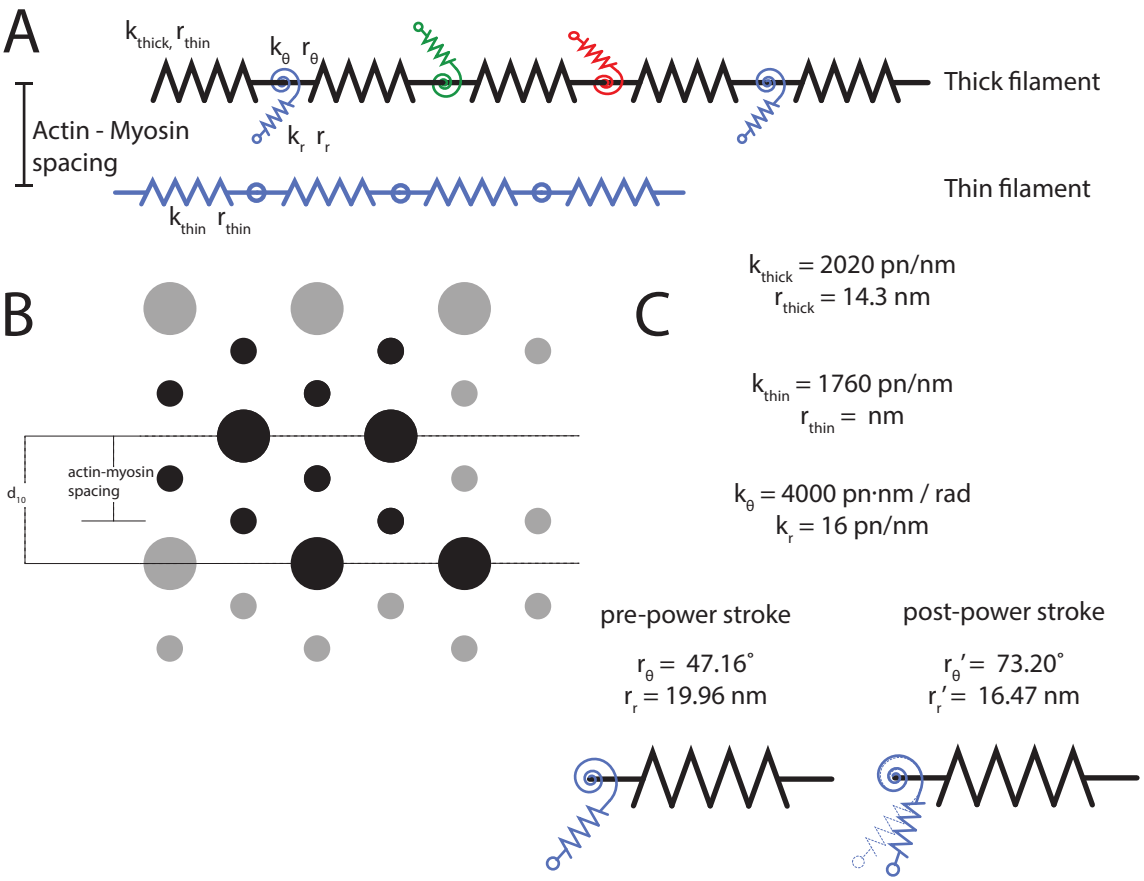

Figure 3.1: **Half sarcomere geometry and spring element stiffnesses.** The geometry of the spring lattice defines repeating motif that models the half sarcomere. A) A 2-D longitudinal view of a segment of a thick filament and one thin filament with which it interacts. Each myosin head faces a certain actin-containing thin filament with which it can potentially bind. B) A cross-sectional view of the half sarcomere, showing the four thick filaments and 8 thin filaments present in model. The d_{10} spacing is the lattice spacing of the crystal unit cell, measured by x-ray diffraction [28]. The actin-myosin spacing (minus the diameter of the thick and thin filaments) is the main parameter we vary in the model. C) The thick and thin filaments are composed of series spring elements of stiffness k_{thick} and k_{thin} taken from empirical estimates. Equilibrium lengths are r_{thick} and r_{thin}. Each myosin head is governed by a three state kinetic model, but the free energy of each state is modified by the strain on the head. We use a two spring model for myosin composed of a linear torsional spring at the base (k_θ and r_θ) and a linear transitional spring in the arm (k_r and r_r), as in [33]. The power stroke is mechanically represented by a change in the rest angle and length of the myosin motor.

Each node of the thick filaments contains triplets of myosin heads, referred to as crowns. The elastic links between adjacent crowns are described as linear springs with a set length

of 14.3 nm, consistent with the 14.3 nm repeat in muscle which gives the helical repeat of the myosin heads [98]. Myosin head triplets are azimuthally distributed by 120°and adjacent crowns are rotated by 60°. Thin filaments are similarly composed of crossbridge binding sites which are spaced 38.7 nm apart and are linked together by linear springs. Filament strain can change the local spacing of heads or binding sites and can arise from either muscle stretch or internal stress produced from myosin binding. The out-of-register nature of myosin heads and binding sites (42.9 nm vs 38.7 nm) is a well-known feature of muscle that emphasizes the importance of a spatially explicit model because compliance in the filaments can either promote or suppress binding probability [28, 99].

The stiffness of the thin filaments k_{thin} were originally estimated in [100] from 1 μm long segments of rabbit skeletal muscle to be 65 pN/nm via deflection of a microneedle under a microscope. The stiffness of the thick filaments comes from the observation that thick filaments are about 150% stiffer than thin filaments, as seen by strain changes in the thick and thin filaments via x-ray diffraction of frog skeletal muscle [101]. The repeat distances of 38.7 and 43 nm are then used to scale the stiffness of each segment of the two filaments [99].

Myosin heads themselves are deformable and previous spatially explicit models have incorporated either a single linear spring [96, 63, 102, 99] or two or four springs mixing torsional and linear elements [33, 34]. The single linear spring does not accurately capture the radial force that crossbridges generate, or the radial dependence of the binding probability of myosin heads, but the two and four spring models (2sXB and 4sXB, respectively) have given comparable prior results [33, 63]. We therefore use a torsional and linear spring (Fig. 3.1A) whose initial stiffness were initially based on those in [33]. However, we increased the stiffness of the cross bridge springs in order so that the binding rates of the crossbridges were bound to a physiological regime.

Crossbridges are able to bind to and unbind from binding sites on nodes on thin filaments. Myosin binding during muscle contraction has been modeled with many different

numbers of states [42, 102, 38], but based on prior models and because we primarily wanted to look at the effect of myofilament lattice structure on the force production step we focused on a 3-state model where myosin heads can be: 1-unbound, 2-weakly bound, and 3-strongly bound. The transition from weakly bound to strongly bound representing the primary step in force production, called the power stroke (Fig. 3.1C). The power stroke occurs because ATP hydrolysis causes conformational changes in the structure of the myosin motor, which is represented mechanically as a change in the equilibrium angle and equilibrium length of the torsional and linear springs which comprise the myosin motor [33]. The pre- and post-power stroke equilibrium locations of the myosin head come from electron tomography of quick frozen muscle of insect flight muscle [103, 104].

At the beginning of each time step, transition probabilities are calculated for cross-bridge binding and state transitions based on the current state of each myosin head and its distance to the nearest thin filament binding site. The force on each node is calculated as the force from attached crossbridges as well as the force from displaced neighboring nodes. To solve for the equilibrium state of the half sarcomere, each node's axial location is iteratively adjusted so that the instantaneous force on each node is zero. The net force is then calculated as the force exerted by the node nearest the m-line on each thick filament.

3.2.3 Rate functions

Rate equations for earlier versions of these spatial explicit models were originally established by fitting force under constant velocity data in [105] to a model in which crossbridges were represented by linear (axial only) springs. These rates were subsequently adapted in [99, 63] to include dependence on crossbridge stiffness. Work loops were considered in [96], but only with one dimensional axial springs, meaning actin-myosin spacing was not a factor. Torsional springs were added in [33, 34] in order to examine the effect of actin-myosin spacing but only in the context of muscle's isometric force-length relationship. The

transition rates used in the 2sXB model are given by the following equations:

$$r_{12} = \tau * e^{-d^2} \tag{3.1}$$

$$r_{21} = \frac{r_{12}}{\exp\left(U_0 - U_1\right)} \tag{3.2}$$

$$r_{23} = A * (1 + tanh(C + D(U_1 - U_2))) \tag{3.3}$$

$$r_{32} = \frac{r_{32}}{\exp\left(U_1 - U_2\right)} \tag{3.4}$$

$$r_{31} = G\sqrt{U_2} + H \tag{3.5}$$

$$r_{13} = 0 \tag{3.6}$$

Here, U_i is the free energy in the i^{th} state, d is the distance from the myosin head to actin binding site, and the rate constants τ, A, C, D, G, and H are chosen so that the function has units of 1 ms^{-1}, and the functions yield transitions consistent with previous models [33, 34, 99, 63] and experimental data [105]. Probability of a transition is calculated from the rate as $1 - e^{-r_{ij} \cdot dt}$, where dt is the time step in the simulation.

3.2.4 Actin permissiveness

In passive real muscle, actin bindings sites are obscured by tropomyosin, which wraps helically around actin and is regulated by the troponin complex of proteins. When a muscle is activated, Ca^{2+} rapidly floods the sarcomere, binds to troponin C, which causes a conformational change in tropomyosin, allowing myosin heads to attach. When Ca^{2+} is pumped out of the contractile lattice, tropomyosin reverts to its original confirmation, preventing myosin binding and force generation. This entire process is parameterized in the model by a single 'actin permissiveness' value which is bounded from 0 to 1 and represents the availability of an actin binding site for potential myosin binding. The product of actin permissiveness and the binding probability calculated from spatial configuration equals the actual probability of binding. An actin permissiveness of 0.5 would indicate that only half of the actin binding sites in the sarcomere are available for binding, which in the model is

handled as each instance of binding being 50% less likely. The actin permissiveness is the same for each binding site in the sarcomere even though the binding probability of a given site will depend both on this and the spatial arrangement of available myosin heads.

3.3 Adapting previous models for work loop simulations

Earlier versions of the 2sXB spatially explicit model were used to investigate isometric muscle's force-length dependence on actin-myosin spacing [34, 33]. Those models were able to capture muscle's quasi-static behavior and to show that the force-length relationship in muscle is in fact highly dependent on radial spacing changes of actin and myosin which are coupled to changes in sarcomere axial length [33]. This is what led us to use that model to investigate if the actin-myosin spacing could have a significant effect on net work of a sarcomere.

The net (mass-specific) work of muscle is given by the area enclosed by a stress-strain curve, which is under steady time-periodic conditions is called the muscle's work loop [43, 4]. In work loop experiments, typically the *in vivo* strain amplitude, frequency, and pattern of activation are measured in an intact animal, allowing the same patterns to be input into an excised muscle, from which net work can be measured [16]. After establishing the behavior of the muscle under conditions which mimic its *in vivo* behavior, the parameters of the work loop can be adjusted to explore the properties of muscle [9]. For example, the phase of activation can be adjusted, yielding a phase sweep. The phase of activation is the point in the length cycle when activation occurs. While the phase of activation *in vivo* might be limited, by expanding the range of activation in work loops we can drive the muscle into different force producing regimes to examine its function.

3.3.1 Titin provides passive force in the model

This model also incorporates titin, a protein filament which attaches the thick filaments to the Z-disk, which defines the end of the sarcomere [58]. Each myosin filament is connected

to each of the four myosin-containing thick filaments at one end, and to the z-disk at the location where the actin-containing thick filament intersects the z-disk. Each titin filament therefore exerts a radial and axial force on the lattice. The force of titin is given by the equation $F_{titin} = a \cdot e^{b \cdot \Delta L}$, as in other models [58, 26, 17]. For the parameters a and b, we used the same parameters as in [58]. There it was found that increasing the stiffness of titin increased the amount of cross bridge binding, but actually reduced force output along the descending limb of the length-tension relationship. In real muscle the stiffness of titin is thought to change with Ca^{2+}, and is increasingly recognized as an important contributor to muscle function [21], and it has been suggested that titin stiffness could significantly affect work [58]. Although titin is present in the model, in the current implementation does not undergo activation-dependent changes. Furthermore, titin is not present invertebrates like *M. sexta*, although a number of proteins such as sallimus, kettin, and projectin have been identified which may serve an analogous function [22, 106].

3.3.2 Improving the dynamic regime of the 2sXB model

While ideal for capturing axial and radial force contributions, the prior 2sXB models could not produce significant positive work under *in vivo* frequencies and amplitudes. We simulated work loops using the release version of these models at 25 Hz at 10 phases of activation between 0 and 0.9 and compared the results to phase sweep work loop data taken from *Manduca sexta* isolated, whole muscle experiments [12]. We found that work loops produced orders of magnitude more net negative work (-230 J/Kg at phase of activation of 0) under these conditions (Figure 3.2). It is important to acknowledge that this dynamic regime with high rates of axial shortening and lengthening were not the purpose of the prior 2sXB model and these simulations only serve to illustrate the regime where modifications are necessary to apply such approaches. Other prior models that did not include a second spring, and hence an explicit radial dependency, could emulate work production under cyclic strain strain curves, but cannot test the dependency on lattice spacing [96].

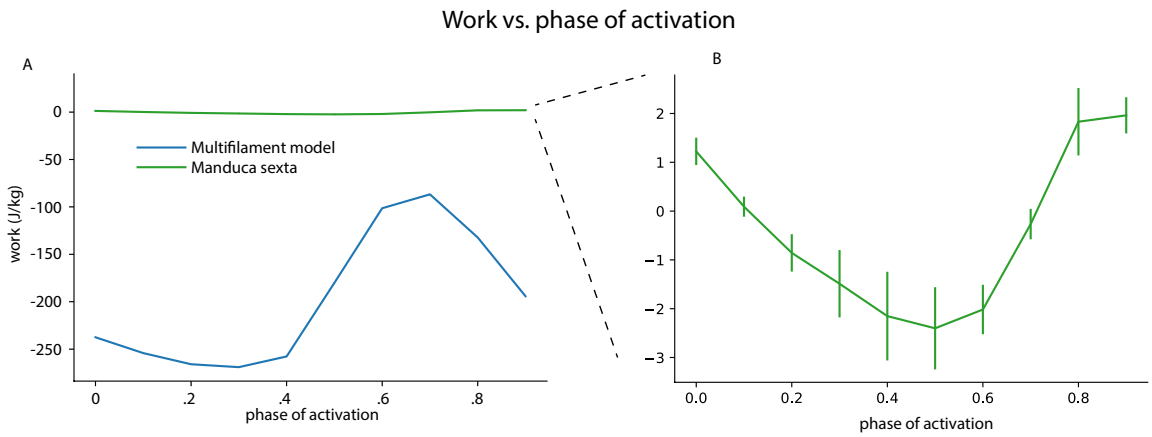

Figure 3.2: A) Work loop simulations were done at 25 Hz and 10% peak-to-peak amplitude, which is the *in vivo* frequency and amplitude of *Manduca sexta*. Blue shows the net work at different phases of activation simulated form the previous 2sXB model, compared to green which shows the net work phase sweep for *Manduca sexta* from experiments [12]. B) The *in vivo M sexta* phase sweep re-plotted to show that net mechanical work changes from positive to negative during the phase sweep, but on a much zoomed in scale.

The origin of the large negative work in the previous 2xSB models arises from many crossbridges being strained in unphysiological conditions. During a single work cycle at physiological strain velocities, a large population of crossbridges transition to the loosely bound state s_2 even when strained at 20 nm, far from their equilibrium strain. They remain attached for some time, being further strained to 45 nm. This is substantially larger extensions than what a crossbridge should experience, which should be less than 10 nm during rapid shortening [102, 105]. These abnormally strained crossbridges generate large amounts of negative force during shortening (Fig. 3.3A). These loosely bound crossbridges are not binding from an unbound state (s_1) but rather are reverting from the strongly bound state (s_3) (Fig. 3.3 B). This is because the r_{31} rate does not increase rapidly enough at high strains, and reverse power stroke rate r_{32}, increases around -20 nm. While this regime of extreme, unphysiological strains were unlikely to have been explored in previous simulations of the 2sXB model that consider isometric conditions, they prevent realistic force under dynamic conditions.

The inappropriate reverse transition to s_2 and persistence in that state comes from the

model exploring the tails of the rate functions. In particular, the unbinding rate r_{21} is the ratio of the binding rate r_{12} and the difference in free energies between two states of the expression $\exp^{U_1-U_2}$ (Fig. 3.4A,B). The falloff of r_{21} is too slow relative to $\exp^{U_1-U2}$, which causes the unbinding rate r_{21} to be 0 at extreme strains, when it should be rapidly rising. This meant that when tightly bound crossbridges revert from the strongly bound to the loosely bound state, instead of nearly instantly dissociating, they instead became negatively strained up to 40 nm during shortening. Similarly, loosely bound crossbridges would become positively strained during lengthening. The large forces caused by these highly strained crossbridges opposing length change in the sarcomere was the major cause of the negative work being done.

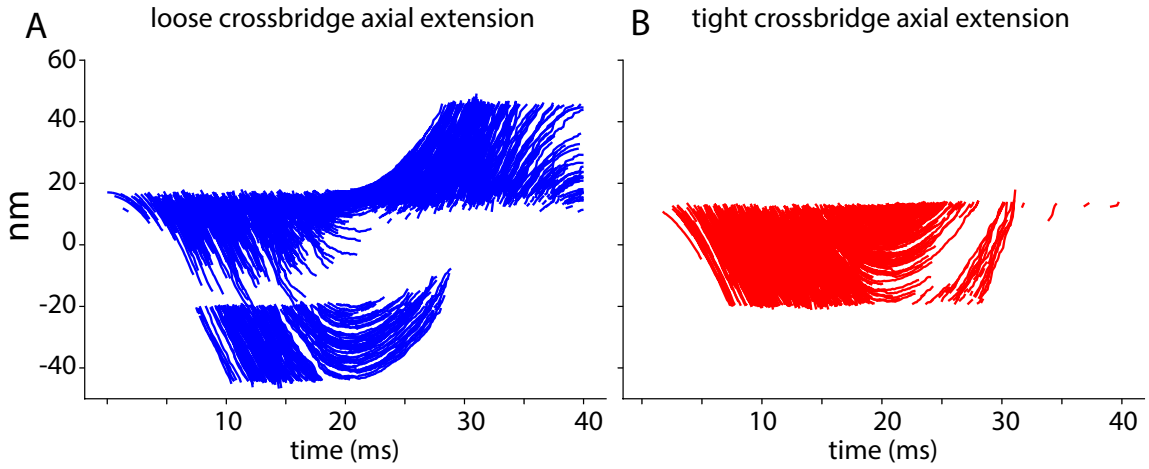

Figure 3.3: A) shows the traces of individual crossbridges in the loosely bound state (s_2) during work loops from the unmodified 2sXB model from [33] B) shows the traces of individual crossbridges in the tightly bound state (s_3). The extreme negative axial extensions during shortening generated considerable force opposite the shortening direction, which generated negative work.

3.3.3 Updated rate functions

Because we wanted to maintain consistency with the previous instances of the spatially explicit model as much as possible, we sought to change the behavior of the rate functions by making rates steeper at higher strains without substantially changing their behavior at

low strains. Comparing to the rate equations which were originally fit in [102, 105], we saw that the binding rate r_{12} exponentially decreases with increasing distance from the binding site just as in later versions of the model. However [105] also added a baseline rate of .005 ms^{-1} to r_{12} which is not present in the 2xSB models. At first glance this seems nonphysical, since it implies that crossbridges have a chance to bind at any axial distance. However the magnitude is too small to practically change r_{12} significantly, and when we re-examine the r_{21} rate, this baseline offset in r_{12} corrects the problem with the binding rates exponential falloff, which enforces an infinite well in the r_{21} rate without substantially changing binding rates in the working range of the myosin head.

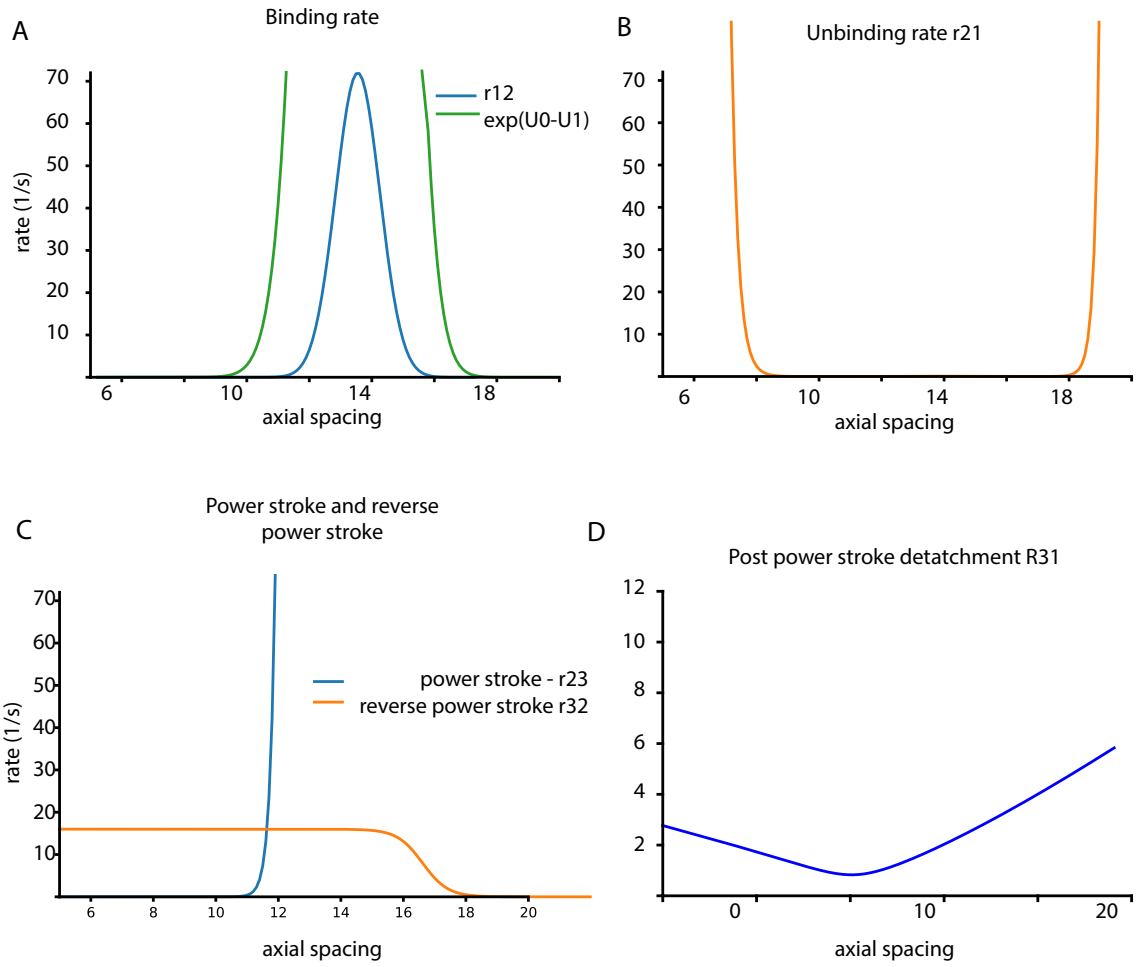

Figure 3.4: Rate equations listed in Eq. 3.6 at an actin-myosin spacing of 15, without thermal forcing. A) The binding rate r_{12} is shown along with the expression $e^{U_0-U_1}$. B) Here we show the r_{21} rate, which is the ratio of the r_{12} rate and $e^{U_0-U_1}$. We found that in the original 2sXB model parameters in [33], the r_{21} rate was not bounded. C) Here we show the powerstoke (r_{23}) and reverse power stroke rate (r_{32}). D) The post power stroke detachment rate r_{31} was not steep enough, which allowed strongly bound bound crossbridges to be strained to unphysiological distances.

While this change was able to account for much of the negative work being done in work loops simulations, we still found that the r_{21} was not tightly constrained compared to previous incarnations of the model [105, 63], causing crossbridges to become nonphysically strained (Fig. 3.4C,D). While individual rate functions could be adjusted, the overall pattern is that myosin heads tend to remain in either s_2 or s_3 at unreasonably large strains. This is consistent with an underestimation of the effective stiffness of the myosin head. We

therefore stiffened the myosin head's torsional spring by a factor of 10 compared to the previous model. This affects the r_{21} rate since it is dependent on the free energy of the myosin head, which is dependent on the stiffness of both spring elements, and also makes the r_{31} rate steeper [99, 63, 33]. We chose to increase the torsional spring stiffness since it is the dominant contributor to the steepness of the rate equations in the axial direction.

3.3.4 Stiffness changes were necessary to match physiological data

After these changes we found that the model produced much less tetanic force than the peak tetanus force of *Manduca sexta* DLM. We also found that the dominant contributor of force was from the loosely bound state, while the tightly bound state contributed little net force. Therefore, we also chose to increase the stiffness of the myosin head's linear spring by a factor of 4, and the power stroke rate constant by a factor of 10. We chose these parameters because this set the average steady-state force of a crossbridge to be about 8-10 pn under isometric tetanus, consistent with estimates of the force of the crossbridge power stroke [107]. Besides more closely matching these physiological observables, increase binding might be expected to match to data from invertebrate flight muscle because the original model in [105] was derived from rabbit psoas, a slower muscle than *M sexta* flight muscle [108, 109]. Although the stiffness we use is larger than what has been reported from single molecule experiments, these experiments may underestimate stiffness *in vivo* [107, 110, 99].

3.3.5 Activation profile was found by matching to twitch force

Since work loops are cyclically activated, we needed to define a periodic function for the actin permissiveness, or activation curve, for the sarcomere. We set the shape the actin permissiveness curve as two exponential functions representing influx and re-uptake of Ca^{2+}. We then simulated an isometric twitch by choosing the influx time and half life of Ca^{2+} re-uptake such that the rise, fall, and peak force during model response matched

twitch data taken from *M. sexta*. The simulated tetanic force and twitch force are shown in figure 3.5, as well as a twitch from *M. sexta*. We used this same activation curve in all following work loop simulations.

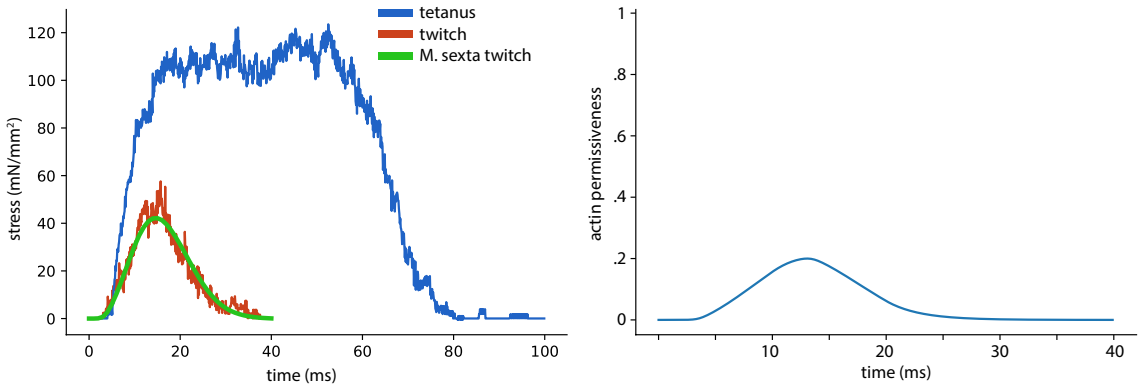

Figure 3.5: We plot the peak isometric tetanic force, then the activation curve which yielded twitch like-force *M. sexta*. This activation curve is then used in all the following work loop simulations.

3.3.6 Actin-Myosin Spacing and d_{10}

We wanted to see if changes in the actin-myosin spacing in a half sarcomere model could modify work output. Since the actin-myosin arrangement in muscle is highly ordered, x-ray diffraction can be used to measure the d_{10} spacing. However, d_{10} is a measurement of the size of the crystallographic unit cell, not a direct measurement of the actin-myosin spacing. It is however, proportional to the actin-myosin spacing, with the proportionality constant depending on the type of muscle. Vertebrate muscle, invertebrate limb muscle, and invertebrate flight muscle all have different proportions and arrangements of actin relative to myosin [27, 18, 31]. In vertebrate muscle, the actin-myosin spacing is given by $\frac{2}{3}d_{10}$ and in invertebrate flight muscle it is $\frac{1}{\sqrt{3}}d_{10}$. Vertebrate d_{10} spacings are typically in the range from 35-40 nm, whereas invertebrate d_{10} spacings tend to be larger, ranging between 40-50 nm. This model and piror 2sXB models, use binding rates originally fit to vertebrate force-velocity curves, and a actin-myosin geometry from vertebrate muscle. We centered our simulations on an actin-myosin spacing of 15 nm (when the radius of the thick and

thin filaments are subtracted out), which corresponds to a d_{10} of 47.5 nm in invertebrate muscle, the average value for *M. sexta* [32]. Because of the different packing arrangements in vertebrate muscle, even though the d_{10} spacing is different from vertebrate muscle, the actin-myosin spacing is similar (12.8 nm actin-myosin spacing at 38 nm d_{10}).

3.4 Results

3.4.1 Simulated work-phase sweep compared to *M sexta* work-phase sweep

After tuning our model to twitch and tetanus data from *M sexta*, we first tested if it could capture realistic levels of mechanical work under dynamic, physiological conditions. We simulated these work loops with a peak-to-peak strain amplitude of 10% and at a frequency of 25 Hz, as in *M sexta* and varied the phase of activation which should cause net work to smoothly transition from positive to negative depending on when myosin heads are actively recruited. Under the crossbridge stiffnesses and rate constant change we made, we simulated work loops at 16 phases of activation. We initially kept a constant lattice spacing of 15 nm, which would correspond to a d_{10} spacing of 47.5 nm in *Manduca sexta*.

Whereas prior models that incorporate explicit radial strain dependence did not generate any net positive work and were multiple orders of magnitude away from predicting force under dynamic conditions 3.3, our revised 2sXB model produced a strong match to physiological work loops at all phases. Each trial included 16 periods, and work was calculated for each period and averaged to obtain means and standard deviations. At a phase of activation of 0 - the average *in vivo* phase for flight in *M sexta* - our model produced 0.6 $\pm$ .2 J/kg (mean $\pm$ s.d.), compared to 1.6 $\pm$ .27 J/kg in *M sexta* whereas the earlier 2sXB model predicted -230 J/Kg. At a phase (0.8) that maximized positive mechanical, our updated 2sXB model produced 1.06 $\pm$ .28 J/kg compared to 2.93 $\pm$ .59 J/kg *in vivo*. During phases of activation around the transition from the end of shortening to the beginning of lengthening (0.5), the model produced more negative work than *M sexta*. For example, the model produced -3.5 $\pm$ 0.5 J/Kg, compared to -1.9 $\pm$ .4 J/kg *in vivo* (mean $\pm$ s.d.). Despite

not being explicitly tuned to match the dynamic conditions of work loops, the model both captures work output to within a factor of 3 (compared to a factor of ¿100) and shows a phase dependency that matches *in vivo* expectations.

Comparing the simulated work loops with real work loops from *M sexta*, there are several notable differences. First of all, there is a large passive component of force in real muscle which is not present in the model. This can be seen from the ramp in force as muscle strain increases (Figure 3.6 C). Because the passive component of force in real muscle is much higher than in our model, we show also *M sexta* work loops which have had the passive component of force subtracted (3.6 D). We found at the *in vivo* phase of activation for *M sexta* of 0 (the start of shortening), that peak passive-subtracted force occurred 5 ms after activation occurred, whereas in simulated work loops the force rose much slower, only peaking 20 ms after activation. At a phase of activation of 0.4 (just before the transition from shortening to lengthening), the force in the simulated work loops rises much faster and higher during the first few milliseconds than in the passive subtracted, however they both exhibit the same plateau of force during lengthening. At a phase of 0.8 the force in *M sexta* work loops is considerably higher than that of simulated work loops, with *M sexta* work loops producing 100 mN/mm^2 compared to peak force of of only 40 mN/mm^2 in simulated work loops.

Many of these differences likely arise from not specifically matching the model to replicate *M. sexta* parameters. One possible avenue of for future research would be to examine if species-specific structural differences could give tighter fits to specific datasets. For example, we should expect variation in the actin:myosin ratio, the orientation of the repeating lattice unit, and the presence of other active filaments and regulatory proteins influence force production under dynamic conditions. Notably, the passive stiffness of titin has been shown to influence the amount of crossbridge binding and force in a spatially explicit muscle model [58]. Since the passive component of our model is so low, increasing the stiffness of titin a significant amount could have a large impact on work. While elaborations could

be made to make the updated 2sXB model more like other specific systems, the fundamental formulation here is sufficient to test if structural variation can drive large changes in work output under physiological conditions.

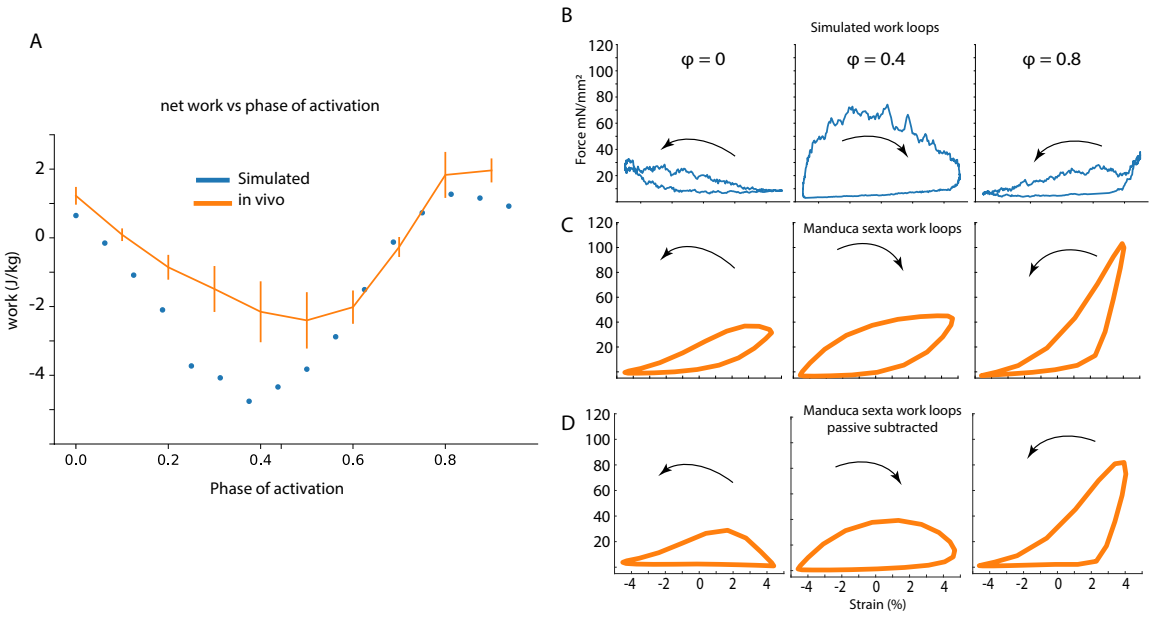

Figure 3.6: A) We plot the net work vs. phase of activation produced by our update 2sXB model (blue) as well as the measured *in vivo* net work for *M sexta* (orange). B) We show example simulated work loops at phases of activation of 0, 0.4, and 0.8. C) We also show real work loops from *M sexta* at the same phases for comparison (Fig. 3.6 C). Because the passive component of force in real muscle is much higher than in our model, we show also *M sexta* work loops which have had the passive component of force subtracted.

3.4.2 1 nm spacing changes can generate positive or negative net work

The updated 2sXB model allows us to test if small differences in the axial spacing of the myofilament lattice can modulate muscle mechanical work, as suggested in [31]. After getting a reasonable phase sweep at 15 nm, we simulated work loops at 14 nm. In invertebrate flight muscle, this would correspond to a d_{10} change of 47.6 to 45.9, a 1.7 nm difference. We found that under these conditions, at a lattice spacing of 14 nm the net work was negative (-0.74 $\pm$ 0.14 J/kg), while the 15 nm produced net positive work (0.72 $\pm$ 0.14 J/kg) (Fig. 3.7). A single nanometer difference in lattice space can cause a switch in the sign of the model's output

We next extended the simulation to lattice spacings from 12 to 17.5 nm, again keeping lattice spacing constant throughout the entire work loop. At the *in vivo* phase of activation lattice spacing had a net work peak at 16 nm (Figure 3.8, $\phi = 0.0$, red). As lattice spacing increased from 12 to 16 nm, net work changed from -4.2 J/Kg to 1.3 J/kg, increasing positive work by 1.3 J/kg nm^{-1}. Similarly, at a phase of activation of 0.85, the net work peaked at a lattice spacing of 15.75, with net work increasing 3.0 J/kg nm^{-1} from 12 to 16 nm. In contrast at a phase of activation of 0.15, net work only slowly increases with lattice spacing, and never peaks. The peak in the phase of activation occurs at an actin myosin spacing equivalent to a d_{10} of 49 nm, while the recorded mean d_{10} spacing in *M sexta* is 47 nm [32].

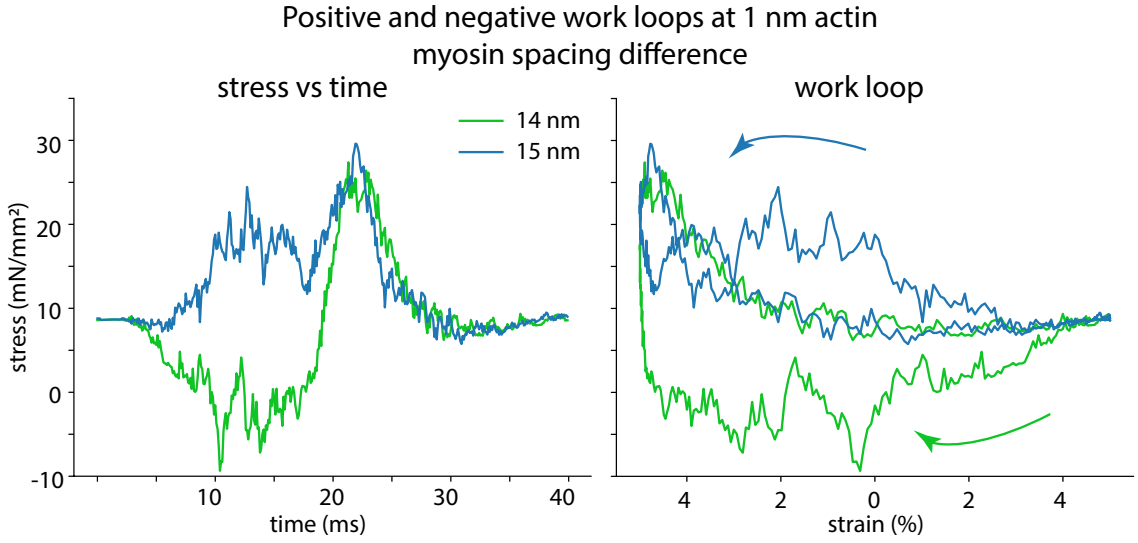

Figure 3.7: We show stress vs time and stress vs strain (work loop) simulated at an actin-myosin spacing of 14 (green) and 15 (blue). Since the model is spatially explicit, there is a high degree of stochasticity, which is why we simulated 16 periods and averaged.

3.4.3 Net work depends on actin-myosin spacing amplitude

We next wanted to show how the net work would depend not only on the mean offset of the lattice spacing, but on the amplitude of the spacing change. In many muscles the lattice spacing in not constant, but depends on the length of the sarcomere [10, 32, 28]. We wanted to see how work would be influenced when we made the actin-myosin spacing depend on

sarcomere length. To start with we chose to make the lattice spacing isovolumetric with length change. We then compared the results of work loops when the lattice spacing was isovolumetric, with work loops that were at constant lattice spacing equal to the mean spacing in the isovolumetric conditions.

We simulated work loops at 25 Hz with the same activation and strain pattern used in work loops as above, and 10% peak to peak strain amplitude. Each point in figure 3.8 consists of 10 periods. Isolattice conditions indicate constant lattice spacing. Isovolumetric conditions indicate the lattice spacing changed with length according to the equation $\Delta d = d(1-(1+\frac{\Delta L}{L})^{-\nu})$, where d is the d_{10} spacing, which we then convert to face-to face actin-myosin spacing, and L is the length of the simulated half sarcomere. The Poisson ratio is given by ν, and $\nu = .5$ will give isovolumetric changes. We simulated here three phases of activation. A phase of 0 is the *in vivo* phase, with ϕ=0.85 and ϕ=0.15 being the limits of the *in vivo* range in *M sexta*.

Radial motions of the lattice can enhance work output, but at large lattice spacing the reverse can also occur. At actin-myosin spacings lower than the peak work output, isovolumetric work loops produced more work than isolattice work loops 3.8. For example, isolattice work loops at $LS = 14$ nm produce -0.5 J/kg, but isovolumetric work loops at $LS = 14$ nm produce 1.0 J/kg . This is due to isolattice work loops producing much less force during shortening (figure 3.8 B and C). Because the radial spacing differences here are the consequence of axial strain, the model shows the potential for multiscale interactions to alter work in a physiological meaningful way.

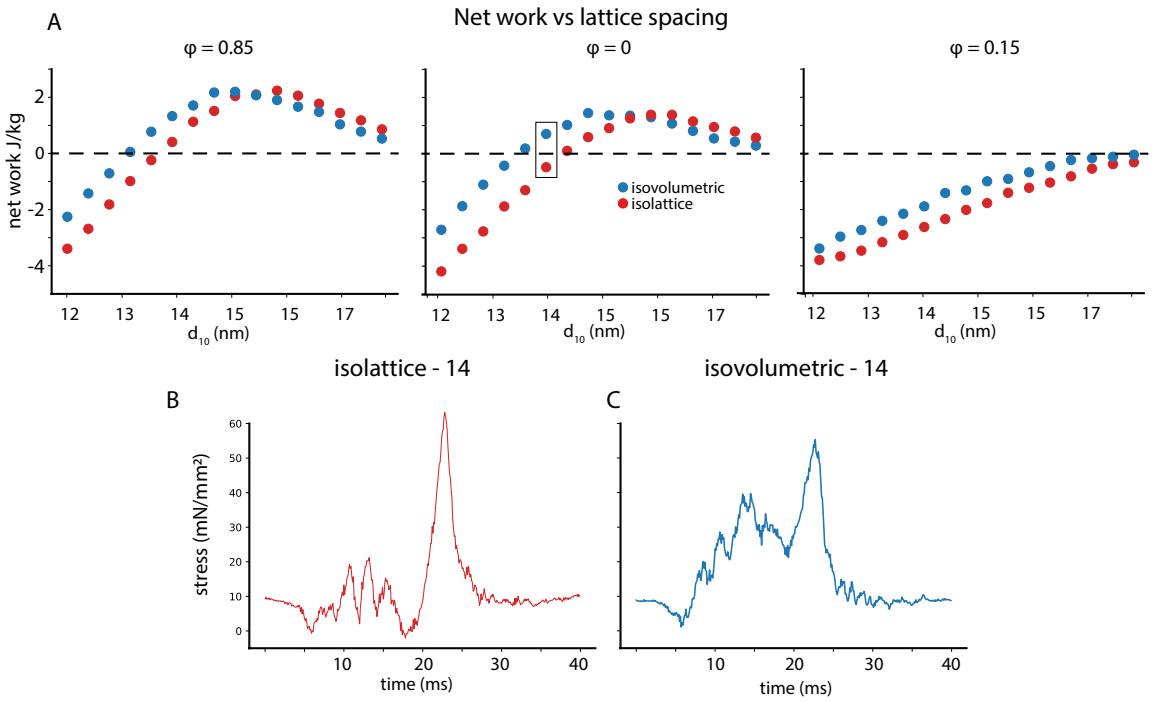

Figure 3.8: A) We show the net work at phases of activation of 0.85, 0.0, and 0.15 under conditions in which the lattice spacing was either constant (isolattice, red), or changed with sarcomere strain (isovolumetric, blue). For isovolumetric conditions, the lattice spacing indicated is the lattice spacing at a strain of 0. We found that the lattice spacing of peak net work shifted to lower d_{10}s under isovolumetric conditions. The box at 14 nm at a phase of activation of 0 indicates the data in B and C. B) shows the stress vs. time for isolattice conditions at an actin-myosin spacing of 14 nm and a phase of activation of 0.0. B) shows stress vs time for isovolumetric actin-myosin spacing changes when the 0 strain spacing was 14 nm.

3.5 Discussion

The updated 2sXB can simulate realistic scales of mechanical work under dynamic conditions and supports the hypothesis that nanometer scale changes in the myofilament lattice can significantly effect the mechanical output of whole muscle. Previously, we showed that lattice spacing differences on the order of 1 nm in two muscles in the cockroach *Blaberus discoidalis* were associated with their different mechanical functions. However, we could not definitively shown that the lattice spacing differences observed were responsible for, rather than just correlated with, modulating work. Our updated 2sXB model results suggest

that the lattice spacing alone has the potential to drive mechanical functional differences, for example switching a motor to a brake.

There are two sources of lattice spacing changes to consider. Time varying spacing can arise from a combination of axial strain and the active production of radial force by myosin crossbridges. Passive offsets in lattice spacing between two muscles, as seen in the cockroach muscle can arise from different radial stiffness and equilibrium position in the lattice likely determined by the titin-like anchoring proteins. In the second test we chose to show the impact of isovolumetric changes, however, the lattice spacing is not necessarily isovolumetric. While we do not know how the lattice spacing's relationship with length is set in muscle, it seems to be muscle specific [29, 32, 31]. However, even though real muscle has a very complicated structure, including many more elements than are in our model, we are still able to show the potential for lattice spacing to affect net work.

The stiffness of the filaments and crossbridges has been shown to be a key parameter in muscle force production in spatially explicit models [99, 58, 33, 63]. In general, there is a trade-off in that high compliance in the thick and thin filaments allow more crossbridge binding, but less force per crossbridge [63]. Also, by increasing the stiffness of the myosin heads, thermal forcing in the unbound state is reduced, which can reduce the number of heads which bind. Higher stiffness, however, can increase the force that each crossbridge can produce. These kind of interacting effects currently can only be shown in a spatially explicit model.

The effects of activatable titin could have a large effect on the amount of work produced. In [58] it was shown that by increasing the stiffness of titin, crossbridge binding could be increased, however force production was lower. They also predicted that stiffening titin could also decrease the negative work produced. By introducing activatable titin, we might expect an even more dramatic dependence of net work on lattice spacing.

Other limitations of the model are the fact that crossbridge attachment in muscle generates not only an axial force, but a radial one as well [33, 35]. This radial force can either

push or pull the actin-myosin spacing in or out. This means there is a coupling between the lattice spacing and crossbridge recruitment. Currently we prescribe the lattice spacing changes, meaning there is no explicit coupling between radial spacing and radial force of the crossbridges present in the model currently. However, future versions could incorporate this behavior, after measuring the effective radial stiffness of the lattice. This could affect the work since crossbridge recruitment could deform the lattice, resulting in more or less crossbridge recruitment. This would require experiments aimed at measuring the radial stiffness of the lattice and sarcomere.

Even though the spacing change is small, it can have a large effect. In most physiological conditions, binding transitions are less likely at higher lattice spacings, as are power stroke transitions. However binding events are also able to generate more force, enough to cause positive work, in contrast to the net work at lower lattice spacings. Furthermore, this effect can be multiscale, since the lattice spacing of a sarcomere will depend on the length of each sarcomere, which may not be uniform in the whole muscle [111]. This means that as muscle oscillates, the lattice spacing can be a determinant of muscle force within each sarcomere, which then influences the length, and therefore lattice spacing and force, of its neighbors [17, 83].

The difference in work between the pair of muscles in *Blaberus discoidalis* was 2.386 $\pm$ 1.8 [16], and the d_{10} spacing difference was 1 nm [31]. In our model with a 1 nm actin-myosin spacing change, meaning a 1.8 nm d_{10} change, the model produced a difference of .6 J/kg. While these work differences are not as large as those in *Blaberus discoidalis*, there could be several reasons why this is so. First, our model lattice structure is based on that found in vertebrate muscle, whereas we want to compare our model to an invertebrate flight muscle *M sexta*. Not only that, but invertebrate limb muscle, such as that found in [31], has a different lattice structure compared to either vertebrate or invertebrate flight structure. Also the stiffness of the spring elements of the filaments and crossbridges can greatly affect the force [63, 99]. However, despite these limitations, we found that we were

able to produce physiological levels of force and work.

3.6 Conclusion

We were able to show in a spatially explicit model with explicit radial spacing difference that we could obtain physiological amounts of force and net work. We showed that the lattice spacing could affect the net work in such a model. This model provides a framework for examining how the biophysics and spatial arrangement of force production in muscle can scale through sarcomeres to the whole muscle scale.

3.7 Model availability

This model will be made available as a github repository.

3.8 Acknowledgments

We would like to thank Tom Daniel, Dave Williams, Joe Powers, and Anthony Asencio for their helpful discussions.

This work was supported by grant W911NF-14-1-0396 from the Army Research Office, National Science Foundation Early Career Development Award MPS/PoLS 1554790, and the Georgia Tech Dunn Family Professorship to S.S. Other support was provided by the National Science Foundation SAVI student research network in physics of living systems (1205878). The original 2sXB model was originally developed with additional support from Army Research office grant W911NF-13-1-0435.

CHAPTER 4

CONNECTING THE DYNAMICS OF MYOFILAMENT NANO-STRUCTURE TO MACROSCOPIC FUNCTION IN INVERTEBRATE FLIGHT MUSCLE

4.1 Introduction

While many biological materials and structures are hierarchically arranged, muscle is unique in that it is both highly ordered and active [19]. Billions of myosin motors are able to form crossbridges between actin-containing thin filaments and myosin-containing thick filaments which generate stress and strain [57]. Muscle is also incredibly versatile, able to meet the changing demands needed for locomotion [4, 10]. Although muscle's structure is very complex, the fact that it is so highly ordered means that x-ray diffraction crystallographic techniques can be used to study its structure [28]. With high speed x-ray detectors, it is possible to study muscle's changing nanometer-scale structure with millisecond-scale time resolution [35, 55, 30, 32, 2, 31]. This makes it possible to infer nanometer-scale mechanisms for the macroscopic performance of muscle.

However, there are limitations to bridging these scales. Tests of many specific mechanistic hypotheses are done under quasi-static conditions, such as constant length or velocity, as well as activation [55, 112]. These can provide support for specific mechanisms, but it can be challenging to connect the results to the versatile function of muscle under dynamic conditions. On the other hand, time resolved work loops with simultaneous x-ray diffraction have either not focused on force production and mechanical function [97], could only

This chapter is the result of collaborative work with Dr. Weikang Ma (IIT/Argonne NL), Prof. Thomas Irving (IIT/Argonne NL), Jeff Gau (Georgia Institute of Technology), and Dr. Brett Aiello (Georgia Institute of Technology). They will appear as co-authors on the final journal manuscript. The current dissertation chapter was written and prepared by Travis Tune.

resolve the primary diffraction peaks [2], or have not be able to replicate full strain amplitude and frequency or physiological work output because of the challenges in maintaining intact muscle viability in the x-ray [2, 31, 56]. Still other studies have looked at the high speed structural data in intact animals such as bees and moths which are undergoing tethered flight [32, 30, 10]. This approach allows the muscle being investigated to operate as close to the *in vivo* conditions as possible while measuring structural data. Unfortunately, it also means that measuring force, as well as prescribing consistent strain and activation patterns is impossible, which necessitates making assumptions about how structural data relates to macroscopic measurements, which are based on quasi-static results like those mentioned above. Moreover, recent work has shown that the structural changes in intact animals are quite variable from individual to individual [32].

We wanted to see if we could test whether hypotheses about muscle structure and mechanisms established under quasi-static conditions could be examined under dynamic work loops. To do this we need to first establish that we are able to get net work consistent with established values and that the structural data we record during work loops is consistent between individuals. We chose the dorsal longitudinal muscles (DLM) of the hawk moth *Manduca sexta* to do this. We chose *Manduca sexta* since its *in-vivo* activation, strain trajectory, frequency, and work dependence on phase of activation have all been well characterized [12, 44, 11]. We can also compare our results with structural data taken from intact animals during tethered flight [32]. There, it was found that variation from individual from individual was quite high, possibly because specimens were free behaving. In this paper, we sought to test four specific hypotheses that form the basis for conclusions of the molecular structure to macroscopic function relationship. First we examine whether a high degree of variability from individual to individual in the fully intact animal preparations is a general feature of structural data acquired under dynamic conditions or comes in part from variables that cannot be controlled without an isolated muscle preparation. It was previously shown that a machine learning model could predict lattice spacing from structural

data in a tethered, intact, behaving *M sexta* well within individuals, but could not be generalized across individuals [32]. If it were possible to develop a model which could predict force in such an experiment across individuals, it could provide a powerful tool for investigating the *in vivo* function of muscle. We hypothesize that by tightly controlling strain, frequency, and stimulation we could constrain variability between individuals and generalize predictions across individuals. We performed work loops at *in vivo* strain frequency and amplitude at different phases of activation in order to drive the muscle into different regimes to explore how structural data relates to macroscopic measurements like force.

Second, it has previously been thought that the spacing of the 7.2 nm meridional peak reports (see figure 4.1) on strain in the myosin filament backbone [113, 114, 54]. Because tension in the myosin filament, either from crossbridge binding or passive sarcomere stretch, strains the filament backbone, it is assumed that axial force can be related to changes in the 7.2 nm reflection. The relationship between the 7.2 nm reflection (called the M6 in vertebrates) and force has been shown to be nonlinear, possibly due to nonlinear elasticity in the myosin filaments [55]. However, this relationship was established under isometric conditions in vertebrate muscle. The presumed one-to-one relationship between the 7.2 reflection and force is important for conclusions from intact preparations. For example, is used to investigate stretch activation in high frequency invertebrate muscle [30, 115], although it hasn't been verified under such conditions. This was done by comparing the timing of force with other structural signals after stretch. We predict that the same relationship would be true in work loops, and that even at different phases of activation the 7.2 nm reflection should have a one-to-one relationship with force. Alternatively, the relationship may be more complex either because of Ca^{2+}-modulated stiffness of some of the titin-like proteins that anchor the thick filament to the z-disk, or because of the proposed mechanosensing activation of thick filaments in vertebrates which has been linked to changes in the 7.2 nm peak [116].

Our third hypothesis concerns the 14.2 nm peak (called the M3 in vertebrates) has been

proposed to report the configuration of the myosin heads rather than thick filament strain [113, 53]. Specifically, the intensity of the peak reports the angle of the heads and the spacing of the peak reporting the spacing between myosin heads. It was shown in [55] that the 14.2 did not change when passively strained, but had a nonlinear relationship with force under active force. If this relationship holds in dynamic muscle, we should expect that the spacing and intensity changes of the 14.2 nm peak in *M sexta* are minimal under passive conditions and vary strongly with phase of activation, rather than having a constant one-to-one relationship with force like the 7.2 nm spacing.

Finally, we test the basic assumption that the 7.2 nm and 14.2 nm peaks are in fact reporting different structural elements in the thick filament, the filament backbone and myosin head configuration respectively [53, 54, 55]. The models and experiments supporting these assumptions are usually based on vertebrate muscle. These assumptions are then sometimes used in intact invertebrate muscle however [30]. However, it has been shown in tarantula muscle that both the 7.2 and 14.2 nm peaks report both the filament backbone and myosin head configuration.

4.2 Materials and Methods

4.2.1 Animals

Specimens of hawk moths were shipped from the University of Washington which maintains an *M sexta* colony. Specimens were 1-2 days post eclosion. Prior to being shipped specimens had their wings and legs removed and were kept moist to prevent desiccation. We kept specimens at 5°C during storage as well as during dissection, only warming specimens to *in vivo* temperature immediately prior to data collection. Our sample size for each condition is indicated in Figure 4.1.

4.2.2 Muscle physiological preparation

Our work loop set up was similar to those found in [12, 11, 117, 3, 2, 32] (Figure 4.1). In brief, we isolated the main thoracic cavity by removing the first thoracic segment and the abdomen. Leaving the second and third thoracic segments intact, we severed the connection from the ventral ganglion which activates the main downstroke flight muscle (dorsolongitudinal muscle, DLM). The dennervation removes all spontaneous activity from the muscles. Using calipers, we measured the distance between the anterior and posterior phragmas, which are exoskeletal invaginations that form the origination and insertion for the DLM, and we defined this length as L_{rest}. We used an ergometer or muscle lever (model 305c, Aurora Scientific, Aurora, Canada), and attached a motor arm with two prongs which we lightly coat with cyanoacrylate glue and inserted into a gap between the posterior phragma and the third thoracic segment. We glue the anterior phragma to a rigid 3D-printed ABS plastic block that has been shaped to the form of the pragma to provide even deformation. Once mounted into the experimental rig, we set the muscle length to .98*L_{rest} = L_0, since the mean length during *in vivo* flight is different from the rest length [12]. We then dissected away the exoskeleton and all muscles other than DLM. During this preparation as well as during experiments, we maintained a stream of *M sexta* saline at 5°C over the DLM. In general we took care to make sure the muscle was never hyper-extended or contracted during the dissection as doing would significantly worsen the performance and durability of the muscle specimen. We ensured that the muscle remained cold up until we wanted to start data collection, since based on our prior experience, this greatly improves the quality and consistency of the diffraction data. After mounting the muscle into the experimental apparatus, we increased temperature to the *in vivo* temperature of 35°C, and all subsequent trials were performed at that constant temperature. After all experiments with each individual were complete, we cut away the DLM from the phragmas and measured its mass. Assuming a density of water (1 g/ml), we estimated muscle cross-sectional area using the length and mass of the muscle.

4.2.3 Simultaneous work loop and x-ray diffraction

Once, mounted, we oscillated the isolated moth DLM (downstroke) muscle with a sinusoidal strain trajectory at 25 Hz with 4.5% strain amplitude, which matches *in vivo* conditions [12]. The *in vivo* phase of activation during flight had been determined via extracellular recordings to be at the start of shortening (.99 $\pm$ .04 [11]), where we define start of shortening as a phase of 0. The entire muscle is innervated by 5 motor neurons each innervating one subunit, but since all fire in synchrony and only produce a single action potential per wing stroke during flight, we could mimic activation with a single 6 V, .5 ms extracellular pulse delivered via a extracellular stimulator (Model 1700 Differential AC Amplifier, A-M Systems, Sequim WA) [3, 118]. We then extracellularly stimulated the muscle at different phases during the strain cycle, first at the *in vivo* phase of activation and then at other phases to explore variation in the force and mechanical work output of the muscle. We measured force and length of the muscle with a dual mode muscle lever while simultaneously recording x-ray diffraction images. We first measured the work done under passive conditions, then measured work under a phase sweep consisting of 10 phases from 0 to 0.9 (proportion of the period, relative to start of shortening) in an order randomized for each individual. Via a video camera inline with the beam, we were able to target the middle half of the C and D subunits between different individuals. We moved the beam a small amount after each trial to mitigate radiation damage.

X-ray images consisted of 1 ms exposure with 1 ms readout time (500 Hz sample rate), and we recorded 20 frames per work loop cycle (25 Hz). Beam flux was 10^{13} photons/s and beam width was 30 by 150 μm at a wavelength of .103 nm. We chose not to attenuate the beam intensity since we wanted to see the fainter meridional peaks. Since the beam shutter speed was too slow, we had to leave the shutter open for each full trial, which was 400 ms for work loops. These factors meant that each individual muscle's viability decreased as experiments continued, but was necessary for the high time resolution and to see the fainter meridional peaks. Diffraction images were recorded on a Pilatus 3 1M pixel array detector

(Dectris Inc).

4.2.4 Data analysis

Work loop experiments consisted of 10 cycles. We phase averaged by taking x-ray frames from the same point within a length cycle from different work loop cycles within the same trial. This improves the signal to noise ratio allowing us to detect fainter peaks. X-ray images were then analysed using MuscleX, a software suite developed by the Illinois Institute of Technology in collaboration with the BioCAT beamline [119]. Because x-ray diffraction images are symmetric, using MuscleX, we can average each of the four quadrants to further improve the signal to noise ratio. Then by taking the intensity profile through the equator and meridian, the intensity and spacing of each peak can be found. We also background subtracted by fitting a circularly symmetric spline to each image. Background subtraction further enhances signal to noise ratio. Data was then filtered using a robust locally weighted regression method (*smooth - rlowess* method, Matlab 2020a, MathWorks). We used this method since it is a high-pass filter which rejects large outliers, since some trials occasionally had individual frames which had low signal to noise, usually when the muscle was most compressed.

We used the mean intensity of the subtracted background in order to assess image quality. Since noncrystalline elements in the muscle increases the amount of scattering, higher intensity backgrounds can be indicative of loss of integrity in the muscle. Trials in which the background scatter had increased by more than 30% relative to the passive work loop (which was always taken first) were rejected as a threshold for when too much x-ray damage had occurred. We also assessed image quality by the intensity of the 10 peak. Trials in which the mean I_{10} had diminished by more than 75% relative to the passive work loop were rejected. Because damage could also compromise physiological function, we also rejected trials that were outliers in terms of net work, as determined by being outside the interquartile range. In each individual we randomized the order in which we did each phase

of activation. We found that in general the trials we later rejected based on image quality or net work were in the last 2-3 trials of each phase sweep.

Sample to detector distance was found by taking diffraction images of silver behenate, which has a known 5.83 nm spacing. In our analysis, where data is shown as percent change, it is relative to the average value at 0% strain during that preparation's passive work loop. During work loops, there are two frames taken at 0% strain, one at t=0, and one at t=20 ms, which we averaged in order to normalize.

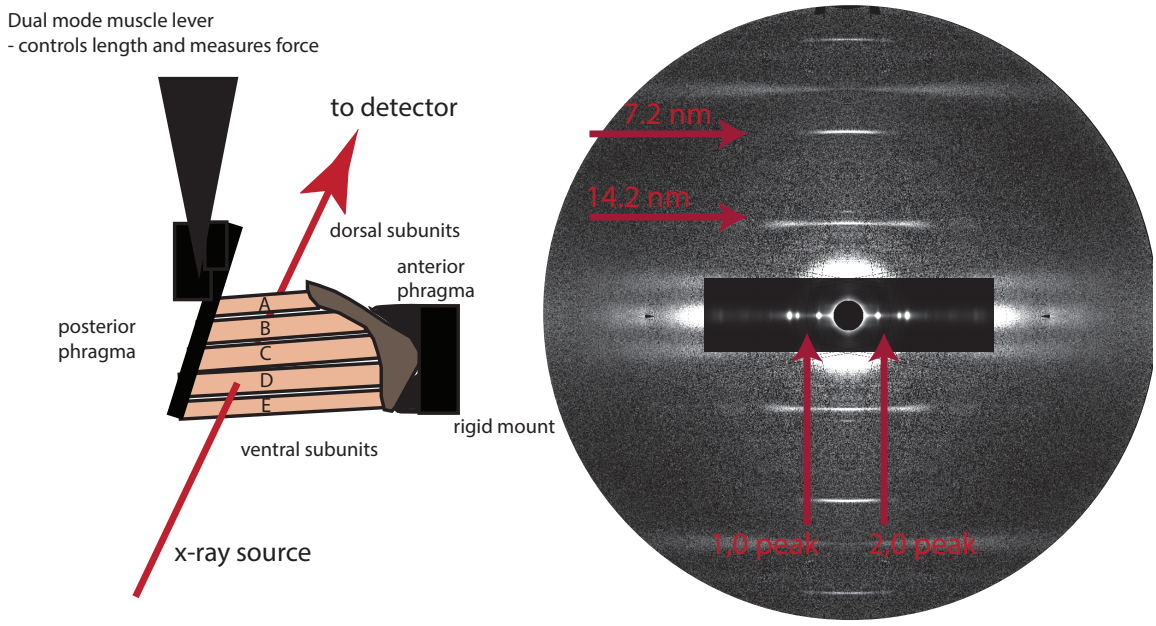

Figure 4.1: Here we show a sketch of the experimental set up with the x-ray beam passing perpendicular to the muscle axis of contraction. We also show an example diffraction image. The brighter inner peaks along the equator are shown on a different intensity scale than fainter outer peaks. The (1,0) and (2,0) peaks indicate the thick-thin filament spacing and the crossbridge binding fraction can be inferred. The 7.2 nm peak is thought to report changes in the thick filament backbone. The 14.2 nm peaks is thought to report changes in the myosin head.

4.3 Results

4.3.1 Force and mechanical work is consistent with prior muscle preparations

Our results show good agreement between the work-phase sweep we recorded with simultaneous x-ray fiber diffraction and data originally established in [12] (Figure 4.2 B). Comparing our data set with data from [12] (Fig.4 C, red) we found no statistical difference between work at phases of 0.9-0.5 ($p = .07$, *ttest* - Matlab 2020a). While we did find statistically significant differences at phases of 0.6, 0.7, and 0.8. The largest difference was at a phase of activation of .8, and was 1.5 $\pm$ .36. This is likely because the data we compare to in [12] is from a single individual. We also note in [12], each individual's *in vivo* conditions were measured during tethered flight and used for that individual's work loop measurements, whereas we used the global mean found in [11, 12]. Overall work varied from a maximum of 2.0 $\pm$ .36 to a minimum of -2.4 $\pm$ .6 with 1.3 $\pm$ .2 at the average *in vivo* phase (means $\pm$ 95% confidence of the mean). These results are in contrast with prior experiments on hawkmoth flight muscle that were unable to realize the same large amplitude strains and work output because of experimental limitations in the in the X-ray experimental apparatus [2]. While work outputs comparable to natural locomotor conditions were not critical for the conclusions drawn in prior studies they were necessary to test hypotheses here.

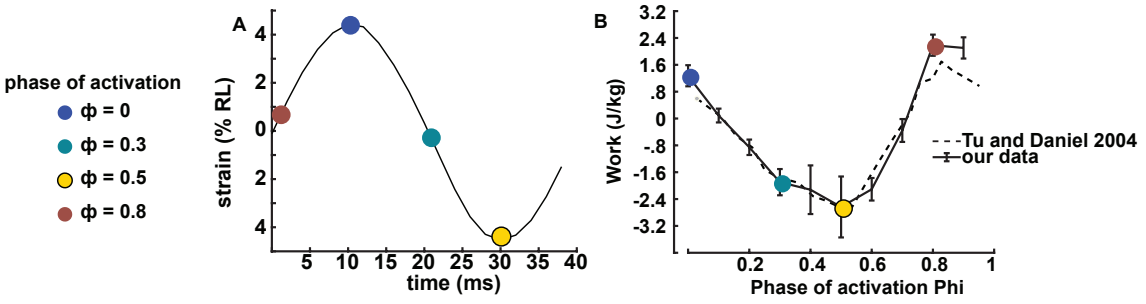

Figure 4.2: Here we show the strain changes imposed on the muscle during work loops as well as the time of activation. We then show the phase sweep response we obtained (mean $\pm$ standard deviation) and compare to the values established in [12].

4.3.2 A Consistent Relationship between Myofilament Structure and Force

When time resolved structural data is acquired in a freely flapping animal there is frequently large variation in the patterns of data making it challenging to infer force from features of the diffraction images. In contrast, one the muscle is isolated and controlled for damage and consistent target location, consistent patterns are evident. We saw that the individuals examined had very large baseline offsets with the mean d_{10} spacing of different passive trials with a mean of 46.9 nm, but a standard deviation of 1.8 nm (Figure 4.3 A). However, when we normalized each measurement in a trial with its corresponding passive value at 0 strain we found consistent behavior between individuals. What is immediately noticeable is that the passive change in lattice space can be quite substantial, and that there are stereotyped differences between the different phases of activation. For example, peak-to-peak change in d_{10} spacing at a phase of activation of 0.0 was 3.95 $\pm$ .57% while at a phase of 0.3 the peak-to-peak change was 2.85 $\pm$ .9 (mean $\pm$ 95% confidence of the mean). A one way ANOVA of the peak-to-peak d_{10} spacing showed a significant effect of phase of activation (p=.0003), which was sinusoidal across all phases of activation (Figure 4.3, C). We also found a statistically significant effect in the phase of the fundamental frequency component of the intensity ratio $\frac{I_{20}}{I_{11}}$ ($p < 10^{-7}$), which was bimodal, peaking at phases of 0.1 (17% $\pm$ 1%) and again at 0.5 (17% $\pm$ 1%).

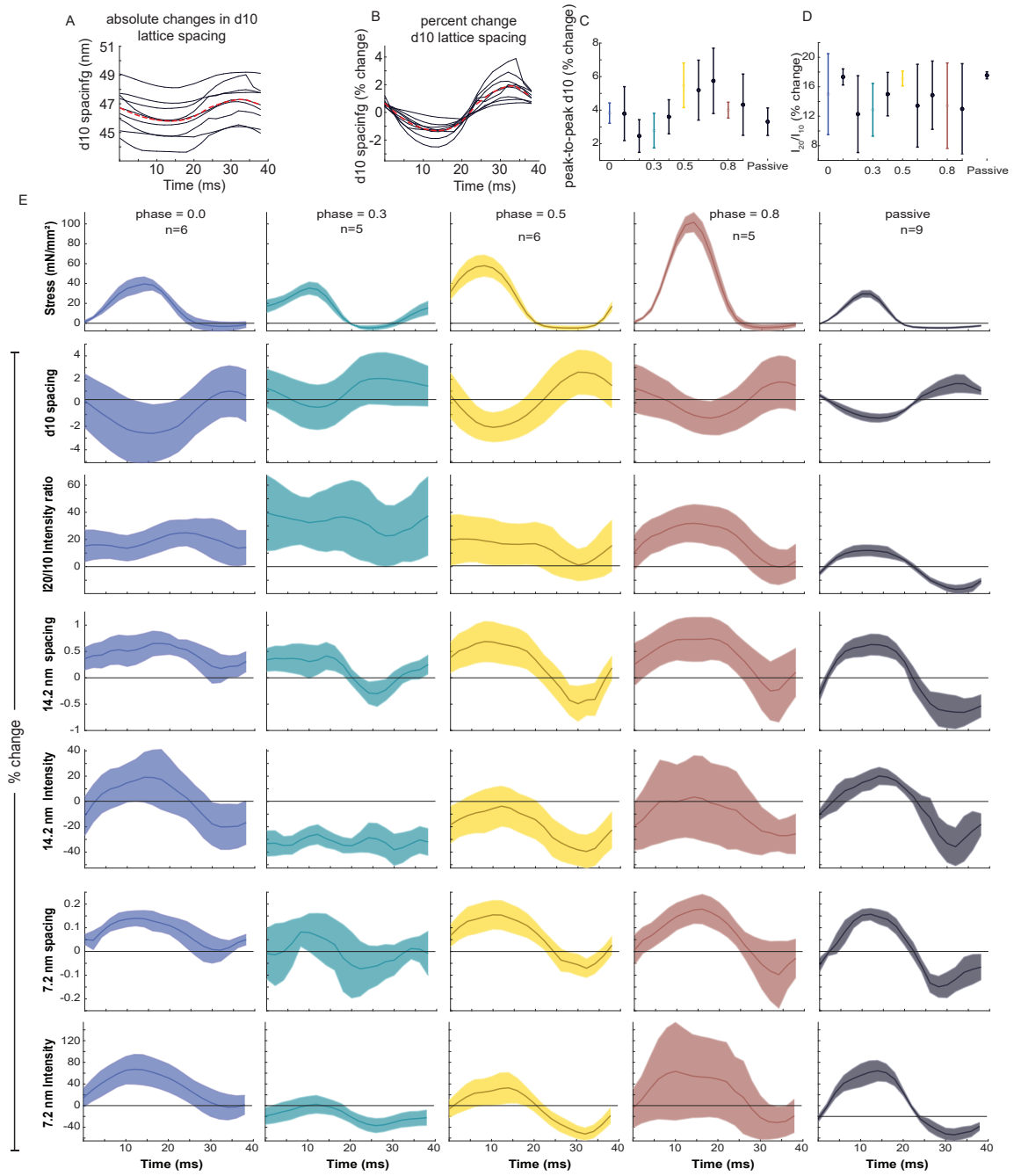

Figure 4.3: A) shows the raw d_{10} spacing changes in units of nm. The red dotted line indicates the mean. B) Shows the same data as percent change relative to the value at 0 strain. C) Shows the time course of stress in units of (mN/mm^2), as well as the d_{10} spacing, $\frac{I_{20}}{I_{11}}$ intensity ratio, 14.2 nm spacing and intensity, and the 7.2 nm spacing and intensity, all as percent change from the within individual passive value at 0 strain. This data is shown as mean $\pm$ 95% confidence interval of the mean. In order from phase of activation of 0 to 0.9, our sample size was 6, 6, 5, 5, 4, 5, 4, 5, 5, 5, and for passive work loops was 9.

The fact that we could find stereotyped differences in the structural data we recorded between phases of activation suggested to us that we could predict phase of activation or force based on the x-ray data we had taken. We first used a long short term memory (LSTM) classifier and predictor [120] to test if we could classify phase of activation based just on the d_{10} spacing and intensity ratio. The LSTM architecture is based on Recurrent Neural Network (RNN) architecture in which cells in the RNN layer output to the cell which represents the next point in the time series as well as cells in the next layer (figure 4.4, A o_t). In an LSTM, there is also a second output within the LSTM layer which carries long term relationship information (figure 4.4, A h_t) [120]. In our model we had the LSTM output into a fully connected layer, followed by a 50% dropout layer (to avoid over training). Because we needed many trials on which to train, for this we chose not to phase average, and instead let each of the 10 work loops from each trial be one instance on which to train. However, without phase averaging, the 7.2 and 14.2 nm peaks weren't intense enough to consistently produce clear signals. Therefore we only trained on the d_{10} and intensity ratio. We trained on 60% of the data and tested on 40%.

To obtain a benchmark for accuracy, we first attempted to predict phase of activation by training on the time series of force produced by the muscle. We found that force could predict phase of activation with 87.4 $\pm$ 1.3% accuracy. We then trained on the d_{10} and intensity ratio. With either feature alone, we obtained accuracies of 63.1 $\pm$ 3.2 and 55.69 $\pm$ 1.3, respectively. When we trained on both features together, our accuracy rose to 76.3 $\pm$ 1.0. In most (26.4%) cases where where the classifier failed, it predicted a phase of activation that was off by only 0.1, an off-by-one error (Fig 4.4 B).

We next tried to predict force itself, rather than just the categorical phase variable. We attempted to predict the time series of force from simultaneous d_{10} and the I_{20}/I_{10} intensity ratio. We found that we could get reasonable force predictions from these features in most trials. Figure 4.4 highlights predicted force traces and their fits for 9 random trials. To compare the predicted fits to the actual values we calculated an R^2 (coefficient of deter-

mination: $1 - \frac{SS_{res}}{SS_{total}}$, where SS_{res} is the residual sum of squares, and SS_{total} is the total sum of squares). 77% of our model's predictions had R^2 values better than 80%, and 51% had R^2 values better than 90% (figure 4.4 D). We obtained a negative R^2, which can be interpreted as models that are entirely not predictive, in only 5% of cases.

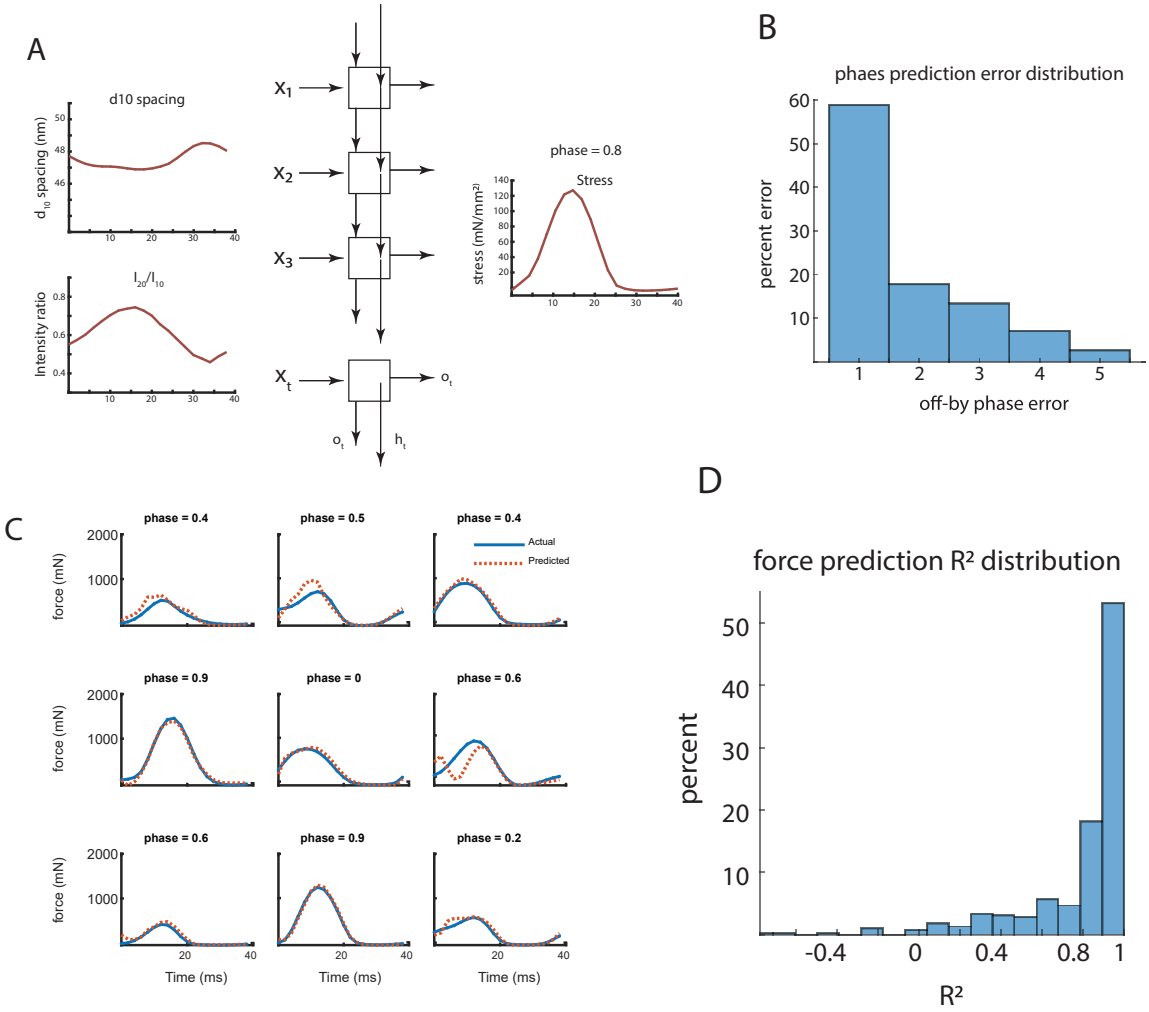

Figure 4.4: A) shows a representation of the LSTM architecture, as well as two sample inputs (d_{10} and $\frac{I_{20}}{I_{11}}$). The inputs x_t are composed of the times series of both d_{10} and $\frac{I_{20}}{I_{11}}$. Each cell in the LSTM layer outputs both to the cell representing the next point in the time series as well as the next layer in the network (o_t). Each cell also outputs into the next cell longer range dependencies in order to capture the history in the system (h_t). We trained two separate models on the same data, one which predicted the categorical phase, and one which predicted the times series of force. B) Shows the distribution of errors made by the phase classifier. It shows that when we predicted off both d_{10} and $\frac{I_{20}}{I_{11}}$, of the 24% of time when an error was made, 60% were errors in which the phase prediction was off by one. C) Shows nine example fits chosen at random from the data we predicted off of. D) Shows the distribution of R^2 vales for the predictions we obtained.

4.3.3 Hysteresis in the position of the 7.2 nm reflection spacing and force

Quasi-static single fiber experiments on vertebrate muscle have shown a ono-to-one relationship between the position of the 7.2 reflection and force [55], which has been used to compare the relative timing of other structural changes in intact preparations. In the periodic stress and strain conditions of the work loops we find the position of the 7.2 reflection does correlate with muscle force consistently (Pearson's linear correlation coefficient ρ = .87 $\pm$ .08 at a phase of activation of 0 (figure 4.5 A,B). As before the relationship is nonlinear with a steeper initial response. The peak-to-peak change in the 7.2 nm peak spacing is significantly reduced compared to the percent change from [55] at similar stress values, at most 0.34 $\pm$ .18% during peak force (phase of activation of 0.8), likely because of the presence of paramyosin in invertebrate thick filaments, which makes thick filaments much stiffer [121].

Most significantly, we also found that while the average response of the 7.2 nm spacing with respect to force was qualitatively similar to previous results, the response was not one-to-one. Instead there was hysteresis in the force- 7.2 nm spacing relationship, which would not be expected based on the prior quasistatic results. We quantified the amount of hysteresis by calculating the cross correlation between the two signals in order to determine the timing differences between the two signals (figure 4.5 C). We found in the passive case that stress lead the 7.2 nm spacing by 2 ms, or 5% of the total period (maximum linear correlation coefficient, ρ = .82 $\pm$ .07), and that depending on the phase of activation the phase difference could be between -2$\pm$3.5 ms and 3.4$\pm$6.5 ms. Positive differences indicates the 7.2 nm spacing lags stress development.

Previous relationships between the 7.2 reflection and force were able to quantify the amount of the passive force due to intracellular (titin-based) components and extracellular matrix. Because extracelluar matrix contributes to the passive force in muscle without necessarily straining the thick filaments, we do not expect the force due to extracellular matrix to correlate at all with the 7.2 nm peak spacing. In [55], they accounted for this by

chemically depolymerizing the thick and thin filaments, which allowed the passive force of the extracellular matrix to be measured and subtracted from the total force, retaining titin-based passive force.

Since our measurement of force includes extracellular contributions to force, we might expect a small phase difference due to viscoelastic effects. However, [55] concluded that passive titin-based stress due to filament strain had the same effect on the 7.2 nm spacing as active force due to myosin cross bridge binding. We therefore account for this potential confounding factor by subtracting the total (titin-based and extracellular based) passive force and total passive 7.2 nm spacing changes. If the hysteresis between the two signals was due to extracellular effect then it should disappear with this correction. Instead, we found that the timing differences of the hysteresis changed significantly, with the largest change being at a phase of activation of 0.7, from 2.4 ms $\pm$ .7 ms to 12.8 ms $\pm$ 5.3 ms ($p = .005$ *t-test*, mean $\pm$ 95% confidence of the mean).

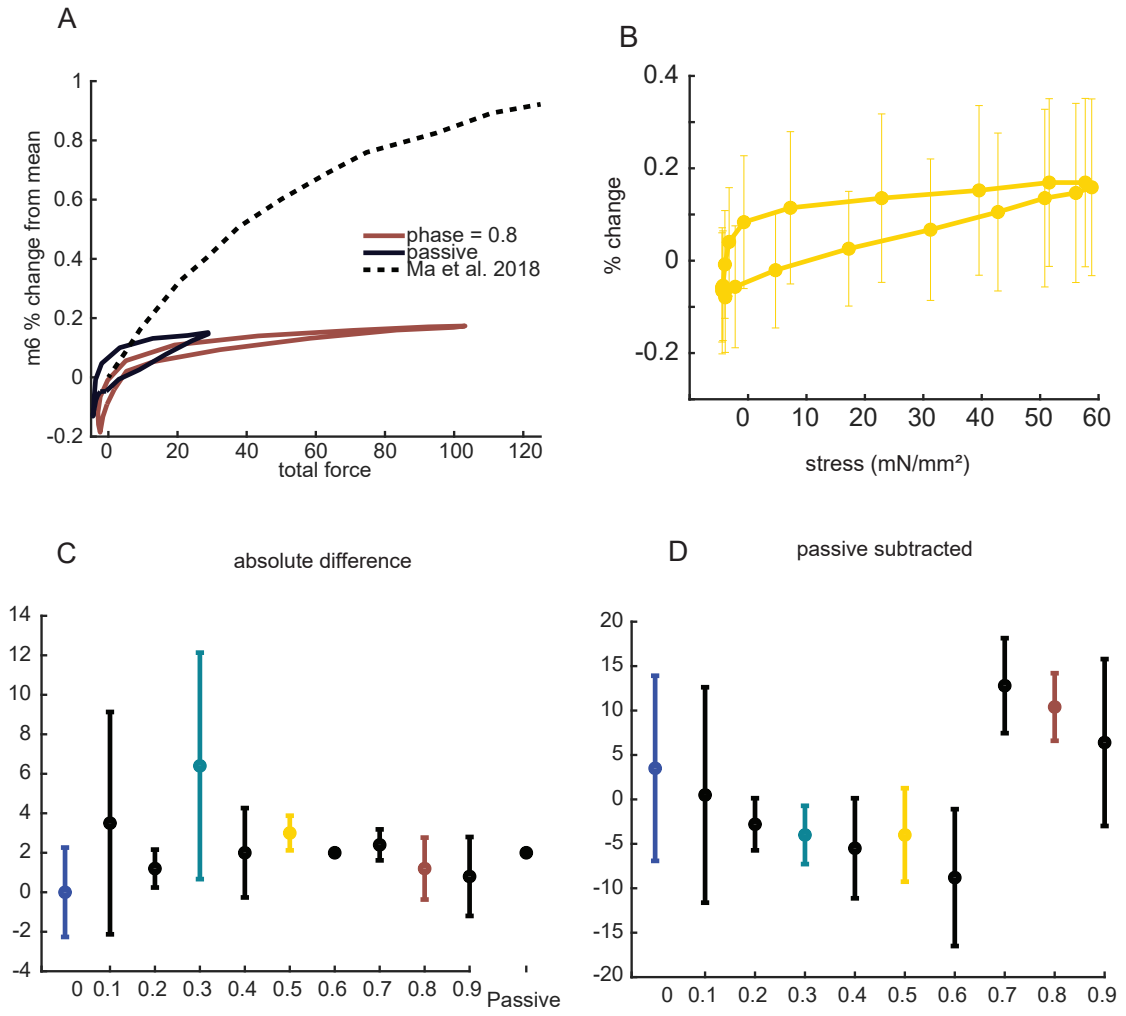

Figure 4.5: A) We plot the force vs 7.2 nm spacing changes during work loops, which we plot along with data from [55], which was taken from isometrically tetanized mouse EDL muscle. For clarity, here we plot only the mean passive and mean ϕ = 0.8 responses. B) Here we plot the stress vs. 7.2 nm changes for ϕ =0.5 in which the timing differences between the 7.2 peak and force were maximal, along with error bars showing standard deviation. C) We quantified the amount of hysteresis between the 7.2 nm spacing and stress by calculating the cross-correlation to determine the lag between stress and the 7.2 nm spacing, with positive differences indicating the 7.2 nm spacing lagged stress development. D) Here we plot the timing difference the 7.2 nm spacing and stress and found when the passive force and passive 7.2 nm spacing responses were subtracted. Since the period is 40 ms, timing differecnes wrap at -20 and +20 ms.

4.3.4 Changes in 14.2 nm reflection intensity are larger in passive than in active muscle

The intensity of the 14.2 nm peak is thought to indicate the angle of the myosin head relative to the thick filament [112]. To test this, we examine the 14.2 peak intensity under passive and active conditions. Contrary to expectation, we find a much larger amplitude of intensity change in passive work loops than in active work loops. At the *in vivo* phase of activation of 0, the peak-to-peak change in the intensity of the 14.2 nm peak was 45% $\pm$ 18.2%, while in passive work loops the peak-to-peak intensity change was 71.5% $\pm$ 18% ($p = .03$, *t-test*, means $\pm$ 95% confidence of the mean). When we look across all phases of activation, we found a statistically significant effect in the peak-to-peak intensity change with respect to phase of activation ($p = .005$, one way ANOVA). This might indicate that activation minimizes peak-to-peak angle changes during work loops in *M. sexta*.

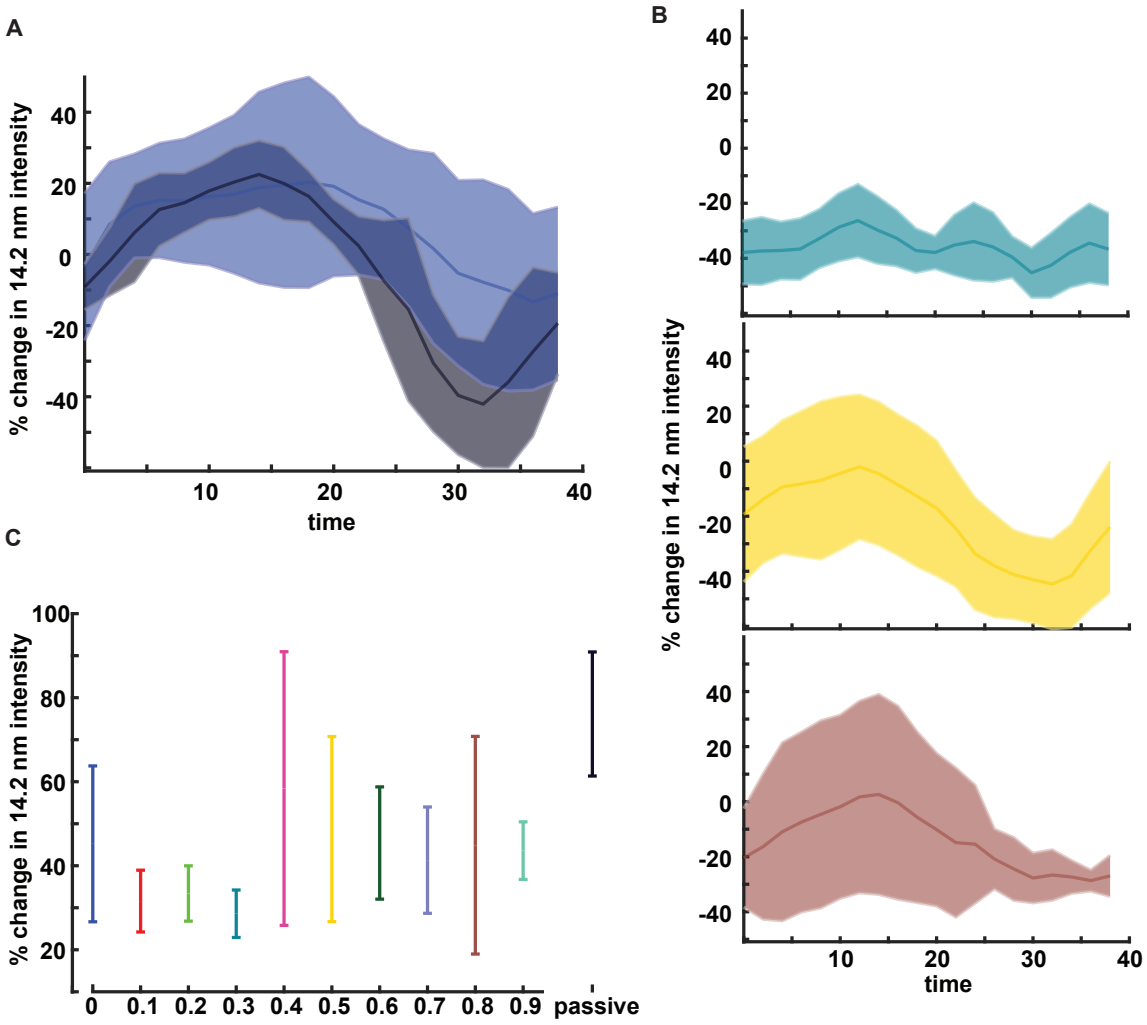

Figure 4.6: A) shows the percent change in intensity of the 14.2 nm peak under passive (black) and work loops with a phase of activation of 0, the *in vivo* condition (blue). B shows the percent change of the intensity of the 14.2 nm peak under phases of activation of 0.3, 0.5, and 0.8. C) shows the mean peak-to-peak amplitude of the 14.2 nm intensity changes during every phase of activation. We saw the amplitude was lower at almost every phase. Since the intensity of this peak is thought to relate to the angle of the myosin head relative to the thick filament, this seems to indicate the myosin head angle is constrained during active work loops compared to passive.

4.3.5 Passive changes in the 14.2 peak spacing were also larger than active work loops and comparable to changes in the 7.2 peak.

The 14.2 nm peak is thought to report changes in myosin head spacing, rather than thick filament backbone strain like the 7.2 nm peak. From previous quasistatic results [55], where

crossbridges are all presumably unattached in unactivated muscle, we expected minimal changes in the 14.2 nm peak spacing during passive work loops and larger spacing changes changes (about 1%) during work loops. We instead found that the change in the 14.2 nm spacing had a peak-to-peak change of $1.6 \pm 0.39\%$ during passive work loops, and during the *in vivo* phase of activation of 0.0 the 14.2 nm spacing was actually constrained with a peak-to-peak change of $0.5 \pm 0.29\%$ ($p < 10^{-3}$, *two sample t-test*, 4.7). More generally, when we considered only activation during shortening (phases of activation 0.0, 0.1, 0.2, 0.3, and 0.4) we could detect no statistically significant difference between the subset of phases ($p = 0.7$, one way ANOVA). Similarly, we found no statistically significant difference in peak-to-peak spacing change for activation during lengthening ($p = .15$, one way ANOVA). However, there is a statistically significant difference between shortening and lengthening ($p = .005$, one way ANOVA). Taken together these patterns of 14.2 peak spacing are comparable to those of the 7.2 peak, and hence seem to report similar changes in structure (compare Fig. 4.7 to Fig. 4.5).

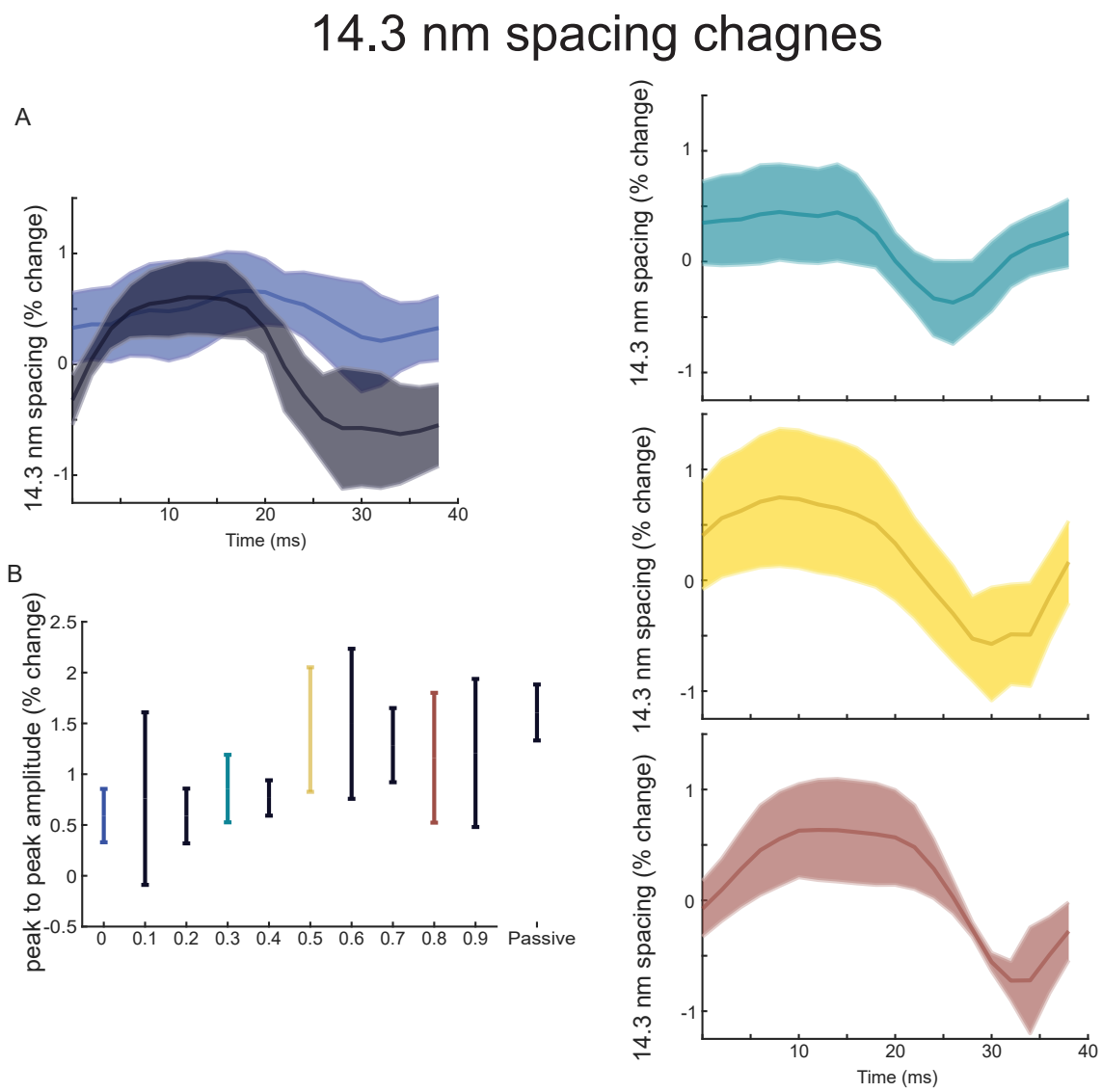

Figure 4.7: Here we show the time series for spacing changes of the 14.2 nm peak at phases of activation of 0.0, 0.3, 0.5, 0.8, as well as unactivated passive work loops. We also show the peak-to-peak changes across all phases (mean $\pm$ 95% confidence of the mean)

4.4 Discussion

By strictly controlling the frequency, amplitude, phase of activation, temperature, and mean offset of a muscle, we were able to obtain structural data from time resolved x-ray diffraction that shows consistent behavior with characteristic patterns that differ with phase of activation. *M. sexta* flight muscle is a synchronous flight muscle that is used a model for

invertebrate muscle function. It is not thought to have the same properties of the specialized asynchronous flight muscle whose mechanisms of strain-dependent activation have been extensively studied with x-ray diffraction methods [51, 115, 30]. However it does seem to share some of the same underlying and most important features. Neither the synchronous nor asynchronous flight muscle has been investigated with time resolved fiber diffraction under intact, physiological conditions that produce comparable force and mechanical work to *in vivo* conditions. As a result several hypotheses or assumptions have necessarily gone unexamined. In contrast to expectations we find that in this intact muscle preparation that the 14.2 nm intensity changes were quite large under passive conditions. We expected them to be small based on results seen in passive stretch experiments [55]. However, passive changes have been seen in the asynchronous flight muscle of *lethocerus* [56].

4.4.1 Under tightly controlled conditions variability between conditions could be constrained

The fact that force can be predicted from x-ray diffraction has implications for possible experiments. For example, there is a discrepancy between how much power insect flight muscle work loop experiments produce under *in vivo* activation, and the estimated power necessary for flight based on aerodynamic considerations [122]. While the maximum power output of muscle is capable of reaching the necessary output [123, 12], the flight muscles in fact don't operate at peak power *in vivo* [44]. This discrepancy might be the result of the dissection and mounting process, which could, for example, remove the presence of neuromodulators like octopamine which is known to be present during *in vivo* behavior and can increase work output in work loops in locust [124]. While our neural network model might not be reliable enough to be able to predict subtle changes in force, the magnitude of the discrepancy between the estimated power necessary for lift and work loop measurements is quite large, with work loop experiments produce half what is estimated to be necessary [122]. Machine learning models based on *ex vivo* work loops might be able to indicate if

intact, *in vivo* tethered flying insects are in fact producing considerably more force than work loop measurements.

4.4.2 Hysteresis between force and 7.2 nm spacing impacts conclusions about the timing of force production

A common assumption made about the 7.2 nm spacing is that since it is thought to be indicative of thick filament strain, it should be a good indicator of the axial force on the myofilaments. This assumption was checked in [55], in which mouse EDL muscle was isometrically tetanized with simultaneous measurement of the 7.2 nm spacing. They found that when passive stress due to extracellular matrix was subtracted, that passive, titin-based (intracellular) stress due to filament strain had the same relationship with the 7.2 nm spacing as active force due to myosin cross bridge binding. However, even when we account for passive forces which in intact muscle preps could include extracellular viscoelastic forcing, we found that there was a distinct timing difference between force and 7.2 spacing.

Accounting for these timing changes can be important for interpreting data taken from intact tethered animals in which force can not be measured. Although the timing differences seem small, and are in fact minimal at the mean *in vivo* phase of activation, 4 ms represents 10% of the total period of the work loop, and was seen in both active and passive work loops. Previously, timing differences in x-ray diffraction signals have been used to infer mechanisms for stretch activation in *Bombus* [30]. There it was seen that the intensity of off-meridional peaks preceded force development which was inferred from the 14.2 nm peak, not measured. Force (the 14.2 nm peak) was then followed by peaks indicating increased cross bridge binding, presumably from cooperative effects. This timing of this chain of events was determined by the phase component of the dominant frequency of each signal and was less than 10% of the total period [30].

One possible explanation for the hysteresis between force and the 7.2 nm spacing is the activation of a series spring element. For example, invertebrates have proteins analogous

to titin, called projectin, sallimus, and kettin [22]. These proteins, like titin, are expected to be activatable with Ca^{2+}. Activated titin-like molecules respond to Ca^{2+} by binding an intermediate domain (PEVK in titin) to the thin filament. This activation can result in a variable stiffness and equilibrium point which could translate into hysteresis if activated for only part of the contraction cycle. A simple model for these activatable proteins is that they are spring like elements whose stiffness and set point changes with Ca^{2+}. So if we assume the 7.2 nm spacing is reporting the strain within only one spring element (the thick filament) in a system of two series springs, and that the stiffness and set point of the other spring (i.e. projectin, sallimus, or kettin) is changing, we might expect timing differences between force and the 7.2 nm spacing to be introduced on activation.

4.4.3 Stiffness differences in *M. sexta* subunits could not predict 7.2 nm spacing changes

While we cannot directly examine whether activatable titin-analogs are responsible for the hysteresis in intact muscle, we can indirectly test it by taking advantage of natural variation in the system. In *M. sexta* DLM there are five separate subunits, and dorsal subunits have lower expression levels of projectin, sallimus, and kettin [22] relative to thick filament proteins, than ventral subunits. From this we can infer the dorsal subunits are likely more compliant than ventral subunits. We also know that under the constant 35°C used in our experiments, when the three dorsal most subunits are compared to the two ventral most subunits, there is no difference in their twitch dynamics [117], or power output (although there are significant power output differences at lower temperatures) [3]. So if we assume that the major difference between these muscles is dominated by the relative expression of titin-analogs, a simple hypothesis might be that in subunits with stiffer titin-like elements, the 7.2 nm spacing changes would be larger than in subunits with more compliant titin-like elements, since strain changes should higher in the more compliant part of the system. In *M sexta*, this hypothesis would predict that the dorsal subunits would have lower magnitude changes than the ventral subunits.

We tested this by comparing x-ray diffraction patterns from the ventral (E) and dorsal (A) subunits (Figure 4.1), expecting amplitude changes in the 7.2 nm spacing in the dorsal subunits to be smaller. When we plotted the time course of 7.2 nm spacing changes for dorsal and ventral subunits, we found instead that the amplitude of the dorsal subunit was $0.11\% \pm .04\%$, while the amplitude of the ventral subunits was $0.23\% \pm .1\%$ ($p = .05$, *t-test*).

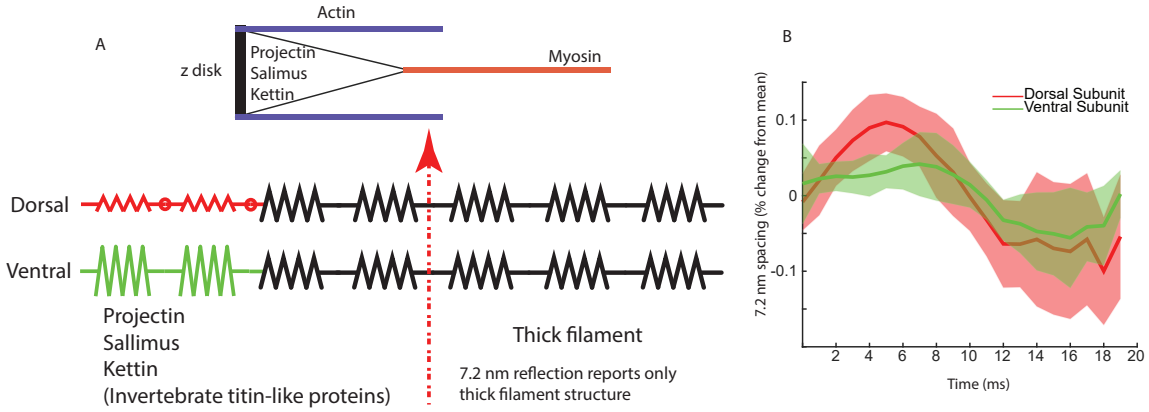

Figure 4.8: Dorsal and ventral 7.2 nm reflection changes with standard deviation. Since the 7.2 nm peak only reports the structure of the thick filament, we hypothesised that different subunits would have different 7.2 nm spacing changes, since they have different amounts of projectin, kettin, and salimus, the titin-analogs in invertebrates. The different stiffnesses might influence 7.2 nm spacing changes. N=6 for dorsal (A) subunits, and N=4 for ventral (E) subunits.

While our results do not support a titin-like mechanism for the hysteresis in thick filament strain, we cannot entirely discount this mechanism with an indirect examination because other differences between the subunits may obscure the expected differences. One way to test this hypothesis directly might be to treat muscles to blebbistatin and then measure the 7.2 nm spacing changes under the same conditions as untreated muscle. Blebbistatin is used to inhibit crossbridge formation. Therefore if significant hysteresis between force and the 7.2 nm spacing could still be observed, it might lend support to the idea that the time constant implied by the existence of the hysteresis in the system is due to activatable titin-analogues.

Alternatively hysteresis might be due to some property intrinsic to the thick filament and crossbridge formation. One such mechanism might be the strain dependent thick filament activation idea proposed in [116]. They propose that below half the maximum tetanus force (T_0) the m6 spacing are not due to filament (non-linear) stiffness, but are due to structural changes in the backbone which then facilitate myosin crossbridge formation, and it's only above $.5T_0$ that the m6 spacing represents force. All of our data is under or at that threshold ($T_0 = 200\frac{mN}{mm^2}$ for *M. sexta* DLM). Under dynamic work loop conditions, a mechanism for activatable thick filaments might introduce hysteresis in the system. It has been suggested, however, that this mechanism may be less prevalent in invertebrate muscles [125].

4.4.4 14.2 nm intensity changes in passive work loops might indicate existence of troponin bridges

The passive changes in 14.2 are surprising given past results. We expected since the spacing and intensity of the 14.2 nm peak are related to myosin head changes would be minimal in unactivated passive work loops, since myosin heads would be unbound. The intensity of the 14.2 nm peak is thought to relate to the angle the myosin head makes with the thick filament, which should change minimally under passive conditions. However, instead we saw that passive peak-to-peak changes in the m3 spacing were larger than every phase of activation (Figure 4.6, C). Since the intensity of any peak in an x-ray diffraction image comes from the underlying order, this might be explained by the myosin heads being much more highly ordered under passive conditions. The 14.2 nm spacing changes also indicate that under active conditions, the spacing between myosin heads has been reduced compared to passive work loops (Figure 4.7, B). This might be the result of cooperativity between myosin heads. When crossbridges bind, they can strain the filament, which can pull neighboring myosin heads closer, allowing them to bind as well.

Another explanation for the large intensity changes in the 14.2 nm intensity may come from the similarity of *M sexta* to asynchronous flight muscle. The flight muscle of many

invertebrates is what is known as asynchronous muscle, where activation of antagonist muscle pairs can create a self excitatory system allowing high wing beat frequencies with high power output. This is in part accomplished by delayed stretch activation, whereby stretching a muscle can cause a delayed rise in force [126]. Stretch activation is also an important property of vertebrate cardiac muscle [127]. The presence of large intensity changes in the 14.2 nm peak in passive work loops may be indicative of troponin bridges, a mechanism which may be responsible for stretch activation [56].

Troponin bridges are a class of crossbridge which bind crossbridges to actin filaments halfway between troponins, and have been directly observed in chemically fixed relaxed muscle [103]. In [56], it was proposed that if troponin bridges existed in passive, intact, dynamically oscillating muscle, it might manifest as large changes in the intensity of the 14.2 nm peak, since the 14.2 nm intensity is thought to report myosin head angle. It should also show up in the A6 and A7 peaks (5.1 and 5.9 nm peaks off-meridional peaks, which indicate thin filament strain. While we were not able to resolve the A6 or A7 peaks at the high temporal sampling frequency of our data, we were able to see very large peak-to-peak changes in the intensity of the 14.2 nm peak (Figure 4.6), which might indicate the presences of troponin bridges in *M sexta*, even though the flight muscles of *M sexta* are not asynchronous. Troponin C isoforms which have previously been implicated in stretch delayed activation in asynchronous muscles have been found in *M. sexta*, indicating some features thought to be important in asynchronous behavior may be prevalent in synchronous muscle as well [128]. Our results may also indicate this.

4.4.5 Consistency of 7.2 and 14.2 nm spacing changes might indicate contributions from both filament backbone and myosin heads

While it is a common assumption that the 7.2 nm spacing arises from structures in the filament backbone, and that the 14.2 nm spacing arises from the structure of the myosin heads [53, 54, 55], these are primarily established in vertebrates. Recently, it was shown

in tarantula leg muscle that the 7.2 nm peak contained contributions from both the filament backbone and the myosin heads [125]. This was due to the high degree of order in the myosin heads, which meant there was contribution from the second order reflection of the 14.2 nm peak at 7.2 nm. While we saw similar peak-to-peak changes in the 7.2 nm spacing as in *Drosophila*, an asynchronous muscle [115], we saw much larger changes than in *lethocerus*, another asynchronous. The wide variability in thick filament structure in invertebrate muscle might make it difficult to generalize results between species [129].

4.5 Conclusion

We were able to show that in at intact muscle operating at *in vivo* strain frequency, amplitude, length offset, and temperature across multiple phases of activation could yield highly time resolved structural changes through x-ray diffraction which showed consistent changes through a range of phase of activation. We were able to show that by tightly constraining the conditions under which the muscle operated, we could reliably predict force through a machine learning model, using equatorial information only. Because tethered experiments necessarily preclude measuring force, this consistency from extracted work loops experiments could be used in tandem with tethered experiments in order to provide an estimate of force. This is important since we see timing differences between force and the 7.2 nm peak. Since the 7.2 nm peak is commonly interpreted as force, this might impact how we draw conclusions from experiments where force can not be directly measured. We also suggest the possibility that *M. sexta* synchronous flight muscle may have structural features typically thought to be important in asynchronous muscle, inline with other studies [128].

4.6 Acknowledgments

We would like to thank Tom Daniel and Sage Malingen for their helpful discussions.

This work was supported by grant W911NF-14-1-0396 from the Army Research Of-

fice, National Science Foundation Early Career Development Award MPS/PoLS 1554790, and the Georgia Tech Dunn Family Professorship to S.S. Other support was provided by the National Science Foundation SAVI student research network in physics of living systems (1205878). This research used resources of the Advanced Photon Source, a U.S. Department of Energy (DOE) Office of Science User Facility operated for the DOE Office of Science by Argonne National Laboratory under Contract No. DE-AC02-06CH11357. The work was supported by GUP beamtime awards 60758. Use of the Pilatus 3 1M detector was provided by grant 1S10OD018090-01 from the National Institute of General Medical Sciences of the National Institutes of Health. This project was also supported by grant 9 P41 GM103622 from NIGMS. The content is solely the responsibility of the authors and does not necessarily reflect the official views of the National Institute of General Medical Sciences or the National Institutes of Health.

Appendices

APPENDIX A

HYSTERESIS IN NM SCALE STRUCTURAL DATA DURING WORK LOOPS

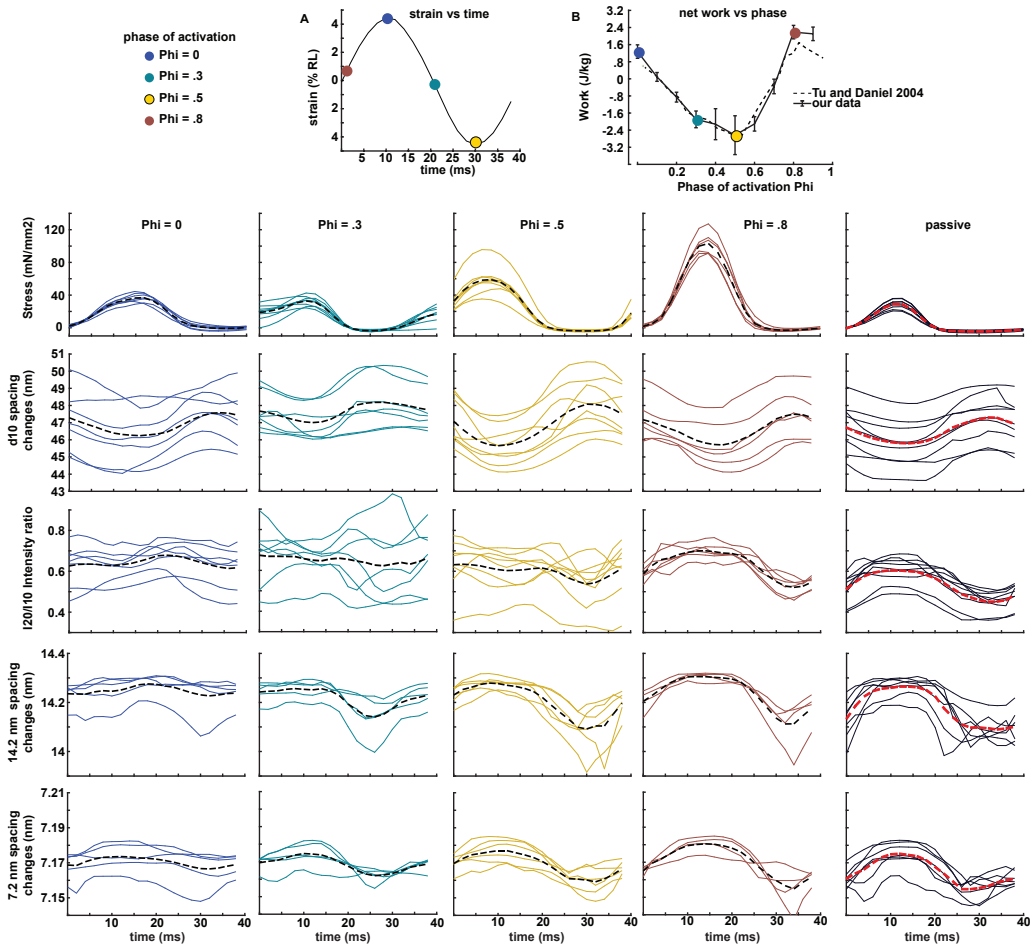

Figure A.1: A) We oscillated isolated whole-muscle moth DLM (downstroke) muscle with a sinusoidal strain trajectory at 25 Hz with 4.5% strain amplitude. We would then extracellularly stimulate the muscle at different phases during the strain cycle. We measure force and length of the muscle while simultaneously recording x-ray diffraction images. B) We defined ϕ = 0 to be the start of shortening, and sampled phases of 0, 0.1, 0.2, 0.3, 0.4, 0.5, 0.6, 0.7, 0.8, and 0.9. We show example data from figure 4C (red trace) from [12] for comparison to our data. C) We show here in each column time resolved measurements we took at phases of 0, 0.3, 0.5, and 0.8. In each row we show the stress, d_{10} spacing, intensity ratio $\frac{I_{20}}{I_{10}}$, 14.2 nm spacing, and 7.2 nm spacing. The mean response for each measurement is shown as black dotted lines in each case, except in passive case where is shown as red.

REFERENCES

[1] R. K. Josephson, "Dissecting muscle power output," *Journal Of Experimental Biology*, vol. 202, no. 23, pp. 3369–3375, 1999.

[2] N. T. George, T. C. Irving, C. D. Williams, and T. L. Daniel, "The cross-bridge spring: can cool muscles store elastic energy?" *Science*, vol. 340, no. 6137, pp. 1217–1220, Jun. 2013.

[3] N. T. George, S Sponberg, and T. L. Daniel, "Temperature gradients drive mechanical energy gradients in the flight muscle of *Manduca sexta.*," *Journal Of Experimental Biology*, vol. 215, pp. 471–479, Feb. 2012.

[4] R. K. Josephson, "Mechanical power output from striated-muscle during cyclic contraction," *Journal Of Experimental Biology*, vol. 114, no. JAN, pp. 493–512, 1985.

[5] A. A. BIEWENER, K. P. DIAL, and G. E. GOSLOW, "Pectoralis muscle force and power output during flight in the starling," *Journal of Experimental Biology*, vol. 164, no. 1, pp. 1–18, 1992. eprint: https://jeb.biologists.org/content/164/1/1.full.pdf.

[6] R. J. Full, D. R. Stokes, A. N. Ahn, and R. K. Josephson, "Energy absorption during running by leg muscles in a cockroach," *Journal Of Experimental Biology*, vol. 201 (Pt 7), pp. 997–1012, Apr. 1998.

[7] T. J. Roberts, R. L. Marsh, P. G. Weyland, and C. R. Taylor, "Muscular Force in Running Turkeys: The Economy of Minimizing Work," *Science*, vol. 275, pp. 1113–1114, Feb. 1997.

[8] K. E. Machin, J. W. S. Pringle, and F. W. Darwin, "The physiology of insect fibrillar muscle iii. the effect of sinusoidal changes of length on a beetle flight muscle," *Proceedings of the Royal Society of London. Series B. Biological Sciences*, vol. 152, no. 948, pp. 311–330, 1960. eprint: https://royalsocietypublishing.org/doi/pdf/10.1098/rspb.1960.0041.

[9] R. K. Josephson, "Contraction dynamics and power output of skeletal muscle," *Annual Review of Physiology*, vol. 55, no. 1, pp. 527–546, 1993, PMID: 8466183. eprint: https://doi.org/10.1146/annurev.ph.55.030193.002523.

[10] M. H. Dickinson, C. T. Farley, R. J. Full, M. A. Koehl, R Kram, and S Lehman, "How animals move: an integrative view.," *Science*, vol. 288, no. 5463, pp. 100–106, Apr. 2000.

[11] M. S. Tu and T. L. Daniel, "Cardiac-like behavior of an insect flight muscle," *Journal of Experimental Biology*, vol. 207, no. 14, pp. 2455–2464, 2004.

[12] ——, "Submaximal power output from the dorsolongitudinal flight muscles of the hawkmot manduca sexta," *Journal of Experimental Biology*, vol. 207, no. 26, pp. 4651–4662, 2004.

[13] A. N. Ahn and R. J. Full, "A motor and a brake: two leg extensor muscles acting at the same joint manage energy differently in a running insect," *Journal Of Experimental Biology*, vol. 205, no. 3, pp. 379–389, 2002.

[14] A. A. Biewener, R. Blickhan, A. K. Perry, N. C. Heglund, and C. R. Taylor, "Muscle forces during locomotion in kangaroo rats: Force platform and tendon buckle measurements compared," *Journal of Experimental Biology*, vol. 137, no. 1, pp. 191–205, 1988. eprint: `https://jeb.biologists.org/content/137/1/191.full.pdf`.

[15] R. Griffiths, "Ultrasound transit time gives direct measurement of muscle fibre length in vivo," *Journal of Neuroscience Methods*, vol. 21, no. 2, pp. 159 –165, 1987.

[16] A. N. Ahn, K Meijer, and R. J. Full, "*IN SITU* MUSCLE POWER DIFFERS WITHOUT VARYING *IN VITRO* MECHANICAL PROPERTIES IN TWO INSECT LEG MUSCLES INNERVATED BY THE SAME MOTOR NEURON," *Journal Of Experimental Biology*, vol. 209, no. 17, pp. 3370–3382, 2006.

[17] S. G. Campbell, P. C. Hatfield, and K. S. Campbell, "A Mathematical Model of Muscle Containing Heterogeneous Half-Sarcomeres Exhibits Residual Force Enhancement," *Plos Computational Biology*, vol. 7, no. 9, e1002156, 2011.

[18] J. Squire, "Special issue: The actin-myosin interaction in muscle: Background and overview," *International Journal of Molecular Sciences*, vol. 20, no. 11, Nov. 2019.

[19] A. D. McCulloch, "Systems Biophysics: Multiscale Biophysical Modeling of Organ Systems," *Biophysical Journal*, vol. 110, no. 5, pp. 1023–1027, 2016.

[20] R. L. Lieber and J Friden, "Functional and clinical signnificance of skeletal muscle architecture," *Muscle Nerve*, vol. 23, no. 11, pp. 1647–1666, 2000.

[21] H. L. Granzier and S. Labeit, "Titin and its associated proteins: The third myofilament system of the sarcomere," in *Fibrous Proteins: Muscle and Molecular Motors*, ser. Advances in Protein Chemistry, vol. 71, Academic Press, 2005, pp. 89 –119.

[22] C.-C. Yuan, W. Ma, P. Schemmel, Y.-S. Cheng, J. Liu, G. Tsaprailis, S. Feldman, A. A. Southgate, and T. C. Irving, "Elastic proteins in the flight muscle of manduca sexta," *Archives of Biochemistry and Biophysics*, vol. 568, pp. 16 –27, 2015.

[23] S. Labeit, C. A. Ottenheijm, and H. Granzier, "Nebulin, a major player in muscle health and disease," *FASEB J.*, vol. 25, no. 3, pp. 822–829, 2011.

[24] Q. Q. Gao and E. M. McNally, "The Dystrophin Complex: Structure, Function, and Implications for Therapy," *Compr Physiol*, vol. 5, no. 3, pp. 1223–1239, 2015.

[25] A. M. Gordon, A. F. Huxley, and F. J. Julian, "The variation in isometric tension with sarcomere length in vertebrate muscle fibres," *The Journal of Physiology*, vol. 184, no. 1, pp. 170–192, 1966.

[26] K. Campbell, "Interactions between Connected Half-Sarcomeres Produce Emergent Mechanical Behavior in a Mathematical Model of Muscle," *PLOS Computational Biology*, vol. 5,11, no. JAN, 2009.

[27] B. Millman, "The filament lattice of striated muscle," *Physiological Reviews*, vol. 78, pp. 359–391, 1998.

[28] T. C. Irving, J. Konhilas, D. Perry, R. Fischetti, and P. P. de Tombe, "Myofilament lattice spacing as a function of sarcomere length in isolated rat myocardium," *Am J Physiol*, vol. 279, H2568–H2573, May 2000.

[29] T. C. Irving and D. W. Maughan, "In Vivo X-Ray Diffraction of Indirect Flight Muscle from Drosophila melanogaster," *Biophysics Journal*, vol. 78, pp. 2511–2515, May 2000.

[30] H. Iwamoto, "Synchrotron radiation x-ray diffraction techniques applied to insect flight muscle," *International Journal of Molecular Sciences*, vol. 19, no. 6, 2018.

[31] T. C. Tune, W. Ma, T. Irving, and S. Sponberg, "Nanometer-scale structure differences in the myofilament lattice spacing of two cockroach leg muscles correspond to their different functions," *Journal of Experimental Biology*, vol. 223, no. 9, 2020. eprint: `https://jeb.biologists.org/content/223/9/jeb212829.full.pdf`.

[32] S. Malingen, A. Asencio, J. Cass, W Ma, T. Irving, and T. Daniel, "In vivo x-ray diffraction and simultaneous emg reveal the time course of myofilament lattice dilation and filament stretch," *bioRxiv*, 2020.

[33] C. D. Williams, M Regnier, and T. L. Daniel, "Axial and Radial Forces of Cross-bridges Depend on Lattice Spacing," *PLOS Computational Biology*, vol. 6, no. e1001018, pp. 1–10, Dec. 2010.

[34] C. D. Williams, M. K. Salcedo, T. C. Irving, M Regnier, and T. L. Daniel, "The length-tension curve in muscle depends on lattice spacing," *Proceedings. Biological sciences / The Royal Society*, vol. 280, no. 1766, pp. 20 130 697–20 130 697, Jul. 2013.

[35] G Cecchi, M. Bagni, P. Griffiths, C. Ashley, and Y Maeda, "Detection of radial crossbridge force by lattice spacing changes in intact single muscle fibers," *Science*, vol. 250, pp. 1409–1411, Dec. 1990.

[36] H. Huxley and J. Hanson, "Changes in the Cross Striations of Muscle during Contraction and Stretch and their Structural Interpretation," *Nature*, vol. 173, no. 4412, pp. 973–976, May 1954.

[37] A. F. Huxley and R. Niedergerke, "Structural Changes in Muscle During Contraction: Interference Microscopy of Living Muscle Fibres," *Nature*, vol. 173, no. 4412, pp. 971–973, May 1954.

[38] A. F. Huxley and R. M. Simmons, "Proposed Mechanism of Force Generation in Striated Muscle," *Nature*, vol. 233, pp. 533–538, Oct. 1971.

[39] M. Kawai and P. Brandt, "Sinusoidal analysis: A high resolution method for correlating biochemical reactions with physiological processes in activated skeletal muscles of rabbit, frog and crayfish," *Journal of Muscle Research and Cell Motility*, vol. 1, pp. 279–303, 1980.

[40] I. Y. Kuo and B. E. Ehrlich, "Signaling in Muscle Contraction," *Cold Spring Harbor Perspectives in Biology*, vol. 7, pp. 255–318, 2 2015.

[41] D. Randall, W. Burggren, and K. French, *Eckert Animal Phsiology: Mechanisms and Adaptations*, 5th ed. New York: W. H. Freeman and Company, 2002, ISBN: 0-7167-3863-5.

[42] R. W. Lymn and E. W. Taylor, "Mechanism of Adenosine Triphosphate Hydrolysis by Actomyosin," *Biochemistry*, vol. 10, no. 25, pp. 4617–4623, Jul. 1971.

[43] A. N. Ahn, "How Muscles Function - the Work Loop Technique," *Journal of Experimental Biology*, vol. 215, no. 7, pp. 1051–1052, 2012.

[44] S. Sponberg and T. L. Daniel, "Abdicating power for control: a precision timing strategy to modulate function of flight power muscles," *Proceedings of the Royal Society B: Biological Sciences*, vol. 270, pp. 3958–3966, Jul. 2012.

[45] A. A. Biewener and M. A. Daley, "Unsteady locomotion: Integrating muscle function with whole body dynamics and neuromuscular control," *Journal of Experimental Biology*, vol. 210, no. 17, pp. 2949–2960, 2007. eprint: https://jeb.biologists.org/content/210/17/2949.full.pdf.

[46] A. V. Hill, "The heat of shortening and the dynamic constants of muscle," *Proceedings of the Royal Society B*, vol. 126, pp. 136–195, 1938.

[47] A. V. Huxley, "Muscle structure and theories of contraction," *Progress in Biophysics and Biophysical Chemistry*, vol. 7, pp. 255–318, 1957.

[48] J. H. Belanger, "Contrasting Tactics in Motor Control by Vertebrates and Arthropods1," *Integrative and Comparative Biology*, vol. 45, no. 4, pp. 672–678, Aug. 2005. eprint: https://academic.oup.com/icb/article-pdf/45/4/672/1782361/i1540-7063-045-04-0672.pdf.

[49] S. Sponberg, T. Libby, C. Mullens, and R. Full, "Shifts in a single muscle's control potential of body dynamics are determined by mechanical feedback," *Philosophical Transactions of the Royal Society B*, vol. 366, pp. 1606–1620, May 2011.

[50] T. Libby, C. Chukwueke, and S. Sponberg, "History-dependent perturbation response in limb muscle," *Journal of Experimental Biology*, 2019. eprint: https://jeb.biologists.org/content/early/2019/12/06/jeb.199018.full.pdf.

[51] T. C. Irving, "X-ray diffraction of indirect flight muscle from drosophila in vivo," in *Nature's Versatile Engine: Insect Flight Muscle Inside and Out*, J. Vigoreaux, Ed., Landes Bioscience, 2006, ch. 16, pp. 197–211.

[52] D. W. Maughan and R. E. Godt, "Radial Forces within Muscle Fibers in Rigor," *Journal of General Physiology*, vol. 77, pp. 49–64, Jan. 1981.

[53] H. E. Huxley, "Recent x-ray diffraction studies of muscle contraction and their implications," *Phil. Trans. R. Soc*, vol. 359, no. 10, pp. 1879–1882, 2004.

[54] M. Linari, G. Piazzesi, I. Dobbie, N. Koubassova, M. Reconditi, T. Narayanan, O. Diat, M. Irving, and V. Lombardi, "Interference fine structure and sarcomere length dependence of the axial x-ray pattern from active single muscle fibers," *Proceedings of the National Academy of Sciences*, vol. 97, no. 13, pp. 7226–7231, 2000. eprint: https://www.pnas.org/content/97/13/7226.full.pdf.

[55] W. Ma, H. Gong, B. Kiss, E.-J. Lee, H. Granzier, and T. Irving, "Thick-filament extensibility in intact skeletal muscle," *Biophysical Journal*, vol. 115, no. 8, pp. 1580 –1588, 2018.

[56] R. J. Perz-Edwards, T. C. Irving, B. A. J. Baumann, D. Gore, D. C. Hutchinson, U. Kržič, R. L. Porter, A. B. Ward, and M. K. Reedy, "X-ray diffraction evidence for myosin-troponin connections and tropomyosin movement during stretch activation of insect flight muscle," *Proceedings of the National Academy of Sciences*, vol. 108, no. 1, pp. 120–125, 2011. eprint: `https://www.pnas.org/content/108/1/120.full.pdf`.

[57] D. W. Maughan and J. O. Vigoreaux, "An Integrated View of Insect Flight Muscle: Genes, Motor Molecules, and Motion," *Physiology*, vol. 14, no. 3, pp. 87–92, 1999.

[58] J. D. Powers, C. D. Williams, M. Regnier, and T. L. Daniel, "A Spatially Explicit Model Shows How Titin Stiffness Modulates Muscle Mechanics and Energetics," *INTEGRATIVE AND COMPARATIVE BIOLOGY*, vol. 58, no. 2, 186–193, 2018.

[59] E. D. Tytell, J. A. Carr, N. Danos, C. Wagenbach, C. M. Sullivan, T. Kiemel, N. J. Cowan, and M. M. Ankarali, "Body stiffness and damping depend sensitively on the timing of muscle activation in lampreys," *Integrative and Comparative Biology*, vol. 58, no. 5, pp. 860–873, Jun. 2018.

[60] T. J. Roberts, R. L. Marsh, P. G. Weyand, and C. R. Taylor, "Muscular force in running turkeys: The economy of minimizing work," *Science*, vol. 275, no. 5303, pp. 1113–1115, 1997. eprint: `https://science.sciencemag.org/content/275/5303/1113.full.pdf`.

[61] M. A. Bagni, G. Cecchi, P. J. Griffiths, Y. Maeda, G. Rapp, and C. C. Ashley, "Lattice spacing changes accompanying isometric tension development in intact single muscle fibers," *Biophys. J.*, vol. 67, no. 5, pp. 1965–1975, 1994.

[62] M. Schoenberg, "Geometrical factors influencing muscle force development. II. Radial forces," *Biophysical Journal*, vol. 30, pp. 69–77, Apr. 1980.

[63] B. C. W. Tanner, T. L. Daniel, and M. Regnier, "Sarcomere lattice geometry influences cooperative myosin binding in muscle," *Plos Computational Biology*, vol. 3, no. 7, pp. 1195–1211, 2007.

[64] B. C. Tanner, G. P. Farman, T. C. Irving, D. W. Maughan, B. M. Palmer, and M. S. Miller, "Thick-to-thin filament surface distance modulates cross-bridge kinetics in Drosophila flight muscle," *Biophysical Journal*, vol. 103, no. 6, pp. 1275–1284, 2012.

[65] F. Fuchs and Y.-P. Wang, "Sarcomere Length Versus Interfilament Spacing as Determinants of Cardiac Myofilament Ca^{2+} Sensitivity and Ca^{2+} Binding," *Journal of Molecular and Cellular Cardiology*, vol. 28, no. 7, pp. 1375 –1383, 1996.

[66] B. B. Adhikari, M. Regnier, A. J. Rivera, K. L. Kreutziger, and D. A. Martyn, "Cardiac length dependence of force and force redevelopment kinetics with altered cross-bridge cycling," *Biophysical Journal*, vol. 87, pp. 1784–1794, Sep. 2004.

[67] G Becht and D Dresden, "Physiology of the Locomotory Muscles in the Cockroach," *Nature*, vol. 177, no. 4514, pp. 836–837, 1956.

[68] K. G. Pearson and J. F. Iles, "Innervation of coxal depressor muscles in the cockroach, Periplaneta americana.," *Journal of Experimental Biology*, vol. 54, no. 1, pp. 215–232, 1971.

[69] G. Becht, G. Hoyle, and P. Usherwood, "Neuromuscular transmission in the coxal muscles of the cockroach," *Journal of Insect Physiology*, vol. 4, no. 3, pp. 191–201, 1960.

[70] J. M. Squire, H. A. Al-khayat, C. Knupp, and P. K. Luther, "Molecular architecture in muscle contractile assemblies," in *Fibrous Proteins: Muscle and Molecular Motors*, ser. Advances in Protein Chemistry, vol. 71, Academic Press, 2005, pp. 17 –87.

[71] C. S. Carbonell, "The Thoracic Muscles of the Cockroach Periplaneta Americana (L.)," *Smithsonian Miscellaneous Collections*, vol. 107, no. 2, pp. 1–23, 1947.

[72] C. D. Williams, M. Balazinska, and T. L. Daniel, "Automated Analysis of Muscle X-ray Diffraction Imaging with MCMC," in *Biomedical Data Management and Graph Online Querying*, Springer, 2015, pp. 126–133.

[73] M. Wojdyr, "Fityk: a general-purpose peak fitting program," *Journal of Applied Crystallography*, vol. 43, pp. 1126–1128, Oct. 2010.

[74] S. S. Jahromi and H. L. Atwood, "Structural Features of Muscle Fibers in the Cockroach Leg," *Journal of Insect Physiology*, vol. 15, pp. 2255–2262, Jun. 1969.

[75] S. Dutta, C. Tsiros, S. L. Sundar, H. Athar, J. Moore, B. Nelson, M. J. Gage, and K. Nishikawa, "Calcium increases titin n2a binding to f-actin and regulated thin filaments," *Scientific Reports*, vol. 8, no. 1, p. 14 575, 2018.

[76] J. J. Widrick, J. G. Romatowski, K. M. Norenberg, S. T. Knuth, J. L. W. Bain, D. A. Riley, S. W. Trappe, T. A. Trappe, D. L. Costill, and R. H. Fitts, "Functional properties of slow and fast gastrocnemius muscle fibers after a 17-day spaceflight," *Journal of Applied Physiology*, vol. 90, no. 6, pp. 2203–2211, 2001.

[77] C. J. Hawkins and P. M. Bennett, "Evaluation of freeze substitution in rabbit skeletal muscle. comparison of electron microscopy to x-ray diffraction," *Journal of Muscle Research & Cell Motility*, vol. 16, pp. 303–318, 1995.

[78] P. Luther and J. Squire, "The intriguing dual lattices of the myosin filaments in vertebrate striated muscles: Evolution and advantage," *Biology*, vol. 3, pp. 846–865, Dec. 2014.

[79] A. Miller and R. T. Tregear, "Evidence concerning crossbridge attachment during muscle contraction," vol. 226, no. 5250, pp. 1060–1061, 1970.

[80] N. Yagi and I. Matsubara, "The equatorial x-ray diffraction patterns of crustacean striated muscles," *Journal of Molecular Biology*, vol. 117, no. 3, pp. 797 –803, 1977.

[81] E. W. April, P. W. Brandt, and G. F. Elliott, "The myofilament lattice: Studies on isolated fibers," *The Journal of Cell Biology*, vol. 51, no. 1, pp. 72–82, 1971. eprint: http://jcb.rupress.org/content/51/1/72.full.pdf.

[82] T. Shimomura, H. Iwamoto, T. T. Vo Doan, S. Ishiwata, H. Sato, and M. Suzuki, "A beetle flight muscle displays leg muscle microstructure," *Biophysical Journal*, vol. 111, pp. 1295–1303, Sep. 2016.

[83] S. G. Campbell, C. Hatfield, and K. S. Campbell, "A model with Heterogeneous Half-Sarcomeres Exhibits Residual Force Enhancement After Active Stretch," *Biophysical Journal*, vol. 100, no. 3, 12a, 2011.

[84] I. Matsubara and G. F. Elliot, "X-ray diffraction studies on skinned single fibres of frog skeletal muscle," *Journal of Molecular Biology*, vol. 72, pp. 657–669, Dec. 1972.

[85] F. Fuchs and D. A. Martyn, "Length-dependent Ca^{2+} activation in cardiac muscle: some remaining questions," *Journal of Muscle Research and Cell Motility*, vol. 26, pp. 199–212, Apr. 2005.

[86] O. Cazorla, Y. Wu, T. Irving, and H. Granzier, "Titin-Based Modulation of Calcium Sensitivity of Active Tension in Mouse Skinned Cardiac Myocytes Materials and Methods Preparations and Solutions," *Circulation Research*, vol. 88, no. 10, pp. 1028–1035, 2001.

[87] N. Fukuda, Y. Wu, G. Farman, T. C. Irving, and H. Granzier, "Titin isoform variance and length dependence of activation in skinned bovine cardiac muscle," *The Journal of Physiology*, vol. 553, no. 1, pp. 147–154, 2003. eprint: https://physoc.onlinelibrary.wiley.com/doi/pdf/10.1113/jphysiol.2003.049759.

[88] B. Bullard, C. Burkart, S. Labeit, and K. Leonard, "The function of elastic proteins in the oscillatory contraction of insect flight muscle," *Journal of Muscle Research & Cell Motility*, vol. 26, no. 6, pp. 479–485, 2005.

[89] B. Bullard, T. Garcia, V. Benes, M. C. Leake, W. A. Linke, and A. F. Oberhauser, "The molecular elasticity of the insect flight muscle proteins projectin and kettin," *Proceedings of the National Academy of Sciences*, vol. 103, no. 12, pp. 4451–4456, 2006.

[90] C. Burkart, F. Qiu, S. Brendel, V. Benes, P. Hååg, S. Labeit, K. Leonard, and B. Bullard, "Modular proteins from the drosophila sallimus (sls) gene and their expression in muscles with different extensibility," *Journal of Molecular Biology*, vol. 367, no. 4, pp. 953 –969, 2007.

[91] S. L. Hooper and J. B. Thuma, "Invertebrate Muscles: Muscle Specific Genes and Proteins," *Physiological reviews*, vol. 85, no. 3, pp. 1001–1060, 2005.

[92] S. Sponberg, A. J. Spence, C. H. Mullens, and R. J. Full, "A single muscle's multifunctional control potential of body dynamics for postural control and running," *Philosophical Transactions of the Royal Society B*, vol. 366, pp. 1592–1605, Apr. 2011.

[93] Y. P. Wang and F Fuchs, "Osmotic compression of skinned cardiac and skeletal muscle bundles: Effects on force generation, $ca2 =$ sensitivity and $ca2 =$ binding," *Journal of Molecular Cell Cardiology*, vol. 27, 1995.

[94] A. M. Gordon, E. Homsher, and M. Regnier, "Regulation of contraction in striated muscle," *Physiol. Rev.*, vol. 80, no. 2, pp. 853–924, 2000.

[95] K. S. Campbell, "Dynamic coupling of regulated binding sites and cycling myosin heads in striated muscle," *Journal of General Physiology*, vol. 143, no. 3, pp. 387–399, Feb. 2014. eprint: `https://rupress.org/jgp/article-pdf/143/3/387/649273/jgp\_201311078.pdf`.

[96] B. C. W. Tanner, M. Regnier, and T. L. Daniel, "A spatially explicit model of muscle contraction explains a relationship between activation phase, power and atp utilization in insect flight," *Journal of Experimental Biology*, vol. 211, no. 2, pp. 180–186, 2008.

[97] J. A. Cass, C. D. Williams, T. C. Irving, T. L. Daniel, and S. N. Sponberg, "A mechanism for sarcomere breating: volume changes and advective flow within the myofilament lattice," *arXiv*, Apr. 2019.

[98] H. Huxley, A. Stewart, H. Sosa, and T. Irving, "X-ray diffraction measurements of the extensibility of actin and myosin filaments in contracting muscle," *Biophysical Journal*, vol. 67, no. 6, pp. 2411 –2421, 1994.

[99] T. L. Daniel, A. C. Trimble, and P. B. Chase, "Compliant realignment of binding sites in muscle: Transient behavior and mechanical tuning," *Biophysical Journal*, vol. 74, 1998.

[100] H. Kojima, A. Ishuima, and T. Yanagida, "Direct measurement of stiffness of single actin filaments with and without tropmyosin by *in vitro* nanomanipulation," *Proceedings of the National Academy of Sciences of the United States of America*, vol. 91, 1994.

[101] K. Wakabayashi, Y Sugimoto, H. Tanaka, Y. Ueno, Y. Takezawa, and Y. Amemiya, "X-ray diffraction evidence for the extensibility of actin and myosin filaments during muscle contraction," *Biophysical Journal*, vol. 67, 1994.

[102] E. Pate and R. Cooke, "A model for the Interaction of Muscle Cross-bridges with Ligands which compete with ATP," *Journal of Theoretical Biology*, vol. 118, pp. 215–230, 1986.

[103] J. Liu, W. Shenping, M. C. Reedy, H. Winkler, C. Lucaveche, Y. Cheng, M. K. Reedy, and K. A. Taylor, "Electron tomography of swollen rigor fibers of insect flight muscle reveals a short and variably angles s2 domain," *Journal of Molecular Biology*, vol. 362, 2006.

[104] K. A. Taylor, H. Schmitz, M. C. Reedy, Y. E. Goldman, C. Franzini-Armstrong, H. Sasaki, R. T. Tregear, K. Poole, C. Lucaveche, E. R. J., L. F. Chen, H. Winkler, and M. Reedy, "Tomograhpic 3d reconstruction of quick-frozen, $ca2+$-activated contracting insect flight muscle," *Cell*, vol. 99, 1999.

[105] E. Pate and R. Cooke, "A model of crossbridge action: the effects of ATP, ADP, and P_i," *Journal of Muscle Research and Cell Motility*, vol. 10, pp. 181–196, 1989.

[106] C. Burkart, F. Qiu, S. Brendel, V. Benes, P. H??g, S. Labeit, K. Leonard, and B. Bullard, "Modular proteins from the Drosophila sallimus (sls) gene and their expression in muscles with different extensibility," *J. Mol. Biol.*, vol. 367, no. 4, pp. 953–969, 2007.

[107] G. Piazzesi, L. Lucii, and V. Lombardi, "The size and the speed of the working stroke of muscle myosin and its dependence on force," vol. 545, pp. 145–151, 2002.

[108] D. Caterini, W. Gittings, J. Huang, and R. Vandenboom, "The effect of work cycle frequency on the potentiation of dynamic force in mouse fast twitch skeletal muscle," *Journal of Molecular Experimental Biology*, vol. 214, 2011.

[109] G. Askew, I. Young, and A. J.D., "Fatigue of mouse soleus muscle, using the work loop technique," *Journal of Molecular Experimental Biology*, vol. 200, 1997.

[110] J. Molloy, J. Burns, J. Kendrick-Jones, R. Tregear, and D. White, "Movement and force produced by a single myosin head," *Nature*, vol. 378, pp. 209–212, 1995.

[111] F. J. Julian and D. L. Morgan, "The effect on tension of non-uniform distribution of length changes applied to frog muscle fibres," *J. Physiol. (Lond.)*, vol. 293, pp. 379–392, 1979.

[112] M Irving, V Lombardi, G Piazzesi, and M. A. Ferenczi, "Myosin head movements are synchronous with the elementary force-generating process in muscle," *Nature*, vol. 357, 1992.

[113] M. Reconditi, "Recent improvements in small angle x-ray diffraction for the study of muscle physiology," *Reports on Progress in Physics*, vol. 69, no. 10, pp. 2709–2759, 2006.

[114] H. E. Huxley, "Recent X-ray diffraction studies of muscle contraction and their implications," *Philos. Trans. R. Soc. Lond., B, Biol. Sci.*, vol. 359, no. 1452, pp. 1879–1882, 2004.

[115] M. Dickinson, G. Farman, M. Frye, T. Bekyarova, D. Gore, D. Maughan, and T. Irving, "Molecular dynamics of cyclically contracting insect flight muscle in vivo," *Nature*, vol. 433, no. 7023, pp. 330–334, 2005.

[116] M. Linari, E. Brunello, M. Reconditi, L. Fusi, M. Caremani, T. Narayanan, G. Piazzesi, V. Lombardi, and M. Irving, "Force generation by skeletal muscle is controlled by mechanosensing in myosin filaments," *Nature*, vol. 528, 276 EP –, 2015.

[117] N. T. George and T. L. Daniel, "Temperature gradients in the flight muscles of manduca sexta imply a spatial gradient in muscle force and energy output," *Journal of Experimental Biology*, vol. 214, no. 6, pp. 894–900, 2011. eprint: `https://jeb.biologists.org/content/214/6/894.full.pdf`.

[118] J. L. Eaton, *Lepidotpteran Anatomy*. J. Wiley Sons, 1988, ISBN: 3257227892.

[119] Jiratrakanvong, J. and Shao, J. and Menendez, M. and Li, X. and Ma, M. Agam, G. and Irving, T., *Musclex: Software suite for x-ray imaging*, version 1.14.4, Aug. 30, 2019.

[120] S. Hochreiter and J. Schmidhuber, "Long short-term memory," *Neural Comput.*, vol. 9, no. 8, 1735–1780, Nov. 1997.

[121] M. Cervera, J. J. Arredondo, and R. M. Ferrreres, "Paramyosin and miniparamyosin," in *Nature's Versatile Engine: Insect Flight Muscle Inside and Out*, J. Vigoreaux, Ed., Landes Bioscience, 2006, ch. 6, pp. 76–85.

[122] A. P. Willmott and C. P. Ellington, "The mechanics of flight in the hawkmoth *Manduca sexta*," *Journal of Experimental Biology*, vol. 200, pp. 2705–2722, 1997.

[123] C. P. Ellington, "Power and Efficiency of Insect Flight Muscle," *Journal of Experimental Biology*, vol. 115, pp. 293–304, Mar. 1985.

[124] J. G. Malamud, A. P. Mizisin, and R. K. Josephson, "The effects of octopamine on contraction kinetics and power output of a locust flight muscle," *Journal of Comparative Physiology A*, vol. 162, pp. 827–835, 1988.

[125] R. Padron, W. Ma, S. Duno-Miranda, N. Koubassova, K. Hwan Lee, A. Pint, L. Alamo, P. Bolanos, A. Tsaturyan, T. Irving, and R. Craig, "The myosin interacting-heads motif present in live tarantula muscle explains tetanic and posttetanic phosphorylation mechanisms," *Procedings of the National Academy Science*, vol. 117, 2020.

[126] R. K. Josephson, J. G. Malmud, and D. R. Stokes, "Asyncronous Muscle: A Primer," *The Journal of Experimental Biology*, vol. 203, pp. 2713–2722, 2000.

[127] J. Stelzer and R. Moss, "Contributions of Stretch Activation to Length-dependent Contraction in Murine Myocardium," *Journal of General Physiology*, vol. 128, no. 4, pp. 461–471, 2006.

[128] A. Ayme-Southgate, S. Feldman, and D. Fulmer, "Myofilament proteins in the synchronous flight muscles of manduca sexta show both similarities and differences to drosophila melanogaster," *Insect Biochemistry and Molecular Biology*, vol. 62, Mar. 2015.

[129] S. L. Hooper, K. H. Hobbs, and J. B. Thuma, "Invertebrate muscles: thin and thick filament structure; molecular basis of contraction and its regulation, catch and asynchronous muscle," *Prog. Neurobiol.*, vol. 86, no. 2, pp. 72–127, 2008.